1-1-1990

Radio observations of several interstellar molecules.

Y. C. Minh
University of Massachusetts Amherst

RADIO OBSERVATIONS OF SEVERAL INTERSTELLAR MOLECULES

A Dissertation Presented

by

YOUNG CHOL MINH

Submitted to the Graduate School of the
University of Massachusetts in partial fulfillment
of the requirements for the degree of

DOCTOR OF PHILOSOPHY

February 1990

Department of Physics and Astronomy

RADIO OBSERVATIONS OF SEVERAL INTERSTELLAR MOLECULES

A Dissertation Presented

by

YOUNG CHOL MINH

Approved as to style and content by:

William M. Irvine, Chairman of Committee

Robert L. Dickman, Member

Paul F. Goldsmith, Member

Robert V. Krotkov, Outside Member

Robert B. Hallock, Department Head
Department of Physics and Astronomy

ACKNOWLEDGEMENTS

When I look back upon the days at Amherst, everything seems to have passed like a dream. Before long I will miss many friendly people here and probably the days I spent at my office and at Quabbin observatory.

I thank my advisor Bill sincerely. The works included in this thesis were, in the first place, possible by his guidance and suggestions. He showed me how to make observations and how to make papers. I had a real valuable time here and I thank Bill again for his support and encouragement.

I am grateful to Lucy Ziurys. Some parts of this thesis were initiated by her kind suggestions and comments. I thank Bob for his encouragement and the hospitality he showed me during my stay at Amherst. I thank Paul for his critical readings of this thesis and suggestions, and Ron, Bob, and Paul for valuable discussions. I thank Mike Brewer for his consultations for computer problems and allowing me to use his LVG model. Without his assistence I might be still debugging my LVG model. I wish to thank Sue Madden who has encouraged me since the first day I came here, and many other students with whom I have had the pleasure of being associated.

I would like to express my special appreciation to FCRAO and its staff for their technical assistance during the observations. I thank a wonderful and powerful team consisted of Jackie, Sally, Denise, Barb, and Jan for their kindness and hospitality. Without

their support, nothing would have worked properly to finish my degree successfully and smoothly.

I thank my parents for their love, support, and encouragement they have given me throughout the entire span of my life. I really don't know how to express my appreciation to them. "Thank you, Mom and Dad !" I also thank my mother-in-law who has prayed for our health and happiness with constant love. I thank my brothers and sisters for their love and encouragement. I thank my son, Hyun-Sik, who has been a constant source of joy during our living at Amherst. I would like to express a special appreciation to my wife, Kyung-Sun, who has sacrificed her achievements in Korea and endured tough time at Amherst, from my heart for her love and faith in me.

Although it is a pleasure to say "*it's done !*", I know it is not the end but just a start. Good-bye everybody and good-bye Amherst ! Thank you !

ABSTRACT

RADIO OBSERVATIONS OF SEVERAL INTERSTELLAR MOLECULES

FEBRUARY 1990

YOUNG CHOL MINH

B.S., M.S., SEOUL NATIONAL UNIVERSITY

Ph.D., UNIVERSITY OF MASSACHUSETTS

Directed by Professor William M. Irvine

We present observations of rotational transitions for several interstellar molecules whose formation may be related to grain processes and discuss their implications for interstellar chemistry.

Interstellar hydrogen sulfide has been observed at fractional abundances $f(H_2S) \sim 10^{-9}$ relative to H_2 towards cold, dark clouds, while its abundance is enhanced by a factor of 1000 in the Orion hot core and the plateau. H_2S may be evaporating from the grain mantles in the hot core, and even in the cold, dark clouds, grain surface reactions may be responsible for the gas-phase H_2S abundances. We also derive an upper limit for the HDS abundance $[HDS]/[H_2S] \leq 6 \times 10^{-4}$ in the Orion hot core.

H_2CS ortho-to-para ratios have been observed to be ~ 1.8 towards TMC-1, which may suggest that H_2CS is in equilibrium with the expected grain temperaure (10 K) and gas-grain exchanges are taking place effectively in cold, dark clouds. We derive a ratio of ~ 3, the statistical value, for Orion(3N1E) and NGC7538, and ~ 2 for Orion(KL).

We derive upper limits of the ethyl cyanide column densities of ~ 3 x 10^{12} cm^{-2} towards TMC-1 and L134N. Together with the detection for vinyl cyanide, there may be no necessity of invoking grain surface synthesis for these highly saturated species in cold clouds, but the desorption processes seem to be quite inefficient for these heavy molecules.

Finally, we have surveyed $HOCO^+$ as a tracer of interstellar CO_2 towards many galactic sources, and derive $f(HOCO^+)$ ~ 10^{-8} - 10^{-9} in the Galactic center and $\leq 10^{-10}$ for cold dark clouds. The observed abundance of $HOCO^+$ in the Galactic center is ~ 3 and ~ 1 orders of magnitude larger than that predicted by ion-molecule chemistry and shock chemistry, respectively. UV photolysis of grain mantles may produce CO_2 efficiently, resulting in a large abundance of $HOCO^+$ in the Galactic center.

Interstellar grains are thought to play crucial roles in the chemistry of interstellar molecular clouds, and our results give some constraints on the *highly uncertain* grain processes, as well as on the gas phase processes.

TABLE OF CONTENTS

LIST OF TABLES

LIST OF FIGURES

CHAPTER 1

INTRODUCTION

1.1 Overview

Interstellar molecules have been used as important probes of the physical and chemical conditions of various types of objects in the universe since the first detection of diatomic radicals and ions in the 1930's and 40's. The molecules in the interstellar medium (ISM) are indeed more than probes; they "provide cooling and heating pathways which govern cloud evolution, including the enhancement or supression of instabilities leading toward clump formation, fragmentation, and ultimately the formation of protostars" (Irvine, Goldsmith, and Hjalmarson 1987). Thus, the evolution of a cloud depends on its chemical conditions as well as on its physical conditions.

Molecular hydrogen, the most abundant and important species in interstellar space, is believed to form on grain surfaces (Hollenbach and Salpeter 1971). The relative contribution of grains to the trace composition of the gas-phase is largely unknown, however. This thesis began as an effort to clarify this issue. The effects of grains are expected to increase with density. Interstellar grains may act as a sink for gas-phase molecules and may also be involved in producing many molecules by surface

catalytic reactions, UV photolysis of grain mantles, evaporation of grain mantles, or disruption by shocks. Details of these processes are, however, currently quite uncertain. Even the questions of grain composition and where and how they form are still controversal. Interstellar grains, including materials such as silicates, graphite, polycyclic aromatic hydrocarbons (PAHs), and amorphous carbon, are believed to form in the outflows of the late-type giants or planetary nebulae. Interstellar grains have been observed to have icy mantles or organic refractory components, probably on top of silicate or graphite cores. Grain surface chemistry to produce "dirty ice" mantles had been suggested as early as 1949 by van de Hulst and later considered in detail by Watson and Salpeter (1972). Surface chemistry involving purely thermodynamic driving forces for grain surface reactions has been considered by Allen and Robinson (1975, 1977). The icy mantles, which form by accretion and reaction of gas-phase species, seem to be ubiquitous in all dense clouds, while the organic refractories have been observed only toward diffuse clouds and the Galactic center (Tielens and Allamandola 1987, and Irvine and Knacke 1989 and references therein).

Recent observations increasingly show that gas and dust can be coupled quite closely. For example, enhanced abundances of oxygen-containing molecules in the Orion compact ridge probably result from H_2O released from grain mantles by the interaction between an outflow and the ambient material (Blake *et al.* 1987), and

NH_3 and H_2O in the Orion hot core are thought to evaporate from grain mantles (Walmsley 1987; Plambeck and Wright 1987). In addition, IR observations towards highly obscured sources have identified several grain mantle components, such as NH_3, H_2O, and CO (Knacke *et al.* 1982; Tielens *et al.* 1984; Lacy *et al.* 1984), that are also present in the gas phase. Recently d'Hendecourt and Muizon (1989) claimed a detection of interstellar carbon dioxide toward three protostars.

Several models have been constructed for the molecular composition of accreting grain mantles (Tielens and Hagen 1982; d'Hendecourt, Allamandola, and Greenberg 1985). One of the most uncertain processes related to grain chemistry is the desorption mechanism. The accretion time scale of the gas-phase species onto the grain ($\sim 3 \times 10^5$ yr for $n \sim 10^4$ cm^{-3}) is supposed to be short relative to both probable molecular cloud lifetimes ($\sim 10^7$ yr) and some of the time scales of the gas-phase chemistry ($\sim 10^7$ yr). Therefore, there must be an efficient desorption mechanism to preserve a gas phase ISM in general (Winnewisser and Herbst 1987). In star-forming regions, desorption may occur easily by interstellar shocks, or by an enhanced UV field, which can disrupt grains or evaporate grain mantles (Dopita 1977; Drain and Salpeter 1979). On the other hand, in the quiescent clouds, desorption may be quite inefficient, but might occur as a result of, for example, heat dissipation of surface reactions, heating via grain-grain

collisions, heavy nuclei cosmic ray bombardment, or X-rays (Leger, Jura, and Omont 1985).

Although interstellar grains have been thought to play important roles in chemical processes in molecular clouds, it is rather difficult to determine observationally that grains are actually involved in producing species other than the hydrogen molecule, and there have been very few radio observations which support grain processes. In this thesis we have studied several molecules whose chemistry may be related to grain processes. We present the observational results for interstellar hydrogen sulfide (H_2S), thioformaldehyde (H_2CS), ethyl cyanide (CH_3CH_2CN), and protonated carbon dioxide ($HOCO^+$), and discuss implications for interstellar chemistry. Each chapter has a format as an individual paper to be published separately: Chapter 2: Minh, Y. C., Irvine, W. M., and Ziurys, L. M. (1989), *Ap. J. (Letters)*, 345, L63; Chapter 3: Minh, Y. C., Ziurys, L. M., Irvine, W. M., and McGonagle, D. (1989), in preparation; Chapter 4: Minh, Y. C., Irvine, W. M., McGonagle, D., and Ziurys, L. M. (1989), in preparation; Chapter 5: Minh, Y. C., Irvine, W. M., and Brewer, M. K. (1989), in preparation; Chapter 6: Minh, Y. C. and Irvine, W. M. (1989), in preparation; Chapter 7: Minh, Y. C., Irvine, W. M., and Ziurys, L. M. (1988), *Ap. J.*, 334, 175; Chapter 8: Minh, Y. C., Brewer, M. K., Irvine, W. M., Friberg, P., and Johansson, L. E. B. (1989), in preparation. Finally in Chapter 9, we summarize our conclusions. The Appendices include the results for statistical equilibrium and LVG model calculations

for H_2CS and $HOCO^+$ in Appendix A, and abundances of several molecules observed towards the Sgr A molecular cloud complex in Appendix B.

1.2 Observed Molecules

1.2.1 Hydrogen sulfide

Interstellar hydrogen sulfide (H_2S) has been suggested as a tracer of high-temperature chemistry and/or grain surface chemistry because crucial gas-phase reactions leading to the formation of H_2S are thought to be appreciably endothermic (Watson and Walmsley 1982; Duley, Millar, and Williams 1980). H_2S was first observed in the ISM by Thaddeus *et al.* (1972) in its 1_{10} - 1_{01} transition at 169 GHz toward several GMC's, but there have been very few published observations of H_2S, at least in part because of the lack of receivers to study the 2 mm region. We have carried out a survey of H_2S at 169 GHz using a new FCRAO 2 mm receiver and present the results in Chapters 2 to 4.

1.2.2 Thioformaldehyde

The ortho/para ratio for molecules which exhibit the appropriate symmetry may be an indicator of dust grain temperatures and dust-gas exchange of material, especially in cold, dark clouds.

However, molecular hydrogen, which has no electric dipole moment, is hard to observe in dense molecular clouds with kinetic temperatures of 10 - 100 K, and formaldehyde (H_2CO) lines are observed to be very optically thick (Kahane *et al.* 1984). H_2CS may be a good candidate to study the ortho-to-para ratio, since the optical depths for the H_2CS lines seem to be much less than those of H_2CO (Irvine *et al.* 1989). In Chapter 5, we discuss the abundances and ortho-to-para ratios for H_2CS observed towards several interstellar clouds.

1.2.3 Ethyl cyanide

Ion-molecule reactions leading to the formation of ethyl cyanide are highly endothermic and proceed quite slowly (Herbst, Adams, and Smith 1983). Heavily saturated molecules such as ethyl cyanide and vinyl cyanide have been suggested to form on grains, since hydrogenation may proceed efficiently on grain surfaces (Irvine and Hjalmarson 1984; Blake *et al.* 1987). We have searched for ethyl cyanide toward TMC-1 in its 2_{02} - 1_{01} transition at 18 GHz and present the result in Chapter 6.

1.2.4 Protonated carbon dioxide

The $HOCO^+$ molecule, the protonated form of CO_2, has been suggested as a tracer of interstellar CO_2, which is conceivably an important carbon and oxygen reservoir, but has no electric dipole

moment (Herbst *et al.* 1977). The major formation route for CO_2 is a neutral-neutral reaction, CO + OH, which is endothermic and hence only effective in shocks or high temperature regions. Another possible pathway for the formation of CO_2 is grain surface reactions. We present our observational results towards many Galactic molecular clouds in Chapters 7 and 8, and discuss chemical implications.

1.3 Sources

Observations have been made towards dense molecular clouds, including cold, dark clouds, star-forming regions in the Galactic disk, and also the Galactic center. We have focused the obsevations on a few well known sources: TMC-1/L134N (Chapters 2, 5, and 6), Orion(KL) (Chapters 3 and 5), and the Galactic center clouds (Sgr B2 and Sgr A; Chapters 7 and 8), while we also include the results for an H_2S survey towards galactic star-forming regions (Chapter 4) and for the extensive search for $HOCO^+$ (Chapter 7).

The morphology and chemistry of TMC-1/L134N, Orion(KL), and Sgr B2 have been reviewed in detail by Irvine, Goldsmith, and Hjalmarson (1987).

1.3.1 TMC-1 and L134N

The cold, dark clouds TMC-1 and L134N are located at a distance ~ 150 pc and are well studied low mass molecular clouds which lack embedded high-luminosity sources. The kinetic temperature (~ 10 K) and density (~ 10^4 cm^{-3}) appear very similar for TMC-1 and L134N, but they have some interesting chemical differences. Carbon-rich species and CS and HCS^+ are more prominant in TMC-1 than in L134N, while some molecular species, including NH_3 and such relatively oxygen-rich molecules as SO, SO_2, and HCOOH, are more abundant in L134N (Irvine *et al.* 1987; Irvine, Good, and Schloerb 1983). It has been suggested that these variations may result from, for example, different initial elemental abundances or from differing cloud ages (Irvine, Goldsmith, and Hjalmarson 1987).

1.3.2 Orion(KL)

The Orion A molecular cloud (OMC-1), where massive star-formation is taking place, is located at a distance ~ 500 pc. Orion(KL), the central core of OMC-1, demonstrates a complex morphology and chemistry (e.g. Plambeck *et al.* 1982; Vogel *et al.* 1984; Blake *et al.* 1987). It contains at least four main components which have distinctive spatial and spectral distributions: the "extended ridge", the "plateau", the "hot core", and the "compact ridge". The extended ridge is a quiescent

component (T_{kin} ~ 50 - 60 K), which is, for example, easily visible in the CS and H_2CO emission, and the molecular processes are probably dominated by ion-molecule chemistry. The emission from the plateau component shows evidence of the energetic outflow driven by the highly luminous IRc 2. Sulfur and silicon containing species are prominent, and shock chemistry dominates molecular processes in the plateau (T_{kin} ~ 100 - 200 K). The hot core is a massive clump which is probably a leftover from the formation of IRc 2, whose radiative heating probably induces kinetic temperatures of the hot core to be ~ 300 K. HCN, HDO, NH_3, and the heavily hydrogenated molecules CH_2CHCN and CH_3CH_2CN are very prominant, which suggests active gas-grain interactions and grain mantle evaporation. An additional recognizable component is the compact ridge (often referred to as the southern condensation; T_{kin} ~ 100 - 150 K) in which large, oxygen-rich molecules are prominent. The compact ridge represents an area where outflow from IRc 2 is thought to be interacting with the quiescent ambient material.

1.3.3 Galactic center clouds

The Sgr B2 molecular cloud is located at a distance ~ 120 - 300 pc from the Galactic center and represents an extreme case of high luminosity star-formation taking place in a very massive giant molecular cloud. A core of 5 - 10 pc diameter contains an extremely rich variety of molecular species. The OH and H_2O masers

are grouped into three condensations: north (N), middle (M), and south (S), each separated by approximately 45 arcseconds in declination. A study of a number of different species shows different distributions; for example, SO strongly peaks at Sgr B2(M), while OCS does at Sgr B2(N) (Goldsmith *et al.* 1987). Because of the large distance and the activities of the Galactic center, however, it is very difficult to disentangle the effects of abundance variations and excitation differences.

The Sgr A molecular complex, situated ~ 100 - 200 pc from the Galactic center, is composed of several condensations of masses greater than 10^5 $M_\odot$, which appear to be related, but the geometry and dynamics are still controversal (Brown and Liszt 1984). The molecular abundances and chemistry of the Sgr A region, however, have not been as well characterized as those of Sgr B2. The total column density toward Sgr A is about a factor of 10 less than that of Sgr B2.

CHAPTER 2

DETECTION OF INTERSTELLAR HYDROGEN SULFIDE IN COLD, DARK CLOUDS

2.1 Summary

We have detected interstellar hydrogen sulfide (H_2S) towards the cold, dark clouds L134N and TMC-1. We derive total column densities of ~ 2.6 x 10^{13} cm^{-2} and ~ 7.0 x 10^{12} cm^{-2} at the SO peak of L134N and at the NH_3 peak of TMC-1, respectively. Since the expected gas phase reactions leading to the formation of H_2S are thought to be endothermic, grain surface reactions may play a major role in the synthesis of this species in cold, dark clouds. If the carbon abundance is high and grain surface reactions are the dominant formation route, H_2CS would be expected to form instead of H_2S, and the abundances of H_2CS have been observed to be high where those of H_2S are low in L134N and TMC-1.

2.2 Introduction

Gas phase ion-molecule reactions have not been very successful in explaining the observed abundances of sulfur-bearing molecules in the interstellar medium, because the initiating reactions of S^+ or S with H_2 are both endothermic (Watson and Walmsley 1982; Smith and Adams 1985). Some species, such as H_2S, SO, and SO_2, are observed

to be overabundant in massive-star-forming regions relative to predictions, an effect which has been ascribed to the widespread occurrence of shocks or other high temperature processes (Hartquist, Oppenheimer, and Dalgarno 1980; Prasad *et al.* 1987). In addition, high abuodances of sulfur-bearing molecules such as HCS^+, H_2CS, C_2S, and C_3S have been reported in cold, dark clouds (Irvine, Good, and Schloerb 1983; Irvine *et al.* 1989; Saito *et al.* 1987; Yamamoto *et al.* 1987), where high temperature reactions should not be important. In fact, the C_2S and C_3S abundances in TMC-1 are vastly greater than those of the oxygen analogs C_2O and C_3O, showing that there are considerable differences between oxygen and sulfur chemistry in cold clouds. Unlike oxygen chemistry, which is thought to be dominated by gas-phase reactions, sulfur chemistry may be dominated by grain surface reactions (e.g. Millar 1982), at least for chemically reduced species. For example, sulfur is expected to react with atomic hydrogen on grain surfaces easily and thereby form the volatile hydride H_2S (Tielens and Alamandola 1987).

H_2S was first observed in the ISM via the lowest frequency (1_{10} - 1_{01}) transition by Thaddeus *et al.* (1972), who obtained column densities ~ 10^{14} cm^{-2} toward several GMC's. The 2_{20} - 2_{11} transition at 217 GHz was detected during the OVRO spectral survey of Orion A (Sutton *et al.* 1985), but, to our knowledge, there have been no other published observations of H_2S in the ISM, at least in part because of the lack of receivers to study the 2 mm region. Using a new FCRAO receiver (Ziurys, Erickson, and Grosslein 1988) to

observe the 1_{10} - 1_{01} transition which occurs near 169 GHz, we have made a survey of H_2S toward many well known star-forming regions and cold, dark clouds. The results for active star-forming regions will be published elsewhere (Minh *et al.* 1989). In this Chapter, we report the first detection of H_2S in cold, dark clouds, and comment on the implications for chemical models.

2.3 Observations

Observations of the lowest frequency transition of H_2S (1_{10} - 1_{01} at ν_o = 168.762762373 GHz; Cupp, Kempf, and Gallagher 1968) were made using the FCRAO 14 m telescope between 1989 January and March. The receiver employed a cooled Schottky diode mixer, which gave total system temperatures, corrected to outside the atmosphere, of 700 - 1000 K. Data were taken by position switching 20 arcminutes in azimuth, and spectra were obtained using a 256-channel filter bank with 100 kHz resolution. The FWHM beamwidth at 169 GHz is 35 arcsec and the antenna main beam efficiency η_B = 0.25. The temperature scale is given as T_A^*, the beam-chopper-corrected antenna temperature. We then approximate the radiation temperature T_R by the main beam brightness temperature $T_{MB} = T_A^*/\eta_B$.

2.4 Results

The observed line parameters are given in Table 2.1, and spectra observed towards L134N and TMC-1 are shown in Figures 2.1a and b, respectively.

H_2S is an asymmetric top, which, because of its two hydrogen spins, possesses both ortho and para species. The $1_{10} - 1_{01}$ transition is the lowest line in the ortho ladder (e.g. see Thaddeus *et al.* 1972, for an energy level diagram). Therefore, to derive the H_2S abundance, the column density was calculated for the ortho levels only, and then extrapolated to a total column density assuming an ortho-to-para ratio. To estimate the ortho species population, the column density in the upper level of the $1_{10} - 1_{01}$ transition was calculated under the optically thin assumption and considering the effect of cosmic background radiation, using the following formula (cf. Irvine, Goldsmith, and Hjalmarson 1987):

$$N_u = \frac{1.94 \times 10^3 \, \nu^2 \, [\mathrm{GHz}] \int T_R dV \, [\mathrm{K\ km\ s^{-1}}]}{A \, [\mathrm{s^{-1}}] \, [1 - J_\nu(T_{bg})/J_\nu(T_{ex})]}$$

In this expression $J_\nu(T) = (h\nu/k)[\exp(h\nu/kT)-1]^{-1}$, A is the Einstein A-coefficient, which for the H_2S $1_{10} - 1_{01}$ transition equals 2.65×10^{-5} s^{-1}, and ν is the frequency of the transition, while T_{bg} is the 2.7 K cosmic background temperature and T_{ex} the excitation temperature of the line involved. Although the H_2S emission was

TABLE 2.1

Summary of Hydrogen Sulfide Observations

Source	T_A^* (K)	V_{LSR} (km s^{-1})	ΔV (km s^{-1})	$\int T_A^* dV$ (K km s^{-1})	N_{tot} (cm^{-2})
L134N	0.13±.03[a]	2.16	0.71	0.09	7.8(12)[c]
L134N(SO)	0.40±.07[a]	2.33	0.74	0.30	2.6(13)
L134N(0,-2)	≤ 0.15[b]	—	—	—	≤ 9.5(12)[d]
L134N(-2.3,2)	≤ 0.21[b]	—	—	—	≤ 1.3(13)[d]
TMC-1	≤ 0.09[b]	—	—	—	≤ 4.7(12)[e]
TMC-1(NH_3)	0.17±.03[a]	5.73	0.50	0.08	7.0(12)

[a] 1 σ uncertainty.

[b] 3 σ upper limit.

[c] A(B) signifies A x 10^B.

[d] ΔV = 0.7 km s^{-1} was assumed.

[e] ΔV = 0.5 km s^{-1} was assumed.

Positions: L134N: RA(1950)= $15^h51^m30^s.0$, Dec(1950)= $-2°43'31''$; L134N(SO): RA(1950)= $15^h51^m26^s.0$, Dec(1950)= $-2°43'31''$; L134N(0,-2): RA(1950)= $15^h51^m22^s.0$, Dec(1950)= $-2°43'31''$; L134N(-2.3,2): RA(1950)= $15^h51^m20^s.8$, Dec(1950)= $-2°41'31''$; TMC-1: RA(1950)= $4^h38^m38^s.6$, Dec(1950)= $25°35'45''$; TMC-1(NH_3): RA(1950)= $4^h38^m22^s.0$, Dec(1950)= $25°41'45''$.

Figure 2.1a - b Spectra of the $1_{10} - 1_{01}$ transition of H_2S taken with the FCRAO 14 m telescope at 100 kHz resolution toward the positions given in Table 2.1 for the dark clouds (a) L134N and (b) TMC-1.

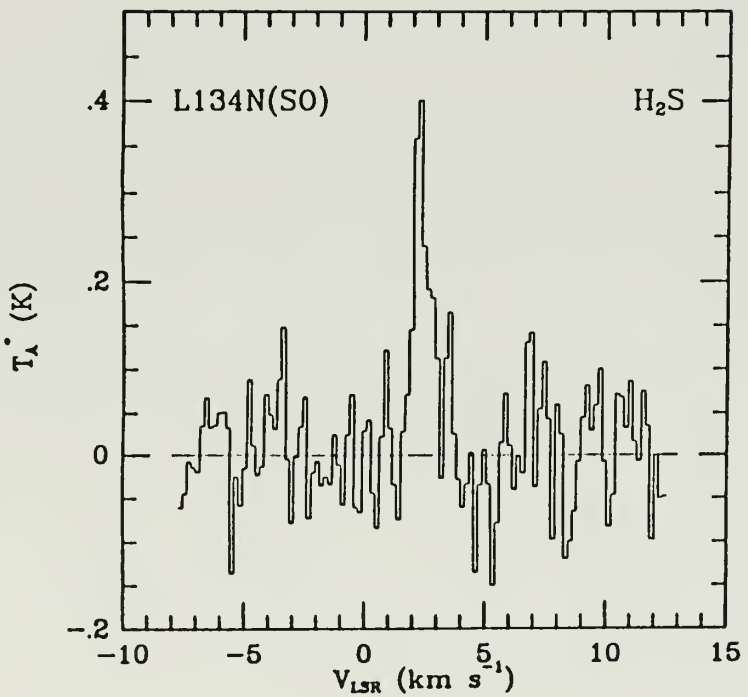
L134N(SO)
H_2S
.4
.2
0
−.2
T_A^* (K)
−10
−5
0
5
10
15
V_{LSR} (km s^{-1})

(a)

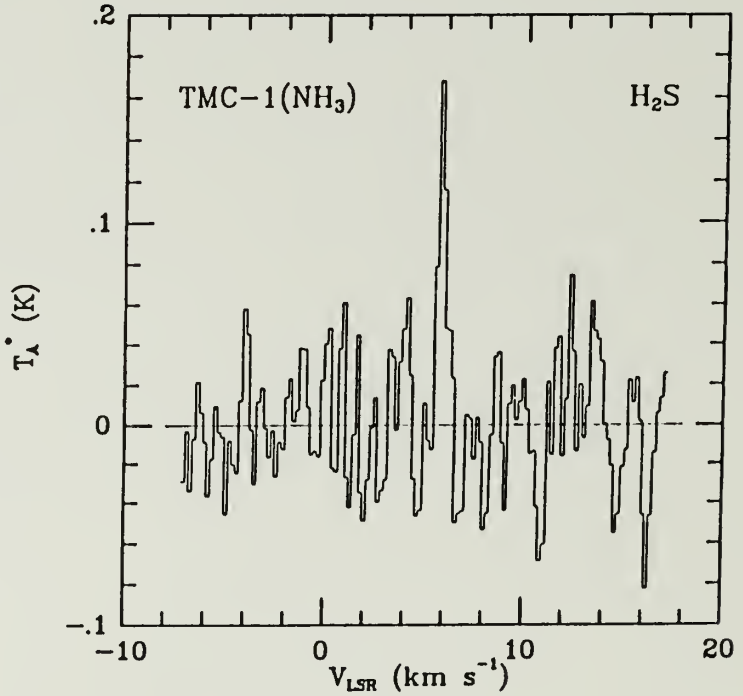
TMC−1(NH_3)
H_2S
.2
.1
0
−.1
T_A^* (K)
−10
0
10
20
V_{LSR} (km s^{-1})

(b)

observed to vary in intensity on an angular scale of an arcmin, it was at least somewhat extended relative to our 35" beam, making the use of $T_R \approx T_{MB}$ appropriate.

The total ortho column density was then derived from N_u by summing over the partition function, assuming a rotational temperature of $T_{rot} = T_{ex} = 5$ K for L134N and TMC-1. Excitation temperatures of about 5 K have been found by Swade (1987) in L134N for several molecules whose fundamental transitions have A-coefficients similar to that for the $1_{10} - 1_{01}$ H_2S line. The partition function for the ortho states was calculated by an explicit summation, using the energy levels given by Helminger, De Lucia, and Kirchoff (1973). As it turns out, for a rotational temperature of 5 K almost all the population for ortho-H_2S is contained in the lowest two levels; i.e., 1_{10} and 1_{01}.

Using this assumptions, a column density of ~ 2 x 10^{13} cm^{-2} was derived for the ortho species of H_2S at the SO peak position in L134N, which implies a total column density for H_2S of N_{tot} ~ 2.6 x 10^{13} cm^{-2}, assuming an ortho-to-para ratio 3 : 1 (see the last column of Table 2.1 for N_{tot} at other observed positions). The ortho-to-para ratio, however, is uncertain. For example, a value of 2 : 1 was found for this ratio for formaldehyde in dark clouds by Kahane *et al.* (1984), who ascribe this deviation from a ratio of 3 : 1 to ortho/para equilibration on grains at a temperature ~ 10 K.

Even if the ratio were as low as 1 : 1 for H_2S, the total column density given here would be underestimated by less than a factor of 2.

A column density of ~ 2.6×10^{13} cm^{-2} for H_2S translates into a fractional abundance of ~ 3×10^{-9} at the SO peak of L134N, assuming $N(H_2) \sim 8.2 \times 10^{21}$ cm^{-2} at the same position (Swade 1987; assuming $N(C^{18}O)/N(H_2) = 1.7 \times 10^{-7}$). For TMC-1 we find for the same assumptions $f(H_2S) < 5 \times 10^{-10}$ at the cyanopolyyne peak and $f \sim 7 \times 10^{-10}$ at the NH_3 maximum, taking $N(H_2) = 10^{22}$ cm^{-2} at both positions (Irvine *et al.* 1987; Friberg and Hjalmarson 1989).

2.5 Discussion

Our detections of hydrogen sulfide in cold, dark clouds are quite interesting, because the most significant gas phase reactions to produce H_2S are appreciably endothermic; consequently, the presence of H_2S has been regarded as an indicator of either shock chemistry or grain surface chemistry (Watson and Walmsley 1982; Smith and Adams 1985; Duley, Millar, and Williams 1980). Since there are no known embedded heating sources in the clouds observed, high temperature chemistry and shock chemistry are presumably unimportant in these regions.

The ion-molecule reactions related to hydrogen sulfide have not been well studied in the laboratory. The radiative association reaction between HS^+ and H_2 has been employed by chemical modelers

as a principal formation route in dense clouds (cf. Herbst, DeFrees, and Koch 1989), but the predicted H_2S abundance is less than that observed at the SO peak of L134N by a factor of 10 - 100 for the models which match the observed abundances of other species (Herbst and Leung 1986; Leung, Herbst, and Huebner 1984). However, given the lack of experimental data, particularly at temperatures ~ 10 K appropriate to dark clouds, ion-molecule reactions cannot be ruled out entirely as a source of H_2S. Other routes that lead to the production of H_2S, for example the reaction between S^+ and H_2CO (Prasad and Huntress 1982), should be studied further.

Nonetheless, grain surface reactions may be a more promising pathway to explain the observed H_2S abundance. It has been suggested that such reactions may greatly alter the abundances of gas phase molecules, especially for sulfur- and nitrogen-bearing species (e.g. Tielens and Allamandola 1987). If sulfur has been depleted onto grains in a dense region, ions like C^+ or H^+ are likely to find SH^- or S^- sites on the grain surfaces, which may lead to the formation of H_2CS or H_2S, respectively (Duley, Millar, and Williams 1980). H_2S has been identified tentatively in the grain mantles toward the compact radio source W33A (Geballe *et al.* 1986). H_2S is relatively volatile and might be easily desorbed in processes such as those described by Greenberg *et al.* (e.g. 1980).

Our failure to detect H_2S towards the cyanopolyyne peak of TMC-1 is of significant chemical interest in this regard. TMC-1 consists of an elongated series of condensations in Taurus; the

cyanopolyyne peak position has the highest column densities among dark clouds for many molecular species, including particularly many chemically unsaturated organic molecules such as the cyanopolyynes ($HC_{2n}CN$, n = 0, ..., 5), the hydrocarbon radicals C_nH (n = 1, ..., 6), the rings C_3H_2 and c-C_3H, and methylated carbon chains (e.g. Irvine *et al.* 1987; Guélin and Cernicharo 1989). In fact, TMC-1 has become a standard source for comparison of observational results with those of models of ion-molecule chemistry (*e.g.* Millar and Nejad 1985). Nontheless, it has been previously pointed out that some molecular species, including NH_3 and such relatively oxygen-rich molecules as SO, SO_2, and HCOOH, are more abundant in L134N than in TMC-1 (Irvine *et al.* 1987; Irvine, Good, and Schloerb 1983). It has been suggested that these variations might reflect differences in the gas phase carbon/oxygen ratio between these clouds. Compared to L134N, TMC-1 at the cyanopolyyne peak has a H_2CS abundance ~ 5 times larger than that found in L134N (Irvine *et al.* 1989) and a H_2S abundance at least ~ 4 times less (see Table 2.1). A higher carbon abundance in TMC-1 versus L134N may lead to the formation of H_2CS instead of H_2S, as well as to the abundant carbon-chain molecules in TMC-1. Indeed, observations of H_2CS in these two cold clouds indicate an anti-correlation between H_2S and H_2CS (Minh and Irvine 1989).

The question also arises as to whether the chemical differences between TMC-1 and L134N may be partly mirrored by chemical gradients *within* each of these clouds. A gradient in the NH_3/cyanopolyyne

abundance seems to be well established in TMC-1 (e.g. Olano, Walmsley, and Wilson 1988), where we detect H_2S only towards the NH_3 maximum. Swade (1987; 1989) has shown that the location of peak column density of SO and SO_2 in L134N differs from the position of maximum intensity for C_3H_2, HCO^+ and the cyanopolyynes, and has speculated that this may be a result of differential depletion of oxygen relative to carbon in the latter region. Such an effect could result from the differing volatility of H_2O and CH_4 (cf. Blake *et al.* 1987). Note that the fractional abundance of H_2S which we determine in L134N appears to correlate with SO and SO_2, rather that with *either* NH_3 or C_3H_2 and the cyanopolyynes. Clearly more data is needed on the relative distribution of these species in cold clouds.

CHAPTER 3

OBSERVATIONS OF H_2S TOWARDS OMC-1

3.1 Summary

Interstellar hydrogen sulfide (H_2S) and its isotopic variant ($H_2{}^{34}S$) have been observed toward several positions in OMC-1 via their $1_{10} - 1_{01}$ transitions near 168 GHz. We derive total column densities towards Orion(KL) of ~ 2×10^{14} cm^{-2} for the Orion extended ridge, ~ 10^{17} cm^{-2} for the plateau, and ~ 10^{18} cm^{-2} for the compact ridge, in addition to values for other positions in OMC-1. The fractional abundance of H_2S ~ 10^{-9} in the quiescent regions of OMC-1, as well as in cold dark clouds (Minh, Irvine, and Ziurys 1989), seems to be difficult to explain by currently known ion-molecule reactions. The fractional abundance of H_2S relative to H_2 is enhanced by a further factor of 1000 in the hot core and the plateau (to ~ 10^{-6}) relative to the quiescent clouds. We suggest that H_2S in the hot core may be evaporating from grain mantles, while H_2S in the plateau may result from either high-temperature gas phase chemistry or grain surface chemistry. From the non-detection of HDS in its $2_{11} - 2_{12}$ transition, we estimate the abundance ratio $[HDS]/[H_2S] \leq 5 \times 10^{-3}$ in the hot core by assuming the same excitation conditions and emission regions for both species.

3.2 Introduction

The abundances of most interstellar molecules can be reproduced via gas-phase ion-molecule reactions which usually have no activation energy barriers and are simple two body processes. Gas-phase ion-molecule reactions, however, have not been very successful in explaining the observed abundances of some sulfur-bearing molecules in the interstellar medium. Species such as SO and SO_2 appear to be unusually abundant in clouds where high mass star-formation is occuring, accompanied by shock waves and high temperatures. Such observations have led to the suggestion that "shock" or "high temperature" chemistry, i.e. chemistry involving gas-phase reactions with activation energies, may be taking place in hot regions and subsequently producing these species (e.g. Hartquist, Oppenheimer, and Dargarno 1980).

Along with elevated temperatures, shocks can also cause the partial or complete destruction of dust grains. Such grain destruction could also contribute to the formation of many of these so-called "high temperature" molecules, since they often contain refractory elements. Also, the UV radiation field from the newly formed massive stars can evaporate grain mantles and consequently release molecules into the gas phase. It is, however, often very difficult to differentiate between gas-phase reactions and grain related processes in the formation of interstellar molecules in shocked regions.

Interstellar hydrogen sulfide (H_2S) has been suggested as a tracer of high-temperature chemistry and/or grain surface chemistry because crucial gas phase reactions leading to the formation of H_2S are thought to be appreciably endothermic (Watson and Walmsley 1982; Smith and Adams 1985; Duley, Millar, and Williams 1980). H_2S was first observed in the ISM via the lowest frequency ortho transition (1_{10} - 1_{01}) by Thaddeus *et al.* (1972), who obtained column densities ~ 10^{14} cm^{-2} toward several GMC's. This transition has recently been detected towards the cold, dark clouds L134N and TMC-1 as well (Minh, Irvine, and Ziurys 1989; Paper 1), where high temperature processes should not be important. Although ion-molecule reactions cannot be ruled out entirely as a source of H_2S, grain surface reactions may be a more promising pathway to explain the observed abundance in cold, dark clouds (Paper 1). H_2S has also been identified tentatively in the grain mantles toward the compact radio source W33A (Geballe *et al.* 1986).

The Orion A molecular cloud (OMC-1), where massive star-formation is taking place, is about 500 pc from the sun, and is one of the most extensively studied sources in the sky. The central core, known as Orion(KL), demonstrates a complex morphology (e.g. Plambeck *et al.* 1982; Vogel *et al.* 1984) and chemistry (e.g. Blake *et al.* 1987). It contains at least three main components which have distinctive spatial and spectral distributions: the "extended ridge", the "hot core", and the "plateau". Their characteristic features have been reviewed in detail by Irvine, Goldsmith, and

Hjalmarson (1987) and Prasad *et al.* (1987). Since regions characterized by outflows and elevated temperatures and also extended cooler, quiescent material are present, Orion(KL) serves as an important test object for grain and shock chemistry as well as for low temperature ion-molecule synthesis. We report here observations of the $1_{10} - 1_{01}$ transition of interstellar hydrogen sulfide (H_2S) and its isotopes towards OMC-1 and comment on the implications for chemical models. Data towards several other star-forming regions for H_2S will be published elsewhere (Minh *et al.* 1989; see also § 4).

3.3 Observations

Observations of H_2S and its isotopic species $H_2{}^{34}S$ and HDS (see transitions and rest frequencies in Table 3.1) were made using the FCRAO 14 m telescope between 1989 January and April. Telescope parameters are also included in Table 3.1. The FCRAO 2 mm receiver (Ziurys, Erickson, and Grosslein 1988) gave total system temperatures, corrected for atmospheric attenuation, of 700 - 1000 K. Data were taken by position switching 30 arcminutes in azimuth, and spectra were obtained using 256-channel filter banks with 250 kHz and 1 MHz resolutions. The temperature scale is given as T_A^*, the beam-chopper-corrected antenna temperature. For calculating column densities, we use the main beam brightness temperature $T_{MB} = T_A^*/\eta_B$.

TABLE 3.1

Line Frequencies and FCRAO Telescope Parameters

Molecule	Transition	Rest Frequency[a] (MHz)	FWHP (arcsec)	η_B
$H_2{}^{32}S$	$1_{10} - 1_{01}$	168762.76237	35	0.25
$H_2{}^{34}S$	$1_{10} - 1_{01}$	167910.516	35	0.25
HDS	$2_{11} - 2_{12}$	153179.160	39	0.30

[a] From Helminger, De Lucia, and Kirchhoff (1973).

3.4 Results

3.4.1 Spectra

The $1_{10} - 1_{01}$ transitions of H_2S and $H_2{}^{34}S$ have been observed towards several selected positions in OMC-1, and the observed line parameters are given in Tables 3.2 and 3.3 for H_2S and $H_2{}^{34}S$, respectively.

The spectra obtained toward the KL position show evidence for three sub-regions, the extended ridge, the plateau, and the hot core. The H_2S spectrum (Figure 3.1) has a "spike" feature at V_{LSR} ~ 9.5 km s^{-1} with FWHP ~ 3.7 km s^{-1}, which agrees quite well with other molecular observations for the extended ridge (Blake *et al.* 1987; Johansson *et al.* 1984). There is no apparent counterpart in the $H_2{}^{34}S$ spectrum, which may indicate that this component is not optically thick. Another ridge component, the compact ridge, has a slightly lower velocity $V_{LSR} \approx 7 - 8$ km s^{-1} and is characterized by a number of large, oxygen-rich species (cf. Irvine, Goldsmith, and Hjalmarson 1987); we find no specific evidence for compact ridge emission in our spectra, and we ignore this component in the analysis. The emission from the plateau is quite visible in the H_2S spectrum, extending from V_{LSR} ~ - 20 to 40 km s^{-1} as shown in Figure 3.1. We regard this component as the "lower velocity" plateau, which is a rather massive disk-like clump in which many molecules have been observed, including sulfur-containing species

TABLE 3.2

Summary of H_2S Observations

Position	T_A^* (K)	V_{LSR} (km s^{-1})	FWHP (km s^{-1})	$\int T_A^* dV$ (K km s^{-1})	N_{column}[a] (x10^{14} cm^{-2})
KL[b] Ridge	1.47	9.5	3.7	5.8	2
KL[b] Hot Core ..	0.39	5.7	12.0	5.0	9000[c] (20000)[d]
KL[b] Plateau ...	1.06	8.0	32.9	37.1	800[c] (3000)[d]
Offset ($\Delta\alpha$,$\Delta\delta$) from KL					
(-0.6,-1.6)(≡ 1.5S)	1.99	7.4	4.8	9.5	5[c] (2)[d]
(1, 3)(≡ 3N1E) ..	1.12	9.8	2.0	2.2	0.1[c] (0.7)[d]
(0 , 1)	1.54	10.0	3.9	6.0	2
(-0.3,-0.8)	2.01	8.7	3.8	7.6	3
(-0.8,-2.4)	1.41	9.1	2.7	3.9	1
(-1, 0)	1.15	8.6	3.3	3.8	1
(-2, 0)	≤ 0.60[e]	—	—	—	≤ 0.5[f]
(1 , 0)	1.06	9.7	5.4	5.7	2
(2 , 0)	≤ 0.53[e]	—	—	—	≤ 0.4[f]
(3 , 0)	0.72	10.2	2.7	1.9	0.7
(4 , 0)	≤ 0.32[e]	—	—	—	≤ 0.3[f]

NOTE. - Spectral resolution is 250 kHz.

Position of KL: RA(1950)= $5^h32^m47^s.0$, Dec(1950)= $-5^\circ24'23''$.

(Continued on next page)

TABLE 3.2

(Continued)

[a] Optically thin emission and T_{ROT} = 30 K have been assumed unless otherwise indicated.

[b] From a gaussian fit by assuming V_{LSR}(Hot Core) = 8.0 km s^{-1} and FWHP (Hot Core) = 12.0 km s^{-1}, and V_{LSR}(Plateau) = 5.7 km s^{-1}.

[c] Using $\tau(H_2S)$ and T_{ROT} from Table 3.5.

[d] Using $\int T_A^*(H_2{}^{34}S)dV$ from Table 3.3, and T_{ROT} and the source size from Table 3.5, assuming $\tau(H_2{}^{34}S) \ll 1$, $S/{}^{34}S = 15$.

[e] 3 σ upper limit.

[f] 3 σ upper limit and FWHP = 2 km s^{-1} were used.

TABLE 3.3

Summary of $H_2{}^{34}S$ Observations[a]

Position	T_A^* (K)	V_{LSR} (km s^{-1})	FWHP (km s^{-1})	$\int T_A^* dV$ (K km s^{-1})
KL[b] Ridge	—	—	—	—
KL[b] Hot Core	0.30	5.7	12.0	3.8
KL[b] Plateau	0.22	8.0	33.2	7.8
1.5S	0.15	6.6	4.3	0.7
3N1E	0.09	9.6	1.1	0.1

NOTE. - Positions in Table 3.2. Spectral resolution is 250 kHz.

[a] Line parameters derived from the gaussian fits.

[b] From a gaussian fit by assuming V_{LSR}(Hot Core) = 5.7 km s^{-1} and FWHP (Hot Core) = 12.0 km s^{-1}, and V_{LSR}(Plateau) = 8.0 km s^{-1}.

Figure 3.1 Spectra of the $1_{10} - 1_{01}$ transitions of H_2S and $H_2{}^{34}S$ taken towards Orion(KL) at a spectral resolution of 250 kHz (position given in Table 3.2). Dotted lines are gaussian fit results and line parameters are included in Tables 3.2 and 3.3.

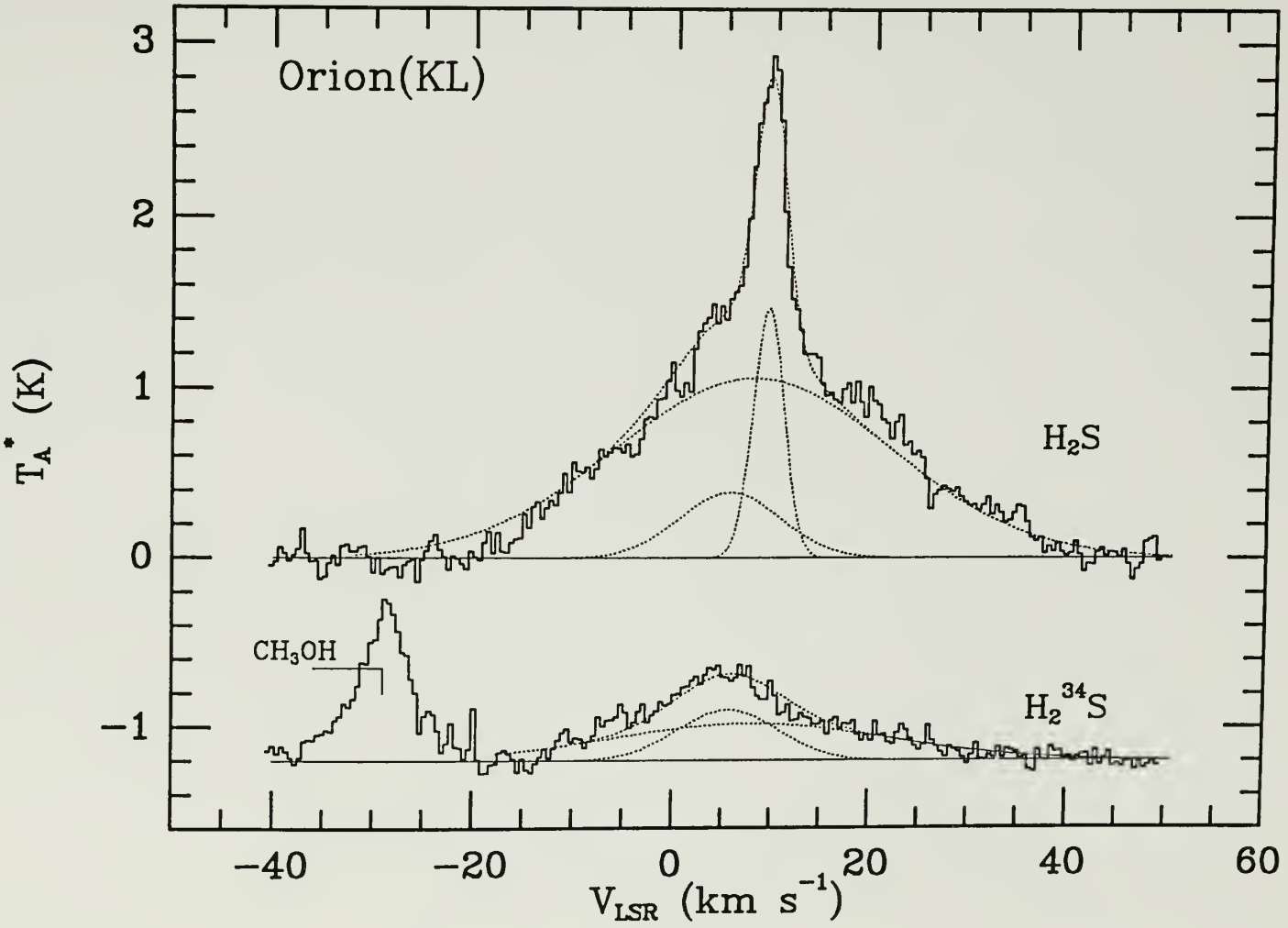
Orion(KL)
H_2S
CH_3OH
$H_2{}^{34}S$
T_A^* (K)
V_{LSR} (km s^{-1})
3
2
1
0
−1
−40
−20
0
20
40
60

and HDO. The hot core, which may be the most massive clump left over from the formation of IRc 2, is characterized by V_{LSR} ~ 5 km s^{-1} and ΔV ~ 5 - 10 km s^{-1} with large abundances of highly saturated molecules, such as H_2O and NH_3. The $H_2{}^{34}S$ spectrum in Figure 3.1 peaks at V_{LSR} ~ 6 km s^{-1}, which is close to the LSR velocity of the hot core. It therefore appears that H_2S is very prominent in the hot core and probably optically very thick in the H_2S spectrum.

In Figure 3.2, we have shown the spectra obtained towards the 1.5S and the 3N1E positions. At the 1.5S position, there is clear evidence for an outflow distinct from that associated with IRc 2 (Ziurys and Friberg 1987; Schmid-Burgk *et al.* 1989; Ziurys, Wilson, and Mauersberger 1989). The broad H_2S line (full width at zero power ~ 12 km s^{-1}) shows some evidence of this. The 3N1E position is a dense and quiescent region, toward which a number of radicals and ions show an emission peak (Turner and Thaddeus 1977; Harris *et al.* 1982).

The ^{34}SO 4_3 - 3_3 line and presumably the CH_3OH 9_1 - 9_0 E1 line have been detected in these observations towards KL and 1.5S. Line parameters for both these species are listed in Table 3.4. The LSR velocity of ~ 8 km s^{-1} of the CH_3OH 9_1 - 9_0 E1 line in KL agrees well with other methanol observations (Johansson *et al.* 1984; Blake *et al.* 1987) of compact ridge molecules. The methanol line is shown in Figure 3.1 together with the $H_2{}^{34}S$ spectrum.

Figure 3.2 Spectra of the $1_{10} - 1_{01}$ transitions of H_2S and $H_2{}^{34}S$ towards Orion 1.5S and 3N1E at a resolution of 250 kHz (positions given in Table 3.2).

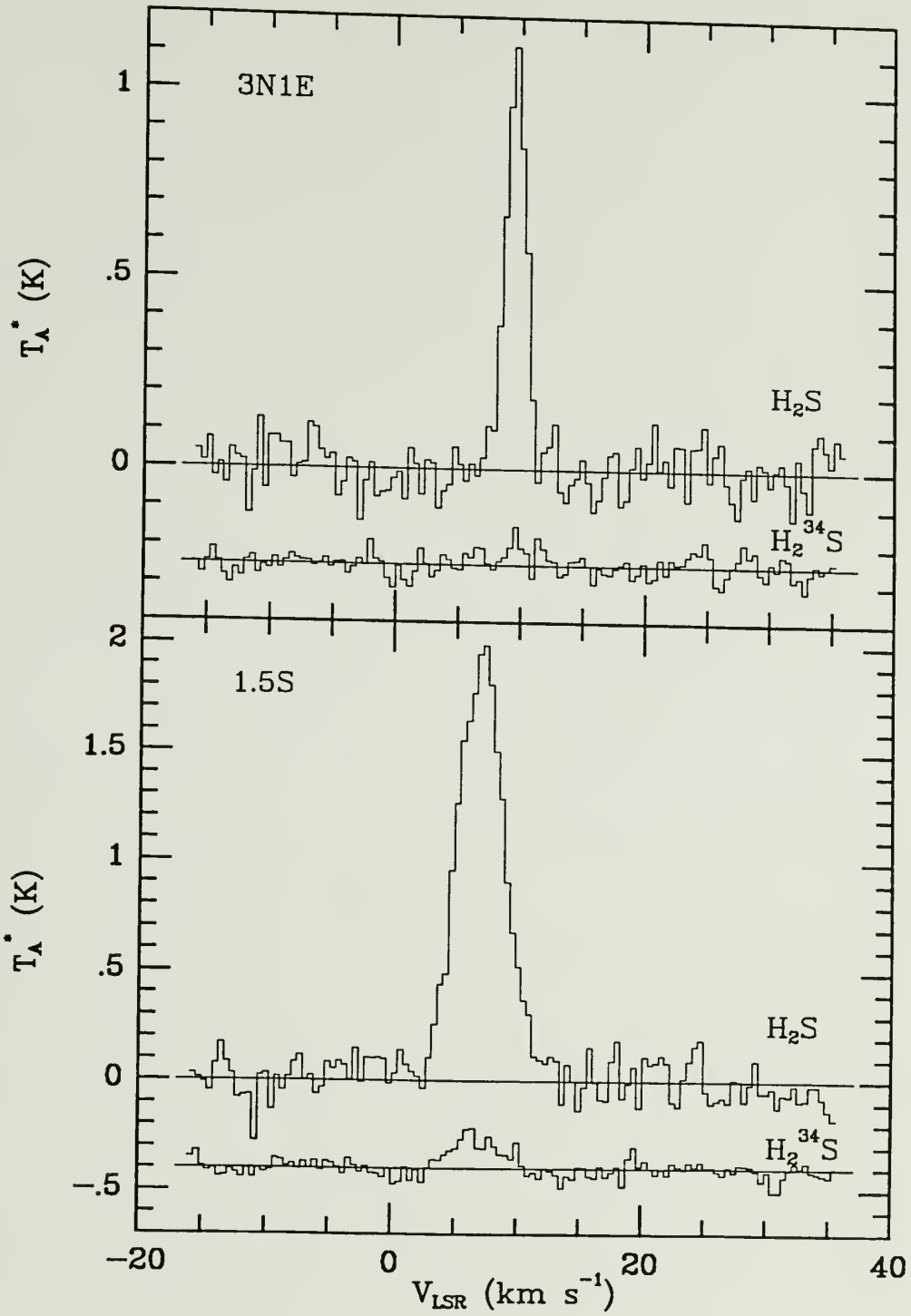
3N1E
1
.5
0
T_A^* (K)
H_2S
$H_2{}^{34}S$
2
1.5S
1.5
1
.5
0
-.5
T_A^* (K)
H_2S
$H_2{}^{34}S$
-20
0
20
40
V_{LSR} (km s^{-1})

TABLE 3.4

Line Parameters for ^{34}SO and CH_3OH

Position	T_A^* (K)	V_{peak} (km s^{-1})	FWHP (km s^{-1})	$\int T_A^* dV$ (K km s^{-1})
	^{34}SO 4_3 - 3_3 Transition			
KL	0.39	6.9	18.9	7.4
1.5S	0.10	3.3	3.9	0.4
	CH_3OH 9_1 - 9_0 E1 Transition			
KL	0.96	8.0	6.6	6.3
1.5S	0.10	8.9	3.8	0.4

NOTE. - Spectral resolutions are 1 MHz for ^{34}SO and 250 kHz for CH_3OH. Positions for KL and 1.5S are in Table 3.2.

Rest frequency: ^{34}SO 4_3 - 3_3 Transition:168.815101 (Hollis *et al.* 1981); CH_3OH 9_1 - 9_0 E1 Transition: 167.93113 (Lovas 1989).

3.4.2 H_2S Abundances

H_2S abundances for each sub-region in KL have been derived by gaussian fitting the spectra. As discussed above, the extended ridge is apparent as a "spike" in the H_2S spectrum, while it has no counterpart in the $H_2{}^{34}S$ spectrum. This suggest that the H_2S emission of the extended ridge is optically thin. A gaussian fit is straightforward for the "spike" in the H_2S spectrum, and we derive an H_2S total column density $N_{tot}(H_2S) \sim 2 \times 10^{14}$ cm^{-2} by assuming an ortho to para ratio of 3 and evaluating the partition function for $T_{rot} \sim 20 - 50$ K (Johansson *et al.* 1984; Blake *et al.* 1987). This corresponds to a fractional abundance of H_2S relative to H_2 of $f(H_2S) \sim 10^{-9}$, taking $N(H_2) \sim 1 - 3 \times 10^{23}$ cm^{-2} for the extended ridge (Blake *et al.* 1987).

Because of the asymmetry of the spectra shown in Figure 3.1, it is difficult to fit to unique components for the plateau and the hot core. So we have set the center velocities for the plateau and the hot core and the line width for the hot core, on the basis of results for other molecules (Johansson *et al.* 1984; Blake *et al.* 1987). Fit results are shown in dotted lines in Figure 3.1, and line parameters are included in Tables 3.2 and 3.3. The emission, of course, does not need to be gaussian, especially for the plateau, but the observed line profiles for both H_2S and $H_2{}^{34}S$ are matched quite well by this procedure. In addition, since the $H_2{}^{34}S$ emission may be assumed to be optically thin and the hot core

component is very apparent in the $H_2{}^{34}S$ spectrum, we can derive reasonable column densities for the hot core and the plateau from the $H_2{}^{34}S$ spectrum (the assumptions are included in the Notes to Tables 3.2 and 3.3; cf. the equation in Irvine, Goldsmith, and Hjalmarson 1987). When we compare column densities so derived for the 1_{10} state to those found from the optical depths obtained comparing the gaussian fit antenna temperatures of the H_2S and $H_2{}^{34}S$ spectra, both results agree well within a factor of a few by assuming the isotopic ratio of $S/^{34}S \sim 15 - 22$ (Schloerb *et al.* 1983).

The Einstein *A* coefficient for the $1_{10} - 1_{01}$ transition for both main and isotope lines was taken to be 2.25×10^{-5} s^{-1} (Thaddeus *et al.* 1972). Thus the $1_{10} - 1_{01}$ line becomes thermalized at densities $\geq 5 \times 10^5$ cm^{-3}. Although such densities probably do not exist over the extended OMC-1 region, they are most likely present towards the KL, 3N1E, and 1.5'S positions. The fraction of the population in the 1_{10} level was evaluated by summing over the partition function for the rotational temperatures indicated in Table 3.2. The resulting total column densities are included in Table 3.2. We derive $N_{tot}(H_2S) \sim 10^{17}$ cm^{-2} and $\sim 10^{18}$ cm^{-2} for the plateau and the hot core, respectively, which corresponds to $f(H_2S) \sim 10^{-6}$ for both components, for $N(H_2) \sim 10^{23}$ cm^{-2} for the plateau and $\sim 10^{24}$ cm^{-2} for the hot core (Blake *et al.* 1987).

The column densities for the 1_{10} state at the 1.5S and 3N1E positions have been derived from the optical depths (Table 3.5) obtained from comparing the H_2S and $H_2{}^{34}S$ spectra, and then total column densities are then given by assuming Boltzmann population distributions at $T_{rot} \sim 75$ K and 15 - 30 K for 1.5S and 3N1E, respectively (cf. Goldsmith *et al.* 1986). Since the 1_{10} energy level of H_2S is about 28 K above the ground state, total column densities are not very sensitive to T_{rot} for values in the range 10 - 50 K. As towards KL, similar values of N_{tot} are obtained from the $H_2{}^{34}S$ spectra alone, on the assumptions of optically thin emission and $S/^{34}S \approx 15$. We find $N_{tot}(H_2S) \sim 4 \times 10^{14}$ cm^{-2} and $\sim 4 \times 10^{13}$ cm^{-2} at 1.5S and 3N1E. For the other positions listed in Table 3.2, we assumed optically thin emission and $T_{rot} \sim 30$ K. We derive $N_{tot}(H_2S) \sim 10^{13} - 10^{14}$ cm^{-2} (included in the last column of the Table 3.2). Optical depths may be greater than one at such locations, which would mean that we underestimate the total column densities in some regions. For example, if $\tau(H_2S) \sim 2$, then the total column density is underestimated by a factor of 2 - 3. The fractional abundances at all the positions are on the order of 10^{-9} for total hydrogen column densities $\sim 0.5 - 5 \times 10^{23}$ cm^{-2} (Table 3.5; Smith *et al.* 1979; Batrla *et al.* 1983).

As a check on our assumptions, we used our derived opacities for the hot core and plateau sources, combined with our measured antenna temperatures and assumed excitation temperatures, to estimate sizes of these regions. The results of these calculations

TABLE 3.5

Abundances of H_2S in OMC-1

Component	T_{rot} [a] (K)	Estimated Source Size [b] (arcsec)	$N(H_2)$ [a,c] (cm^{-2})	$\tau(H_2S)$ [d]	$N(H_2S)$ [c] (cm^{-2})	f [e]
Extended Ridge	30	extended	1-3(23)	< 1	2(14)	1(-9)
Hot Core	200	~ 3	1(24)	23	1(18)	1(-6)
Plateau	100	~ 7	1(23)	3	1(17)	1(-6)
1.5S	75	~ 24	5(23)	0.3	4(14)	1(-9)
3N1E	15-30	extended	7(22)	0.4	4(13)	6(-10)

Numbers in parenthesis are powers of 10.

[a] From Blake *et al.* (1987), Batrla *et al.* (1983), and Goldsmith *et al.* (1986).

[b] Using the equation: $T_R = (T_{ex} - 2.7)(1 - e^{-\tau})(D/HPBW)^2$, where D is the source diameter.

[c] Column density corrected for source size.

[d] Optical depth in the line center, from ratio of H_2S and $H_2{}^{34}S$ data, assuming $S/{}^{34}S = 15$.

[e] Fractional abundance of H_2S relative to H_2.

are given in Table 3.5. As shown in the table, we obtained a source diameter $\theta_s \sim 3"$ for the hot core, and $\theta_s \sim 7"$ for the plateau. Both of these values are less than those derived from other measurements by a factor of ~ 2 (e.g. Plambeck *et al.* 1982; Genzel *et al.* 1982). This disagreement may result from uncertainties in gaussian fit values and estimations of the excitation temperatures, although it is possible that the H_2S emission is more confined than that of some other species. For the 1.5S position, we obtain $\theta_s \sim 24"$, the same value for the outflow as estimated from SiO observations (Ziurys, Wilson, and Mauersberger 1989). Optical depths and abundances for H_2S are summarized in Table 3.5.

We have also made a search for deutrated H_2S (HDS) at the KL postion, but this species has not been detected to a 1 σ level of 33 mK at 250 kHz resolution. Since H_2S seems to be most prominent in the hot core, as we see in the $H_2{}^{34}S$ spectrum in Figure 3.1, we used an excitation temperature ~ 200 K and a source size ~ 3" for the hot core (Table 3.5) to derive an HDS column density. We derive an upper limit $N_{tot}(HDS) \leq 10^{15}$ cm^{-2} in the hot core. Then we estimate the abundance ratio of [HDS]/[H_2S] to be less than ~ 5 x 10^{-4} (see Table 3.2).

3.5 Discussion

Recent ion-molecule chemical models employ the radiative association reaction between SH^+ and H_2 as a principal formation route for the ion H_3S^+ in dense clouds, which is the assumed precursor to H_2S. The predicted abundance of H_2S, therefore, depends on the rate coefficient of the radiative association reaction. Leung, Herbst, and Huebner (1984), following the work of Prasad and Huntress (1982), predicted a fractional abundance of $\sim 10^{-10}$ in quiescent clouds by using a large value of the rate coefficient. Herbst, DeFrees, and Koch (1989) have recalculated the rate coefficient to be about a factor of 2 less than that used by Leung, Herbst, and Huebner (1984). In the quiescent clouds in Orion A, including the extended ridge, our observed fractional abundance is $f(H_2S) \sim 10^{-9}$, which is similar to the value in the cold dark cloud L134N (Paper 1). Thus, the H_2S abundance predicted by standard ion-molecule models is about an order of magnitude less than the observed value. In constrast, Charnley *et al.* (1988) in their dynamical cloud model produce H_2S via the reaction $S^+ + H_2CO \rightarrow H_2S^+ + CO$, followed by $H_2S^+ + e^- \rightarrow H_2S + h\nu$. In this model, the cloud chemistry gets cycled via a collapse/star-formation/expansion sequence. In their slow cycle model, they produce $f(H_2S) \sim 10^{-9}$ in the cloud collapse phase - in good agreement with cold cloud observations. However, as with the other reaction sequence leading

to H_2S, the rates of the reactions used by Charnley *et al.* (1988) are not well known.

It is consequently difficult to establish whether ion-molecule chemistry can produce sufficient H_2S. Given certain assumptions about key rate coefficients, it appears that ion-molecule models can produce $f(H_2S) \sim 10^{-9} - 10^{-10}$, i.e., the values measured for the ambient gas in Orion and for the dark clouds L134N and TMC-1 as well (Minh, Irvine, and Ziurys 1989). However, until such key rate coefficients are determined accurately by experimental methods, the success of ion-molecule synthesis of H_2S remains an open question.

Other processes such as high-temperature chemistry or grain surface chemistry may be important in the Orion hot core and plateau, where the H_2S fractional abundances $f(H_2S) \sim 10^{-6}$ (see Table 3.5). Under high-temperature conditions, the endothermicities or the activation energies can be overcome. Smith and Adams (1985) have suggested that even for moderate increases in the ion velocities relative to H_2 (as would occur in MHD shocks), endothermic reactions which lead to the formation of H_2S could be initiated: $S^+ + H_2$, $SH^+ + H_2$, and $H_2S^+ + H_2$. In MHD shocks, SH^+ is predicted to be formed in observable quantities (Millar *et al.* 1986; Pineau des Forets *et al.* 1986). H_2S can also be formed from atomic sulfur by hydrogen-abstraction reactions with H_2, which have barriers of substantially greater than 7000 K (Hartquist, Oppenheimer, and Dalgarno 1980). The high temperature chemistry models predict a large enhancement of the abundace of sulfur-

containing molecules, including H_2S (e.g. Hartquist, Oppenheimer, and Dargarno 1980; Mitchell 1984), after the passage of shocks, although the final abundances largely depend on the nature of the shock, poorly known reaction rates, and initial abundances.

Grain surface reactions have sometimes been suggested to play an important role in the formation of gas phase interstellar molecules, especially for sulfur- or nitrogen-containing species, although there are a number of serious uncertainties in the grain surface reaction schemes (cf. Prasad *et al.* 1987). One of the major questions is the desorption process, although this may be less of a problem in star-forming regions because of the intense UV field and the strong shock waves generated from the young stellar objects embedded in the cloud. Duley, Millar, and Williams (1980) have invoked grain surface reactions to synthesize H_2S. If sulfur has been depleted onto grain surfaces, ions like C^+ or H^+ are likely to find SH^- or S^- sites on the grain surfaces, which may lead to the formation of H_2CS or H_2S, respectively. Although this model contains many uncertainties and produces too much H_2S, it may be possible that in dense clouds, where sulfur is highly depleted, a variety of sulfur-containing molecules may be formed easily through reactions on the sulphuretted grains (see also Tielens and Alamandola 1987).

The hot core is probably a dense clump or set of clumps in the cavity surrounding IRc 2. The heating mechanism of the hot core is probably radiative (Goldsmith *et al.* 1983), which may warm up the

grains and induce the thermal evaporation of their icy mantles. The large H_2S abundance is consistent with release from the grain mantles directly, such as, for example, has been postulated for NH_3 and HDO, whose abundances are significuantly enhanced in the hot core (Sweitzer 1978; Plambeck and Wright 1987). Plambeck and Wright also suggest that any species released from the grain mantles will survive ~ 1 x 10^3 yrs before being destroyed by gas phase reactions, but this is comparable with the outflow age, and such species could still be overabundant. Therefore, we conclude that the high H_2S abundance $f(H_2S) \sim 10^{-6}$ in the hot core may result from grain mantle evaporation.

Unlike the large deuterium enhancements of the species such as $[HDO]/[H_2O]$ and $[NH_2D]/[NH_3]$ in the hot core (Plambeck and Wright 1987; Walmsley *et al.* 1987), we derive $[HDS]/[H_2S] \leq 5 \times 10^{-4}$. The large deuterium enhancements (as high as ~ 3 x 10^{-3} for $[NH_2D]/[NH_3]$) are thought to originate via deuterium fractionation in the gas-phase followed by freeze out onto grain mantles and subsequent evaporation. Grain surface chemistry may, however, also result in a high deuterium fractionation, mainly by the accretion of atomic deuterium in the gas phase (Tielens and Allamandola 1987; Brown and Millar 1989; Millar, Bennett, and Herbst 1989) Our non-detection of HDS may suggest that there are differences in the formation and fractionation of HDS/H_2S relative to the processes that are important for HDO/H_2O and NH_2D/NH_3.

The plateau emission comes from a violent region within KL which seems to be powered by IRc 2. Shock chemistry may be dominant in the plateau, and is thought to be responsible for the large abundances of SO, SO_2, and SiO. These species may be easily formed in the heated gas because of the enhancements of S, Si, and OH following grain disruption in the shocked region. The large abundance of the fragile molecule H_2CO in the plateau (Blake *et al.* 1987) strongly suggests that small dense condensations also exist in the outflow region, and the high abundance of HDO in the plateau probably suggests that grain surface chemistry may be still important in the plateau. Therefore H_2S may form either in the high-temperature shocked gas or on the grain surfaces in the plateau, and it is difficult to discriminate which chemistry actually plays the major role in producing the observed large abundance of H_2S, $f(H_2S) \sim 10^{-6}$. However, the small condensations in the plateau would contain grains similar to those in the hot core, and the evaporation of grain mantles by UV radiation or shocks would be expected to produce H_2S in the gas phase.

In summary, the H_2S abundances are enhanced by a factor of 1000 in the hot core and the plateau ($f(H_2S) \sim 10^{-6}$) relative to quiescent clouds. The large abundance of H_2S in the hot core may result from grain mantle evaporation, while the large abundance in the plateau could result from high-temperature gas phase chemistry and/or grain-surface chemistry. $f(H_2S) \sim 10^{-9}$ for the quiescent region of OMC-1, which is similar to the value for L134N (Paper 1),

which seems to be difficult to explain by currently known ion-molecule reactions, at least under static cloud conditions. Higher spatial resolution observations should be useful, especially in a region like Orion(KL).

CHAPTER 4

HYDROGEN SULFIDE IN STAR-FORMING REGIONS

4.1 Summary

Interstellar hydrogen sulfide (H_2S) and its isotopic variant $H_2{}^{34}S$ have been observed towards several star-forming regions via their $1_{10} - 1_{01}$ transitions. Where both H_2S and $H_2{}^{34}S$ were observed, the H_2S lines are typically optically thick and H_2S column densities ~ 10^{15} cm^{-2} are found. We set lower limits for the H_2S column densities of ~ 10^{14} cm^{-2} for other sources observed with only the H_2S line. The fractional abundances of H_2S relative to molecular hydrogen are in the range of 10^{-8} to 10^{-9}. H_2S has been searched for unsuccesfully only towards the supernova remnant IC443B, where we set an upper limit 6 x 10^{13} cm^{-2} for the H_2S total column density.

4.2 Introduction

Interstellar hydrogen sulfide (H_2S) was first observed in the ISM via its $1_{10} - 1_{01}$ transition towards several GMCs by Thaddeus *et al.* (1972). Recently, Minh, Irvine, and Ziurys (1989; Paper 1; cf. Chapter 2), and Minh *et al.* (1989; Paper 2; cf. Chapter 3) have observed this transition towards cold dark clouds and towards OMC-1,

and discussed the relative importance of grain-surface reactions, high-temperature shock chemistry, and ion-molecule reactions for the formation of H_2S. Indeed, it is very difficult to differentiate between gas- phase reactions and grain-related processes in the formation of interstellar molecules such as H_2S, although there are clearly large enhancements in the fractional abundance of H_2S in regions of massive star formations (by factors up to 10^3). Even in quiescent regions, the observed fractional abundances of $\sim 10^{-9}$ seems to be difficult to explain with currently known ion-molecule models. H_2S has been suggested as a tracer of high-temperature chemistry or grain surface chemistry because the expected gas phase reactions leading to the formation of H_2S are thought to be appreciably endothermic (Watson and Walmsley 1982; Smith and Adams 1985; Duley, Millar, and Williams 1980). H_2S has been identified tentatively in the grain mantles toward the compact radio source W33A (Geballe *et al.* 1986).

Sulfur-containing molecules appear to be fairly abundant in star formation regions, accompanied by shock waves and high temperatures. Such observations have lead to the postulation that "shock" or "high temperature" chemistry, i.e. chemistry involving gas-phase reactions with activation energies, may be taking place in hot regions and producing these species. Along with elevated temperatures shocks can also cause the partial or complete destruction of dust grains, which would return molecules in the grains to the gas-phase. Also, the UV radiation field from the

newly formed massive stars can evaporate grain mantles and consequently release volatile molecules into the gas phase. Although the strong UV field also can disscociate molecules released from the grain mantles, the high density of gas and dust grains may strongly inhibit such destruction and thus enhance these species in the gas component in star-forming regions.

H_2S abundances in the active regions of Orion(KL), which are enhanced by a factor of 1000 relative to those in quiescent clouds, strongly suggest that the increased H_2S production is related to activities in star formation regions, and possibly to grain-related processes. In this Chapter, we report the results of H_2S and $H_2{}^{34}S$ observations toward several other star forming regions.

4.3 Observations

Observations of the $1_{10} - 1_{01}$ transitions of H_2S and its isotope species $H_2{}^{34}S$ (rest frequencies: 168.76276237 GHz and 167.910516 GHz, respectively, Helminger, De Lucia, and Kirchhoff 1973) were made using the FCRAO 14 m telescope between 1989 January and April. The HPBW and the beam efficiency of the telescope are 35 arcseconds and 0.25 at these frequencies, respectively. The receiver and the observing method are described in § 3.3. The temperature scale is given as T_A^*, the beam-chopper-corrected antenna temperature. We approximate the brightness temperature by main beam brightness temperature $T_{MB} = T_A^*/\eta_B$.

4.4 Results

4.4.1 Sgr B2

The Sgr B2 molecular cloud, situated ~ 120 pc from the Galactic Center, represents a relatively extreme case in terms of mass and column density. A variety of different molecules has been observed in this core, probably because of the large column density and the existence of many different excitation conditions (cf. Irvine, Goldsmith, and Hjalmarson 1987). The H_2S and $H_2{}^{34}S$ spectra obtained at the center (M) and 1N positions are shown in Figure 4.1, and the observed line parameters at these locations and towards more quiescent gas at the position labeled 2N are given in Table 4.1. The H_2S spectra show two peaks at V_{LSR} ~ 50 km s^{-1} and ~ 80 km s^{-1}, which coincide with two peaks of strongly self-absorbed ^{13}CO J=2-1 (Lis 1989). The $H_2{}^{34}S$ spectra, however, may indicate that the H_2S emission in Sgr B2 is not self-absorbed, but traces two different components inside this molecular cloud. Based on the $H_2{}^{34}S$ spectra, we regard the H_2S emission as coming from two different regions, but higher spatial resolution observations would be useful to discriminate the velocity components in Sgr B2 unambiguously.

An estimate of the optical depth can be derived by comparing the antenna temperatures of the same transition of two isotopic variants such as H_2S and $H_2{}^{34}S$. We derive optical depths by assuming the cosmic value of the $S/^{34}S$ ratio ~ 22 and the

TABLE 4.1

H_2S and $H_2{}^{34}S$ Line Parameters Observed towards Sgr B2

Position	T_A^* (K)	V_{LSR} (km s^{-1})	ΔV (km s^{-1})	$\int T_A^* dV$ (K km s^{-1})
SgrB2(M)	0.36	50	10	3.6
	(0.14)	(51)	(13)	(1.9)
	0.18	76	18	3.3
SgrB2(N)	0.30	48	16	5.0
	(0.24)(?)	(56)	(3)	(0.9)
	0.17	84	22	3.9
SgrB2(2N)	0.23	52	7	1.5
	0.15	84	9	1.3

Numbers in parenthesis are for the $H_2{}^{34}S$ (1_{10} - 1_{01}) line.

Spectral resolution is 1 MHz.

Line parameters are derived from gaussian fit.

<u>Positions</u>: SgrB2(M): RA(1950) = $17^h44^m11^s.3$, Dec(1950) = $-28^\circ22'30''$; SgrB2(N): RA(1950) = $17^h44^m11^s.3$, Dec(1950) = $-28^\circ21'30''$; SgrB2(2N): RA(1950) = $17^h44^m11^s.3$, Dec(1950) = $-28^\circ20'30''$.

Figure 4.1 Spectra of the 1_{10} - 1_{01} transitions of H_2S and $H_2{}^{34}S$ taken towards Sgr B2(M) and (N) at a spectral resolution of 1 MHz (positions given in Table 4.1). The CH_3OH (9_1 - 9_0 E1) line is shown in the $H_2{}^{34}S$ spectra.

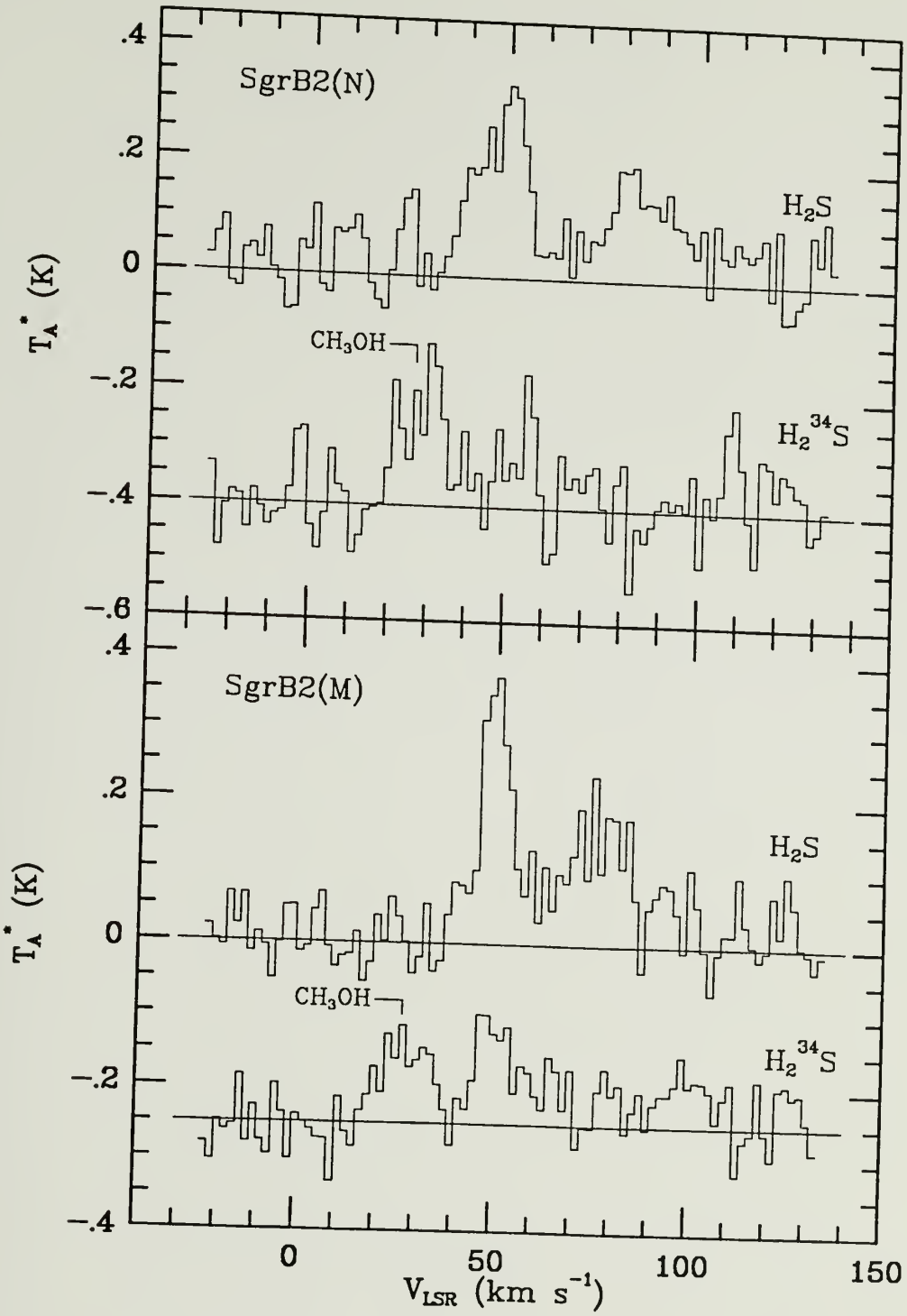
SgrB2(N)
H2S
CH3OH
H2 34S
SgrB2(M)
H2S
CH3OH
H2 34S
T*A (K)
T*A (K)
.4
.2
0
−.2
−.4
−.6
.4
.2
0
−.2
−.4
0
50
100
150
VLSR (km s−1)

co-existence of the two species in the same region with the same excitation temperature. Results are included in Table 4.6. Adoption instead of $S/^{34}S \sim 15$, which seems to be appropriate to Orion (Paper 2), would result in ~ 30 % decrease in the total column density. We have assumed rotational temperatures (T_{rot}) of 20 K, and the effects of varying this assumption in calculating total column densities are shown in Figure 4.2. As shown in the figure, total column densities are relatively insensitive to T_{rot}. For comparison, total column densities have also been derived from the $H_2{}^{34}S$ line using the "standard" equation (Irvine, Goldsmith, and Hjalmarson 1987) for optically thin emission, $T_{rot} = 20$ K, and the isotopic abundance ratio given above. We derive similar values of total column density from both methods, and $N_{total}(H_2S) \sim 10^{15}$ cm^{-2} for each component in Sgr B2(M) and (N). For Sgr B2(2N), we assumed the H_2S line was optically thin. The column densities are included in Table 4.6.

4.4.2 W49

W49, at a distance of 14 kpc, is one of the most active star-formation regions in the Galaxy. It contains the most powerful complex of H_2O masers in the Galaxy (Knowles *et al.* 1974; Genzel *et al.* 1978), with hundreds of spectral features. Several positions have been observed, and the H_2S line parameters are given in Table 4.2 and sample spectra in Figure 4.3. The H_2S spectrum

Figure 4.2 Multiplication factors for determining total column densities of H_2S from values calculated with T_{rot} = 20 K, as a function of rotational temperatures (T_{rot}). Calculation assumes a Boltzmann population distribution. Solid line assumes optically thin lines and dashed line corresponds to calculation with the optical depth as found from the ratio of the H_2S and $H_2{}^{34}S$ transitions.

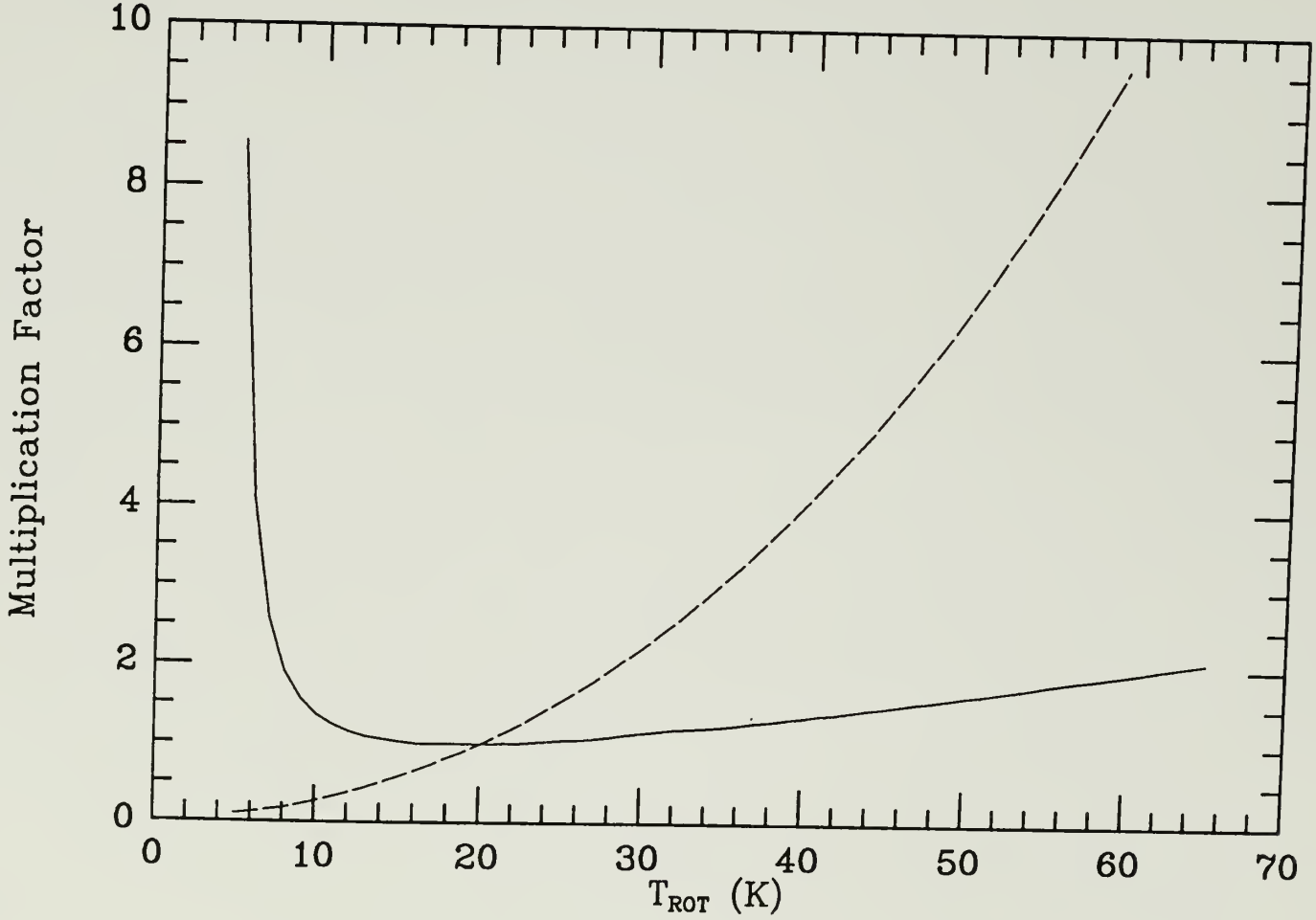
Multiplication Factor
10
8
6
4
2
0
0
10
20
30
40
50
60
70
T_{ROT} (K)

towards W49N is quite similar to the single-dish CO spectrum (HPBW ~ 45"), which shows a strong self-absorption feature (Scoville *et al.* 1986). The H_2S emission is probably self-absorbed, since the $H_2{}^{34}S$ spectrum obtained toward W49N shows a single peak whose V_{LSR} coincides with the absorption feature of the H_2S spectrum (Figure 4.3). The H_2S emission in W49N is fairly extended, and spatial-velocity maps are shown in Figure 4.4. We derive an optical depth ~ 7 at the line center towards the (0, 0) position in Table 4.2 by comparing the H_2S and $H_2{}^{34}S$ spectra, and $N_{total}(H_2S)$ ~ 2×10^{15} cm^{-2} from both the H_2S optical depth and the $H_2{}^{34}S$ line itself with the same assumptions described in § 4.4.1.

4.4.3 W51

The W51 molecular complex is located at a distance of 7 kpc and has two infrared and radio continuum sources associated with bright H_2O masers: W51(M) and W51(N). Genzel and Downes (1982) have suggested that W51(N) has a remarkable morphological similarity to Orion(KL), but the total infrared luminosity is much larger than the luminosity of Orion(KL), and the mass and momentum contained in the high velocity gas are also larger than in Orion by about an order of magnitude. W51(M/S) is located ~ 1′ to the south of W51(N), and has a group of ultra-compact HII regions, and OH and H_2O maser sources. The observed line parameters are included in Table 4.3. The H_2S spectrum for W51(N) shows a "plateau" emission which seems

TABLE 4.2

H_2S Line Parameters Observed toward W49N

Offset[a]		T_A^* [b]	V_{LSR}	ΔV	$\int T_A^* dV$
$\Delta\alpha$	$\Delta\delta$	(K)	(km s^{-1})	(km s^{-1})	(K km s^{-1})
0.	0.	0.39 ±.03	7.4	17.8	7.3
		(0.10 ±.03)	(8.8)	(7.6)	(0.8)
1.	0.	0.29 ±.04	5.3	14.8	4.3
2.	0.	0.31 ±.05	10.7	7.3	2.3
3.	0.	≤ 0.15[c]	—	—	—
-1.	0.	0.36 ±.04	7.8	14.5	5.2
-2.	0.	≤ 0.15[c]	—	—	—
0.	1.	0.18 ±.06	8.9	10.9	2.0
0.	2.	≤ 0.23[c]	—	—	—
0.	-1.	0.28 ±.06	10.6	5.8	1.6
0.	-2.	≤ 0.16[c]	—	—	—

NOTE. - Spectral resolution is 1 MHz.

Numbers in parenthesis are for the $H_2{}^{34}S$ (1_{10} - 1_{01}) line.

[a] In arcmin from RA(1950) = $19^h07^m49^s.8$ and Dec(1950) = $9^\circ01'17''$.

[b] Errors are 1 σ.

[c] 3 σ upper limit.

Figure 4.3 Spectra of the $1_{10} - 1_{01}$ transitions of H_2S and $H_2{}^{34}S$ towards W49N and W49S at a resolution of 1 MHz (positions given in Table 4.2).

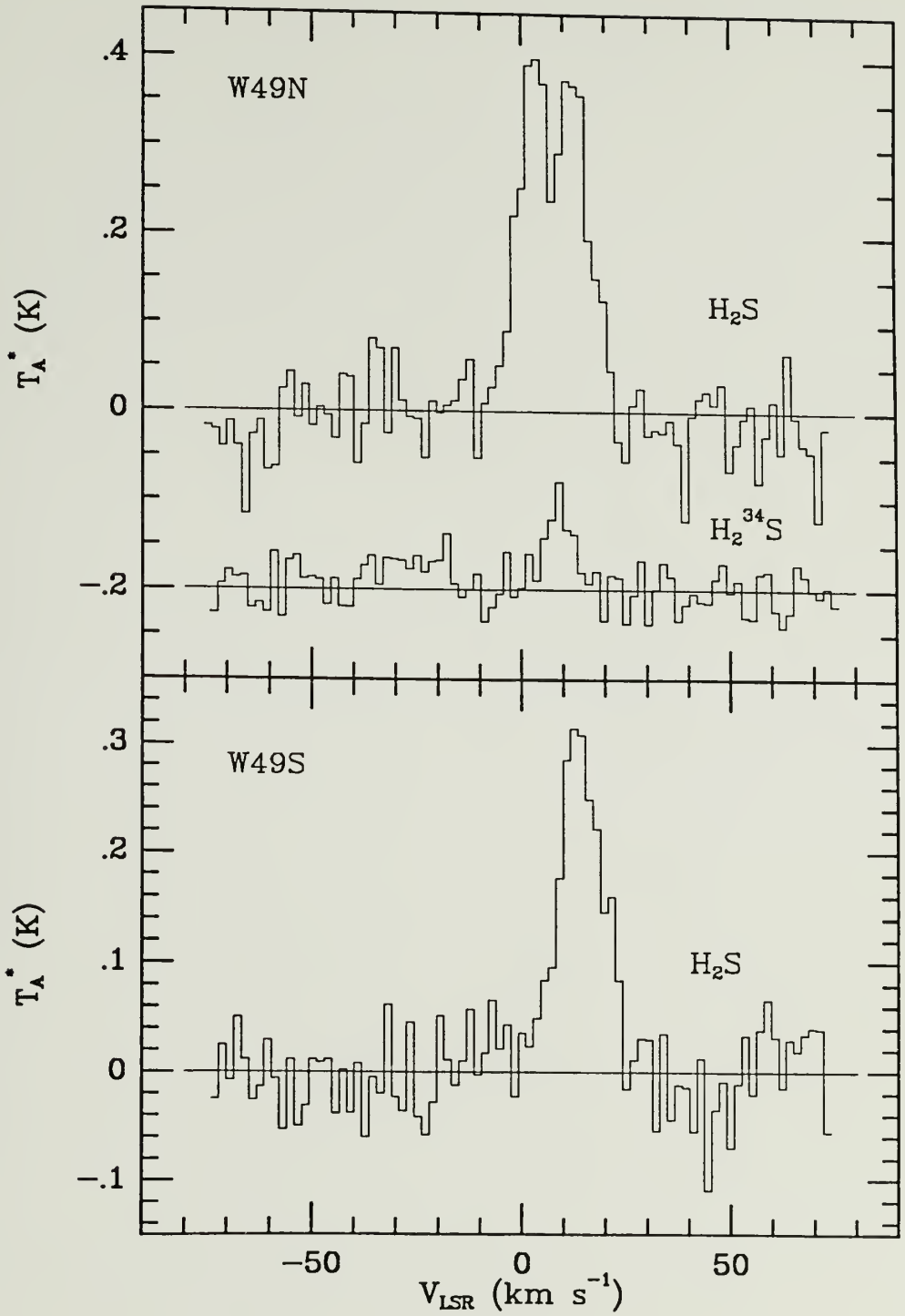
W49N
H2S
H2 34S
W49S
H2S
.4
.2
0
-.2
.3
.2
.1
0
-.1
TA* (K)
TA* (K)
-50
0
50
VLSR (km s-1)

Figure 4.4 Spatial-velocity maps for the observed antenna temperatures obtained toward W49N. Offsets are from the (0, 0) position of W49N in Table 4.2. Lowest contour level is 0.05 K and levels increase by 0.03 K for both panels.

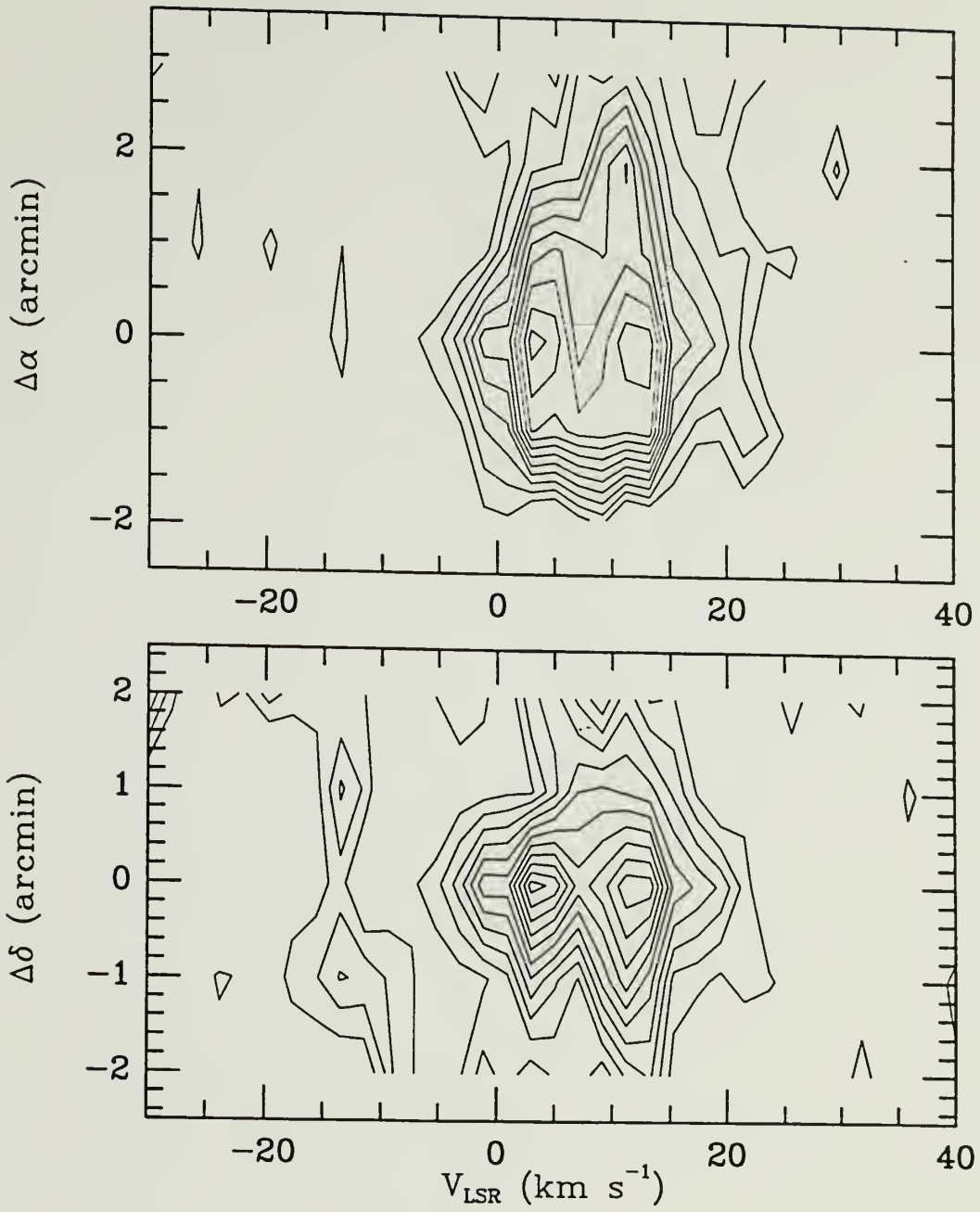
Δα (arcmin)
2
0
−2
−20
0
20
40
Δδ (arcmin)
2
1
0
−1
−2
−20
0
20
40
V_LSR (km s^−1)

to have a center velocity at ~ 50 km s^{-1} and ΔV ~ 15 km s^{-1}. In Figure 4.5, we show the spectrum and a two component gaussian fit. Since $H_2{}^{34}S$ data was not obtained toward W51(N), we calculated the column density from the integrated intensity of the H_2S line by assuming optically thin emission. As a result, the column density may be underestimated by a large factor, because the optical depth could be larger than one and the source size much smaller than the beam size. For W51(M/S), we derive an optical depth of ~ 3 by comparing the H_2S and $H_2{}^{34}S$ intensities, leading to $N_{total}(H_2S)$ ~ 10^{15} cm^{-2}. We have applied the same assumptions to derive column densities as described in § 4.4.1 (see also Figure 4.2 for the effect of T_{rot} in the calculation of column densities).

4.4.4 W3(IRS5)

W3(IRS5) is located at a distance of ~ 2.5 kpc and has a cluster of infrared sources, H_2O masers, and ultra-compact HII regions. The weakness of the radio continuum emission, the lack of high velocity motions and evidence for shock excitation may indicate that W3(IRS5) is in an earlier evolutionary stage than Orion(KL), W51, or W49 (Genzel and Downes 1982). The line parameters are included in Table 4.3 and the spectra in Figure 4.6. We derive an optical depth of ~ 5 for the H_2S line from comparison with the $H_2{}^{34}S$ intensity. This corresponds to $N_{total}(H_2S)$ ~ 10^{15} cm^{-2}, applying the same arguments as described in § 4.4.1.

TABLE 4.3

Line Parameters Observed in W51 and W3

Position	T_A^* (K)	V_{LSR} (km s^{-1})	ΔV (km s^{-1})	$\int T_A^* dV$ (K km s^{-1})
W51(N)	0.14	52.9	15.0	7.9
	0.92	61.1	7.2	7.1
W51(M/S)	1.03	56.8	10.4	11.4
	(0.14)	(55.3)	(13.5)	(2.1)
W3(IRS5)	0.64	-40.8	6.9	4.7
	(0.13)	(-40.9)	(16.5)	(2.3)
W3(OH)	(0.19)	(-43.9)	(4.4)	(0.8)

Numbers in parenthesis are for the $H_2{}^{34}S$ (1_{10} - 1_{01}) line.

Spectral resolution is 1 MHz.

Positions: W51(N): RA(1950) = $19^h21^m22^s.0$, Dec(1950) = $14^\circ25'20''$; W51(M/S) = RA(1950) = $19^h21^m26^s.4$, Dec(1950) = $14^\circ24'42''$; W3(IRS5): RA(1950) = $2^h21^m53^s.0$, Dec(1950) = $61^\circ52'21''$; W3(OH): RA(1950) = $2^h23^m16^s.8$, Dec(1950) = $61^\circ38'57''$.

Figure 4.5 Spectra of the 1_{10} - 1_{01} transitions of H_2S and $H_2{}^{34}S$ towards W51(N) and W51(M/S) at a resolution of 1 MHz (positions given in Table 4.3). Dotted lines in the W51(N) spectrum show gaussian components and line parameters are included in Table 4.3. The CH_3OH (9_1 - 9_0 E1) line is shown in the $H_2{}^{34}S$ spectrum.

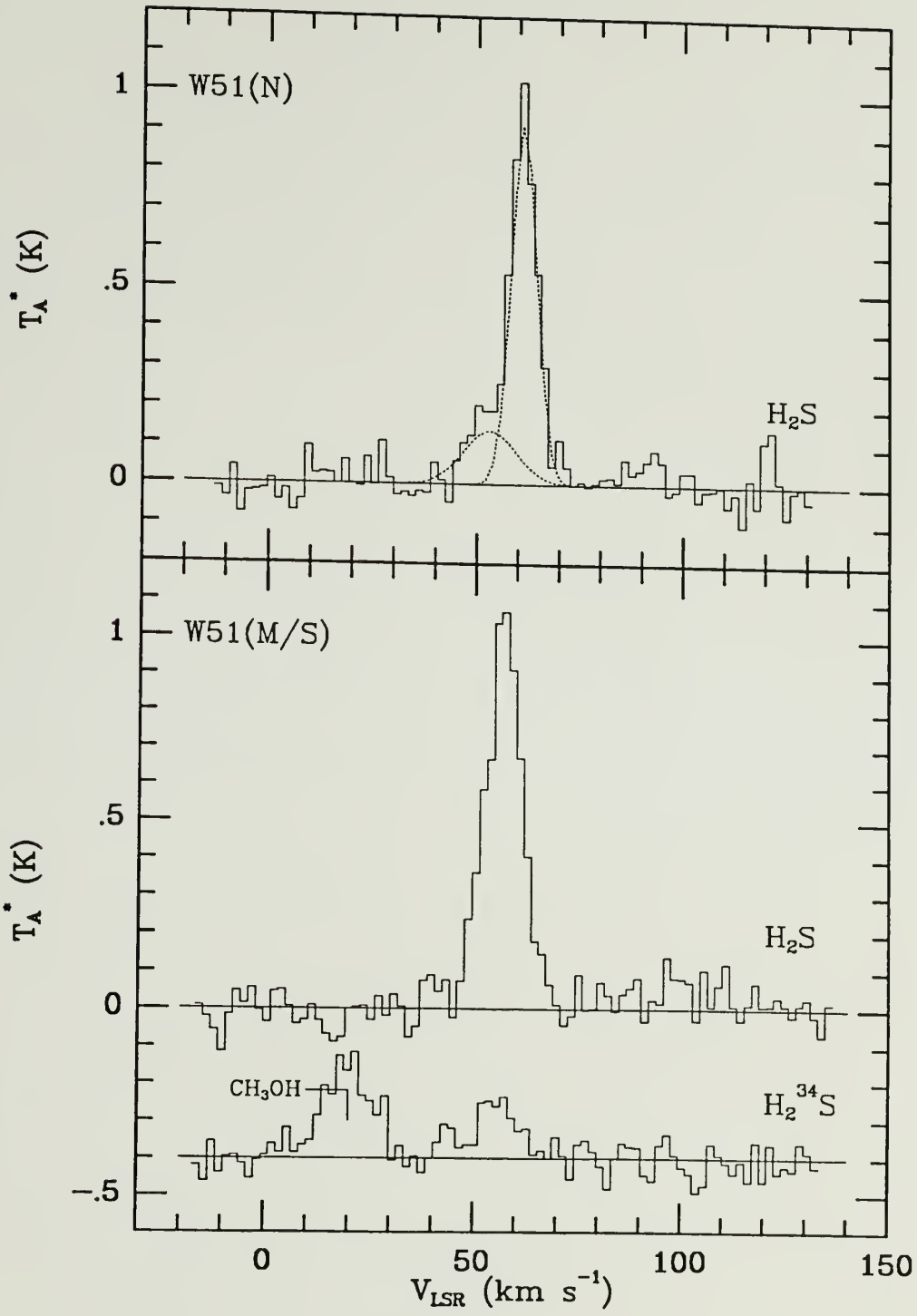
W51(N)
H2S
W51(M/S)
H2S
CH3OH
H2 34S
T*A (K)
T*A (K)
1
.5
0
1
.5
0
−.5
0
50
100
150
VLSR (km s−1)

Figure 4.6 Spectra of the $1_{10} - 1_{01}$ transitions of H_2S and $H_2{}^{34}S$ towards W3(IRS5) at a resolution of 1 MHz (position given in Table 4.3).

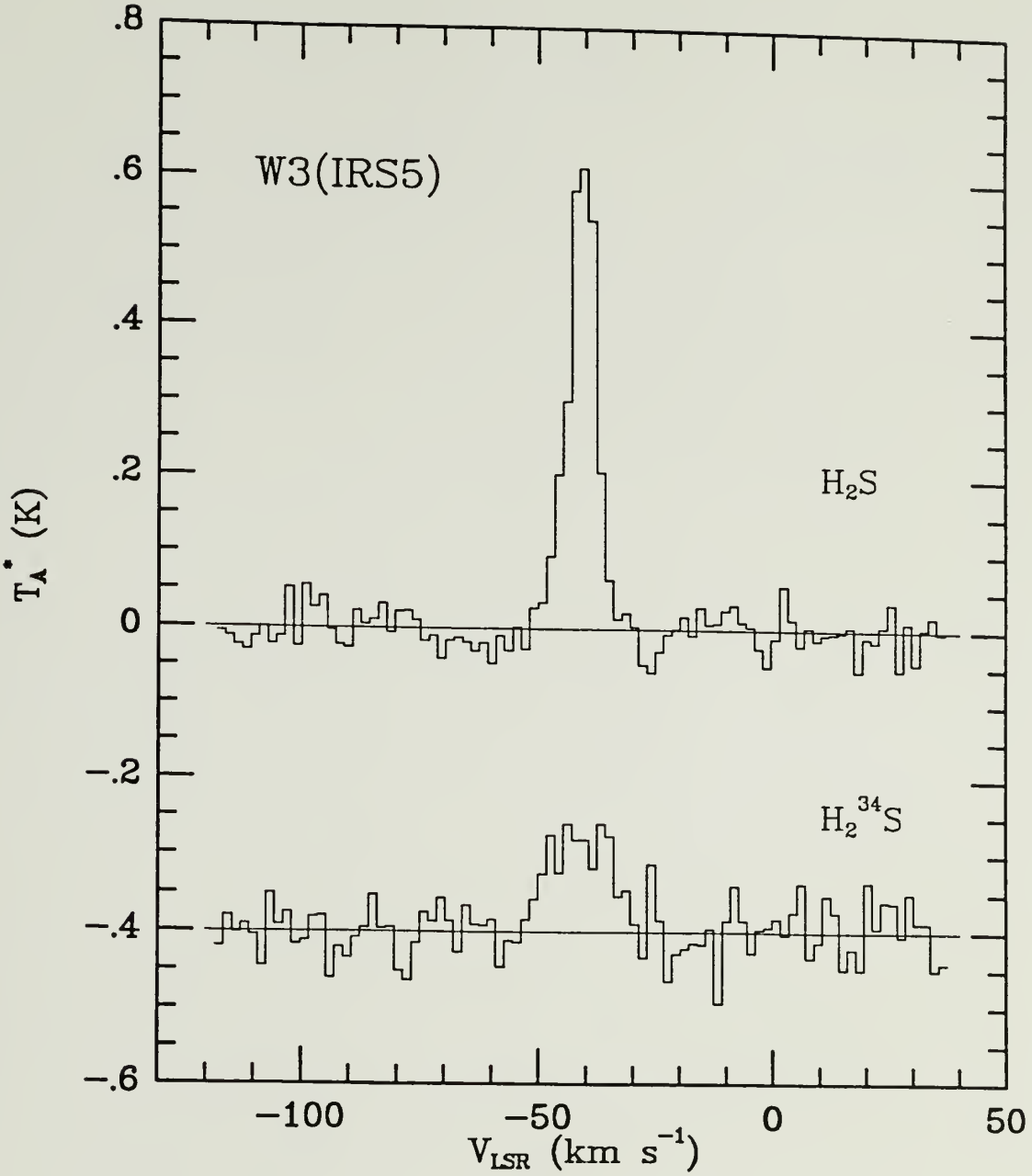
W3(IRS5)
H2S
H2 34S
T*A (K)
VLSR (km s−1)
.8
.6
.4
.2
0
−.2
−.4
−.6
−100
−50
0
50

4.4.5 Other Sources

The H_2S line parameters for other star-forming regions are included in Table 4.4. Most spectra show somewhat asymmetric line profiles, and sample spectra for NGC7538 are shown in Figure 4.7. The $H_2{}^{34}S$ line has not been detected toward NGC7538(N) to a 1 σ value of 40 mK, which indicates that the optical depth of H_2S is less than 2.6. The H_2S total column densitites for these sources have been derived to be ~ 10^{14} cm^{-2} if the H_2S lines are optically thin and the sources fill the antenna beam (see Table 4.6). Most of these sources contain embedded infrared sources, however, and star-formation is probably occuring actively. From the results for the sources in Tables 4.1 - 4.3, it is likely that such regions have optical depths larger than one. The source sizes also could be smaller than the beam size. Therefore, this value of $N_{tot}(H_2S)$ is probably a lower limit.

Among the sources in Table 4.4, the H_2S line has not been detected (to a 3 σ limit of 94 mK) only toward IC443B. We derive $N_{total}(H_2S) \leq 6 \times 10^{13}$ cm^{-2}. SNR IC443 contains several regions which suggest the recent passage of shocks, as evidenced by unusually broad and asymmetric line profiles observed in CO and OH (e.g. DeNoyer and Frerking 1981; Huang, Dickman, and Snell 1986). In Clump B (IC443B), many molecular species have been detected (cf. Ziurys, Snell, and Dickman 1987), and the SiO abundance is significantly enhanced relative to limits in quiescent clouds.

TABLE 4.4

H_2S Line Parameters for Other Sources

Source	T_A^* [a] (K)	V_{LSR} (km s^{-1})	ΔV (km s^{-1})	$\int T_A^* dV$ (K km s^{-1})
AFGL4029	0.28 ±.04	-38.8	2.7	0.8
S235B	0.85 ±.11	-17.0	4.0	3.4
S255	0.82 ±.18	7.7	3.6	2.9
W33A	0.49 ±.05	35.9	8.4	4.2
G34.3+0.2	1.14 ±.05	56.6	4.0	4.5
W49S	0.31 ±.04	12.4	13.5	4.3
S106	0.19 ±.04	-1.4	8.4	1.6
DR21(OH)	0.52 ±.09	-4.2	3.2	1.7
DR21	0.39 ±.13	-1.3	3.9	1.6
S140	1.15 ±.08	-6.7	3.6	4.2
Ceph A	0.58 ±.04	-10.9	5.6	3.3
NGC7538(N)	1.01 ±.07	-57.5	4.8	4.8
NGC7538(S)	0.81 ±.05	-57.0	5.8	4.7
NGC7538(E)	0.39 ±.04	-57.0	4.6	1.8
IC443B	≤ 0.09[b]	—	—	—

[a] Errors are 1 σ.

[b] 3 σ upper limit.

(Continued on next page)

TABLE 4.4

(Continued)

NOTE. - Spectral resolutions are 1 MHz for W33A, W49S, S106, and Ceph A, and 250 kHz for other sources.

Positions: AFGL4029: RA(1950) = $2^h57^m35^s.6$, Dec(1950) = $60°17'22''$; S235B: RA(1950) = $5^h37^m30^s.4$, Dec(1950) = $35°39'57''$; S255:RA(1950) = $6^h09^m58^s.3$, Dec(1950) = $18°00'11''$; W33A: RA(1950) = $18^h11^m19^s.0$, Dec(1950) = $-17°56'46''$; G34.3+0.2: RA(1950) = $18^h50^m46^s.0$, Dec(1950) = $1°11'10''$; W49S: RA(1950) = $19^h07^m58^s.0$, Dec(1950) = $9°00'05''$; S106: RA(1950) = $20^h25^m34^s.0$, Dec(1950) = $37°12'52''$; DR21(OH): RA(1950) = $20^h37^m15^s.0$, Dec(1950) = $42°12'08''$; DR21: RA(1950) = $20^h37^m07^s.6$, Dec(1950) = $42°08'46''$; S140: RA(1950) = $22^h17^m41^s.2$, Dec(1950) = $63°03'41''$; Ceph A: RA(1950) = $22^h54^m19^s.0$, Dec(1950) = $61°45'47''$; NGC7538(N): RA(1950) = $23^h11^m36^s.6$, Dec(1950) = $61°11'48''$; NGC7538(S): RA(1950) = $23^h11^m36^s.6$, Dec(1950) = $61°10'48''$; NGC7538(E): RA(1950) = $23^h11^m53^s.0$, Dec(1950) = $61°10'58''$; IC443B: RA(1950) = $6^h14^m15^s.0$, Dec(1950) = $22°26'50''$.

Figure 4.7 Spectra of the $1_{10} - 1_{01}$ transition of H_2S towards NGC7538(N), (S), and (E) at a resolution of 250 kHz (positions given in Table 4.4).

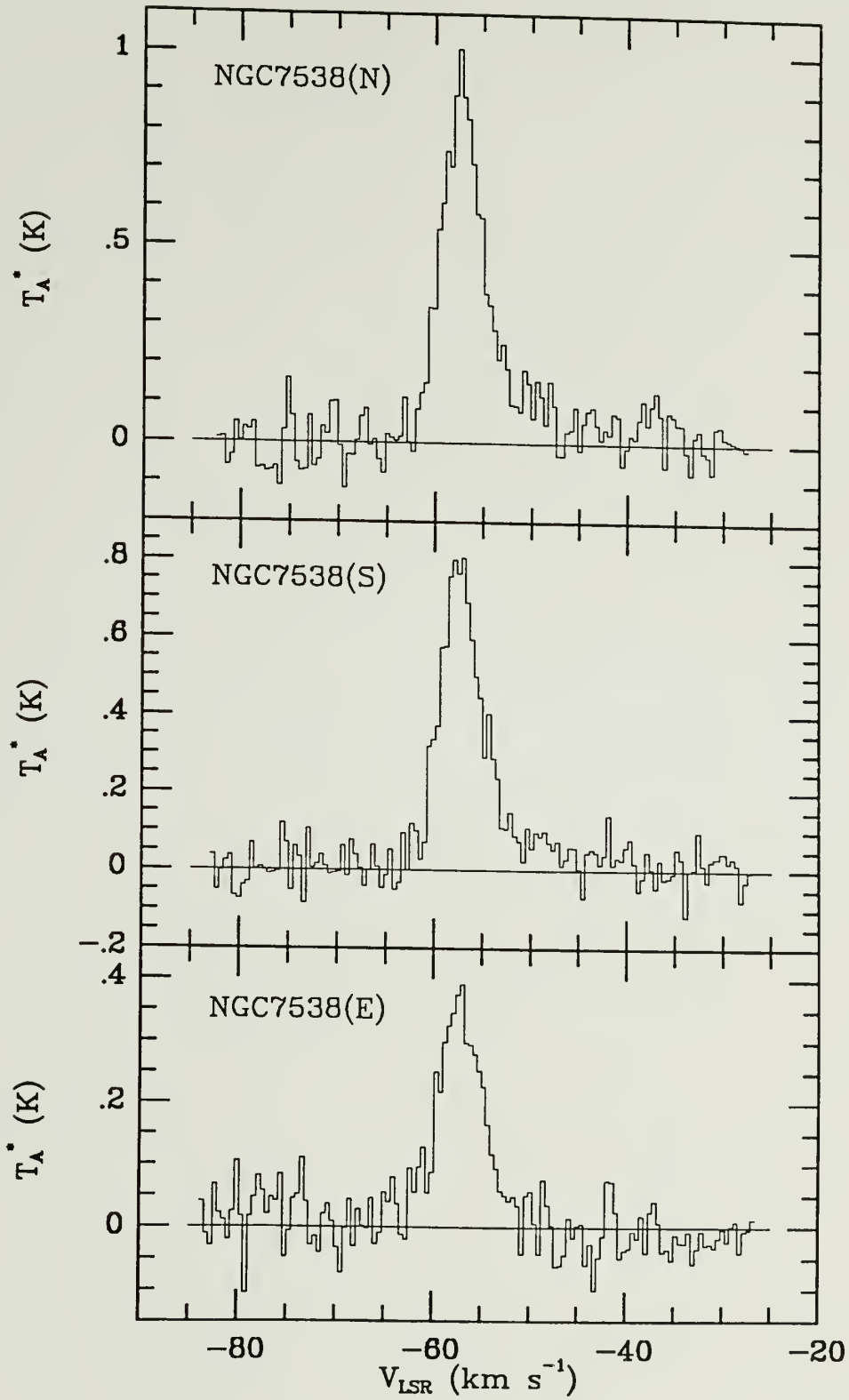
NGC7538(N)
NGC7538(S)
NGC7538(E)
T_A^* (K)
1
.5
0
.8
.6
.4
.2
0
−.2
.4
.2
0
−80
−60
−40
−20
V_{LSR} (km s^{-1})

TABLE 4.5

Line Parameters for ^{34}SO (4_3 - 3_3) and CH_3OH (9_1 - 9_0 E1) Lines

Source	T_A^* [a] (K)	V_{LSR} (km s^{-1})	ΔV (km s^{-1})	$\int T_A^* dV$ (K km s^{-1})
		^{34}SO (4_3 - 3_3)		
SgrB2(M)	0.10 ±.04	58.2	9.5	1.0
W49N(0,0)	0.10 ±.03	7.8	7.8	0.8
		CH_3OH (9_1 - 9_0 E1)		
SgrB2(M)	0.13 ±.05	64.4	12.4	1.7
SgrB2(N)	0.28 ±.07	66.4	9.1	2.6
W51(M/S)	0.25 ±.05	51.4	20.2	3.8

[a] Errors are 1 σ.

NOTE. - Spectral resolution is 1 MHz.

Rest frequency: ^{34}SO (4_3 - 3_3) line: 168.815101 GHz (Hollis *et al.* 1981); CH_3OH (9_1 - 9_0 E1) line: 167.93113 GHz (Lovas 1989).

TABLE 4.6

H_2S Column Densities

Source	$N_{total}(H_2S)$ (cm^{-2})	Comments
SgrB2(M)	~ 2 (15)	Applies to both the 50 km s^{-1} and 80 km s^{-1} components, which have $\tau(H_2S)$ ~ 11 and 7, respectively.
SgrB2(N)	~ 2 (15)	Applies to both the 50 km s^{-1} and 80 km s^{-1} components, which have $\tau(H_2S)$ ~ 6 and 7, respectively.
SgrB2(2N)	≥ 1 (14)	Applies to both the 50 km s^{-1} and 80 km s^{-1} components. From the H_2S line, assuming $\tau(H_2S) \ll 1$.
W49N (0,0)	2 (15)	$\tau(H_2S)$ ~ 7 at the line center.
W51(N)	≥ 1 (14)	Applies to both the 50 km s^{-1} and 60 km s^{-1} gaussian fit components. From the H_2S line, assuming $\tau(H_2S) \ll 1$.
W51(M/S)	1 (15)	$\tau(H_2S)$ ~ 3 at the line center.
W3(IRS5)	1 (15)	$\tau(H_2S)$ ~ 5 at the line center.
IC443B	≤ 6 (13)	With 3σ value, ΔV=20 km s^{-1}, and T_{rot} = 20K.
Other Sources	≥ 1 (14)	Assuming for the H_2S lines $\tau \ll 1$ and T_{rot} = 20 K.

The ^{34}SO 4_3 - 3_3 line and presumably the CH_3OH 9_1 - 9_0 E1 line (Paper 2) have been detected in some sources. Line parameters for both these species are listed in Table 4.5.

4.5 Discussion

We derive H_2S total column densities of ~ 10^{15} cm^{-2} towards several star-forming regions observed in the H_2S and $H_2{}^{34}S$ lines, which is about an order of magnitude larger than suggested by Thaddeus *et al.* (1972), who did not have $H_2{}^{34}S$ data available. We find values $\geq 10^{14}$ cm^{-2} in other sources observed only by the H_2S line. Although total hydrogen column densities are not certain toward many of these locations, the fractional abundances of H_2S relative to H_2 may be ~ 0.2 - 1 x 10^{-8} in Sgr B2 (for $N(H_2)$ ~ 0.2 - 1 x 10^{24} cm^{-2}; Irvine, Goldsmith, and Hjalmarson 1987; Lis 1989), ~ 10^{-7} - 10^{-8} in W49N and W51(M/S) ($N(H_2)$ ~ 1-10 x 10^{22} cm^{-2}; Scoville and Solomon 1973), and probably in the range 10^{-8} - 10^{-9} for other sources (assuming $N(H_2)$ ~ 1-10 x 10^{22} cm^{-2}; e.g. Evans and Blair 1981; Goldsmith and Mao 1983). However, the H_2S abundances for these other star-forming regions may be regarded as lower limits since these values could be increased very much depending on the source sizes, optical depths, and rotational temperatures.

Most of the star-forming regions observed here have infrared sources, compact HII regions, radio continuum sources, and maser sources. The H_2S chemistry has been discussed in Paper 1 and 2,

and the possible grain processes for the formation of H_2S could be also important in the sources discussed here. The H_2S abundances in these regions are in between those for quiescent clouds ($\sim 10^{-9}$), and the Orion hot core and the plateau ($\sim 10^{-6}$) (Paper 1 and 2). Therefore, a part of the H_2S emission may also come from small, hot, and dense regions like the Orion hot core or plateau. Higher spatial resolution observations would be very useful to study H_2S in these regions.

In the supernova remnant IC443B, we derive an upper limit for the H_2S column density $N_{total}(H_2S) \leq 6 \times 10^{13}$ cm^{-2}, which may correspond to a fractional abundance $f(H_2S) \leq 6 \times 10^{-8}$ assuming the H_2 column density estimated from other molecules (Ziurys, Snell, and Dickman 1988). This upper limit is not low enough to determine if the H_2S abundance is significantly enhanced relative to quiescent cloud values, as is predicted in some models of shock chemistry. A better upper limit would be useful to discuss this question.

CHAPTER 5

H_2CS ABUNDANCES AND ORTHO-TO-PARA RATIOS IN INTERSTELLAR CLOUDS

5.1 Summary

Several H_2CS ortho and para transitions have been observed toward interstellar molecular clouds, including cold, dark clouds and star forming regions. We derive H_2CS fractional abundances $f(H_2CS) \sim 1 - 2 \times 10^{-9}$ relative to molecular hydrogen towards TMC-1, Orion A, and NGC7538, and $\sim 5 \times 10^{-10}$ for L134N.

The H_2CS ortho-to-para ratios in TMC-1 are ~ 1.8 towards the cyanopolyyne peak and the ammonia peak, which may indicate the thermalization of H_2CS on 10 K grains. We derive a ratio of ~ 3, the statistical value, for Orion(3N1E) and NGC7538, while we find a value ~ 2 for Orion(KL).

5.2 Introduction

Molecules such as H_2, H_2O, and H_2CO, have two distinct states, depending on the spin of the identical hydrogen nuclei: the para and the ortho states for anti-parallel and parallel spins, respectively. Since radiative or collisional conversion from one form to the other is forbidden, the ortho to para abundance ratio would provide information on the effective formation temperature of the molecules

if only gas phase processes were important subsequent to formation (cf. Kahane *et al.* 1984; hereafter KFLEL). Usually molecular formation temperatures are much larger than the energy difference between ortho and para states, and the corresponding abundance ratio would be given by the relative statistical weights of the respective states.

The ortho-to-para ratio for molecular hydrogen has been studied in diffuse regions or very hot regions, and the ratios are considerably different from the statistical value of 3 (e.g. Spitzer *et al.* 1973; Dalgarno, Black, and Weisheit 1973; Davis, Larson, and Smith 1982; Scoville *et al.* 1982; Gately *et al.* 1987; Takayanagi, Sakimoto, and Onda 1987; Hasegawa *et al.* 1987). However, molecular hydrogen, which has no permanent electric dipole moment, is hard to observe in dense molecular clouds with kinetic temperatures of 10 - 100 K, since its transition probabilities are very small and its rotational levels have energies much larger than the cloud kinetic temperature.

KFLEL have derived H_2CO ortho-to-para ratios ~ 3, the statistical weight value, in Orion A, but they find a ratio ~ 1 - 2 in the cold cloud TMC-1. Gas-phase interconversion mechanisms between ortho and para species, such as proton exchange reactions, are probably too slow to be efficient. However, if thermalization on grain surfaces is important, the ortho-to-para ratio for grains at ~ 10 K would be ~ 1.5, while for $T \geq 30$ K, it approaches the statistical value of 3 (KFLEL). Thus, the observations provide

evidence for gas-grain interactions in cold clouds. The H_2CO lines observed are, however, severely self-absorbed, especially in the dark clouds.

Thioformaldehyde (H_2CS) has been detected in Sgr B2, Orion A, and other star - forming regions (Sinclair *et al.* 1973; Cummins, Linke, and Thaddeus 1986; Loren 1984; Sutton *et al.* 1985; Blake *et al.* 1987; Liszt 1978), and in the cold dark clouds TMC-1 and L134N (Irvine *et al.* 1989). H_2CS is similar to H_2CO in its structure and exists in both ortho and para forms, and H_2CS ortho-to-para ratios ~ 3 have been derived by Gardener *et al.* (1985) in Orion(KL). H_2CS may be a better candidate to study the ortho-to-para ratio than H_2CO, especially in cold dark clouds, since the optical depths for the H_2CS lines seem to be much less than those of H_2CO (Irvine *et al.* 1989). In this Chapter, we report the abundances and ortho-to-para ratios of H_2CS observed in the interstellar molecular clouds TMC-1, L134N, Orion A, and NGC7538.

5.3 Observations

Observations were made using the FCRAO 14 m telescope between 1988 December and 1989 June. Observed H_2CS line frequencies are included in the note to Table 5.1. Both the FCRAO 3 mm and 2 mm receivers employed cooled Schottky diode mixers, which gave total system temperatures, corrected to outside the atmosphere, of 400-600 K for the 100 GHz transitions and 800 - 1000 K for the 140 GHz

TABLE 5.1

H_2CS Line Parameters[a]

Transition	T_A^* [b] (K)	ΔV (km s^{-1})	V_{LSR} (km s^{-1})	$\int T_A^* dV$ (K km s^{-1})
		TMC-1		
3_{03} - 2_{02}	0.52 ±.03	0.61	5.7	0.34
4_{04} - 3_{03}	0.34 ±.07	0.55	5.6	0.20
3_{13} - 2_{12}	0.54 ±.04	0.55	5.6	0.32
3_{12} - 2_{11}	0.51 ±.04	0.67	5.6	0.39
4_{13} - 3_{12}	0.16 ±.05	0.79	5.7	0.13
		L134N		
3_{13} - 2_{12}	0.08 ±.02	0.61	2.2	0.05
		Orion(KL)		
3_{03} - 2_{02} [d]	0.41 ±.02	3.94	8.6	1.62
3_{13} - 2_{12}	0.69 ±.06	3.13	8.5	2.17
3_{12} - 2_{11}	0.52 ±.05	3.18	7.9	1.67
3_{21} - 2_{20}	0.11 ±.02	3.45	7.6	0.39
		NGC7538(N)		
3_{03} - 2_{02}	0.18 ±.02	2.99	-57.1	0.54
3_{13} - 2_{12}	0.27 ±.03	3.29	-57.1	0.90
3_{12} - 2_{11}	0.31 ±.06	2.99	-58.2	0.92

(Continued on next page)

TABLE 5.1

(Continued)

Transition	T_A^* [b] (K)	ΔV (km s^{-1})	V_{LSR} (km s^{-1})	$\int T_A^* dV$ (K km s^{-1})
		TMC-1(NH_3)		
3_{03} - 2_{02}	0.22 ±.05	0.97	5.5	0.23
4_{04} - 3_{03}	——	—	—	—
3_{13} - 2_{12}	0.24 ±.04	0.70	5.7	0.18
3_{12} - 2_{11}	0.23 ±.06	0.56	5.4	0.14
4_{13} - 3_{12}	——	—	—	—
		L134N(SO)		
3_{13} - 2_{12}	≤ 0.09[c]	—	—	—
		Orion(3N1E)		
3_{03} - 2_{02} [d]	0.40 ±.04	1.59	9.4	0.64
3_{13} - 2_{12}	0.53 ±.05	1.70	9.3	0.90
3_{12} - 2_{11}	0.70 ±.10	1.19	9.4	0.84
3_{21} - 2_{20}	≤ 0.11[c]	—	—	—
		NGC7538(S)		
3_{03} - 2_{02}	0.27 ±.03	3.84	-56.4	1.03
3_{13} - 2_{12}	0.44 ±.04	4.63	-56.4	2.03
3_{12} - 2_{11}	0.43 ±.10	4.78	-57.5	2.08

(Continued on next page)

TABLE 5.1

(Continued)

[a] Spectral resolutions are 100 kHz for TMC-1 and L134N, and 250 kHz for Orion and NGC7538.

[b] Errors are 1 σ values.

[c] 3 σ value.

[d] Contaminated by the 3_{22} - 2_{21} transition ($\Delta\nu$ = 0.55 MHz).

NOTE :

Line parameters for TMC-1 have been derived from gaussian fits.

Rest frequency: $\nu_o(3_{03} - 2_{02})$ = 103.040399 GHz; $\nu_o(3_{13} - 2_{12})$ = 101.47753 GHz; $\nu_o(3_{12} - 2_{11})$ = 104.616975 GHz; $\nu_o(3_{21} - 2_{20})$ = 103.051785 GHz; $\nu_o(4_{04} - 3_{03})$ = 137.371043 GHz; $\nu_o(4_{13} - 3_{12})$ = 139.483466 GHz; $\nu_o(3_{21} - 2_{20})$ = 103.051785 GHz (Lovas 1986).

Position: TMC-1: RA(1950) = $4^h38^m38^s.6$, Dec(1950) = $25^\circ35'45''$; TMC-1(NH_3):RA(1950) = $4^h38^m22^s.0$, Dec(1950) = $25^\circ41'45''$; L134N: RA(1950) = $15^h51^m30^s.0$, Dec(1950) = $-2^\circ43'31''$; L134N(SO): RA(1950) = $15^h51^m26^s.0$, Dec(1950) = $-2^\circ43'31''$; Orion(KL): RA(1950) = $5^h32^m47^s.0$, Dec(1950) = $-5^\circ24'23''$; Orion(3N1E): RA(1950) = $5^h32^m51^s.0$; Dec(1950) = $-5^\circ21'23''$; NGC7538(N): RA(1950) = $23^h11^m36^s.6$, Dec(1950) = $61^\circ11'48''$; NGC7538(S): RA(1950) = $23^h11^m36^s.6$; Dec(1950) = $61^\circ10'48''$.

transitions. Data were taken by position switching 30 arcminutes in azimuth, and spectra were obtained using 256-channel filter banks with 100 kHz and 250 kHz resolutions. The FWHP beamwidths are 52 and 43 arcseconds, and the antenna beam efficiencies η_B = 0.57 and 0.40 at 100 GHz and 149 GHz, respectively. The temperature scale is given as T_A^*, the beam-chopper-corrected antenna temperature. We then approximate the radiation temperature T_R by the main beam brightness temperature $T_{MB} = T_A^*/\eta_B$. The observed line parameters are given in Table 5.1 and sample spectra obtained towards TMC-1 and Orion(KL) in Figure 5.1. The observed antenna temperatures are also shown in the rotational diagram in Figure 5.2 for TMC-1 and Orion A.

5.4 Analysis

We have used an LVG statistical equlibrium - radiative transfer model to calculate the antenna brightness temperatures of the H_2CS lines. The model is described in Appendix A. Since the collisional cross-sections for H_2CS are not available, we used the H_2CO collisional de-excitation rates (Green *et al.* 1978) for the corresponding H_2CS levels as a first approximation (Gardener *et al.* 1985), and the collisional excitation rates have beeen calculated by assuming detailed balance. The calculations for TMC-1 (kinetic temperature $T_{kin} \sim$ 10 K) and Orion(3N1E) ($T_{kin} \sim$ 20 K) include 16 levels for ortho-H_2CS and 15 level for para-H_2CS up to energy levels

Figure 5.1 Sample spectra of H_2CS obtained towards TMC-1 and Orion(KL). Positions given in Table 5.1. Spectral resolution is 100 kHz for TMC-1 and 250 kHz for Orion(KL).

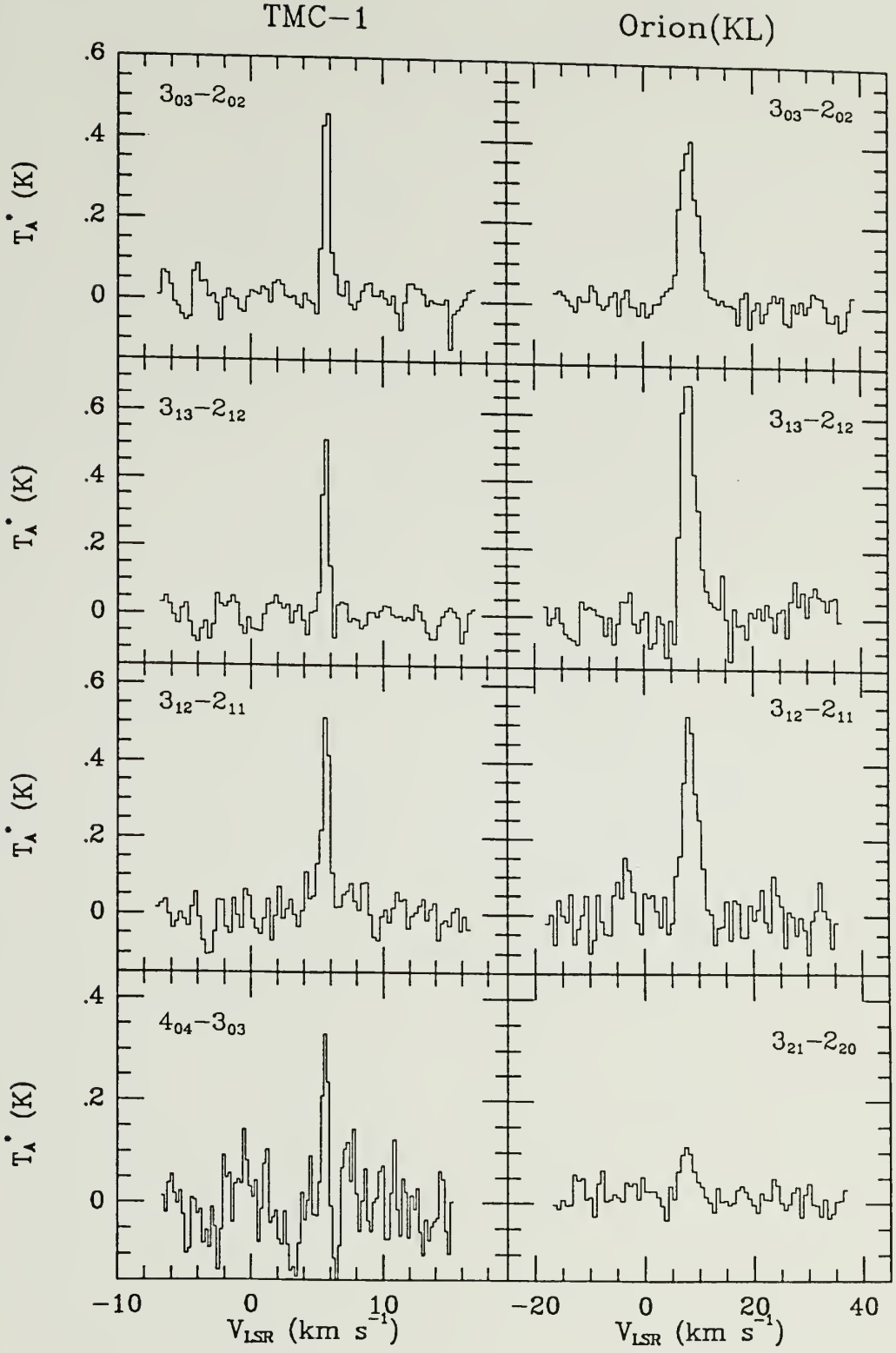
TMC−1
Orion(KL)
$3_{03}-2_{02}$
$3_{13}-2_{12}$
$3_{12}-2_{11}$
$4_{04}-3_{03}$
$3_{21}-2_{20}$
T_A^* (K)
.6
.4
.2
0
−10
0
10
−20
0
20
40
V_{LSR} (km s^{-1})

Figure 5.2 Rotation diagram for the observed H_2CS transitions. In the ordinate, $I = \ln\{1.94\times10^3\ \nu^2(\mathrm{GHz}) \int T_A^* dV\ (\mathrm{K\ km\ s^{-1}}) / A_{UL}\ g_U\ \eta_B\}$, where ν is the rest frequency, A_{UL} the spontaneous emission rate, g_U the statistical weight of the upper level, and η_B the antenna main beam efficiency. A correction for the cosmic background has been made for TMC-1 and L134N with the factor, $[1 - J_\nu(T_{BG})/J_\nu(T_{ex})]^{-1}$, where $J_\nu(T) = (h\nu/k)[\exp(h\nu/kT) - 1]^{-1}$, $T_{BG} = 2.7$ K, and $T_{ex} = 5$ K.

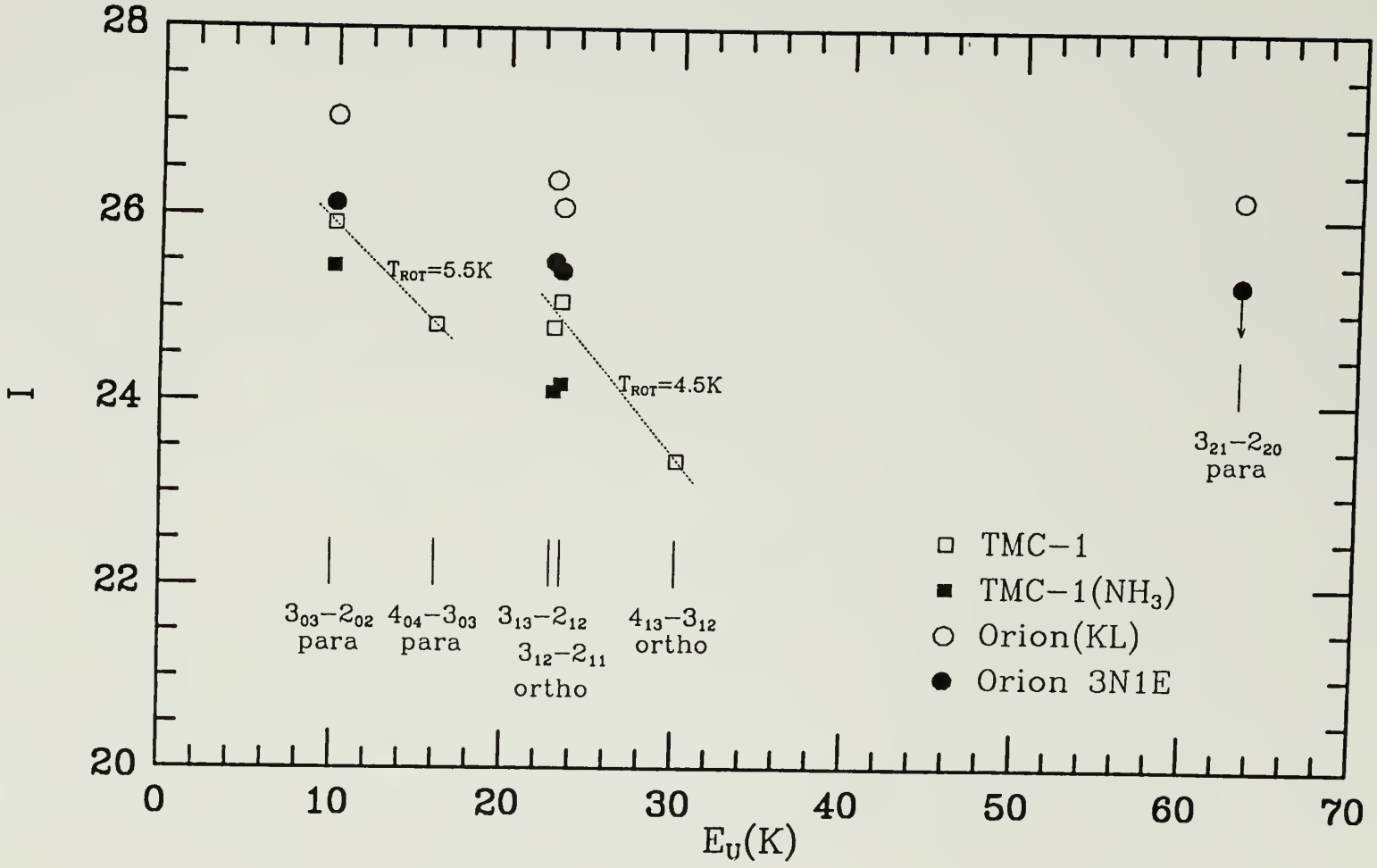
28
26
24
22
20
I
0
10
20
30
40
50
60
70
E_U(K)
T_{ROT}=5.5K
T_{ROT}=4.5K
$3_{03}-2_{02}$ para
$4_{04}-3_{03}$ para
$3_{13}-2_{12}$
$3_{12}-2_{11}$ ortho
$4_{13}-3_{12}$ ortho
$3_{21}-2_{20}$ para
TMC−1
TMC−1(NH_3)
Orion(KL)
Orion 3N1E

70 K above the ground state for each species. Since the de-excitation rates are not sensitive to kinetic temperatures or ΔJ values, we extrapolate the H_2CO de-excitation rates up to energy levels of 300 K to calculate for the Orion compact ridge, which has $T_{kin} \sim 100$ K. We include 60 levels of ortho-H_2CS and 49 levels of para-H_2CS in the LVG analysis for Orion(KL). Some of the results are shown in Appendix A.

In Figure 5.3 we have shown the calculation results for TMC-1, where the observed brightness temperatures and 3 σ values for each transition are indicated. It was assumed that the emission from all of the observed transitions filled the telescope beam. The shaded region in the left panel of Figure 5.3 is the most probable region confined by the three ortho transitions. We have obtained $n(H_2) \sim 10^5 - 10^6$ cm^{-3} in this analysis, and applied this H_2 volume density to also derive the corresponding para abundance. The H_2 density, however, has been suggested to be $0.5 - 1 \times 10^5$ cm^{-3} for the whole TMC-1 molecular cloud by Schloerb, Snell, and Young (1983) from observations of HC_3N lines and $\leq 10^5$ cm^{-3} by Bujarrabal *et al.* (1981) from HC_3N and HC_5N data, which is smaller than our result by a factor of a few. The difference may result from a scaling factor of the collisional cross sections for H_2CS from those of H_2CO. The results from the LVG analysis are included in Table 5.3, together with the abundances derived by assuming optically thin emission and a rotational temperature of 5 K (cf. Irvine, Goldsmith, and Hjalmarson 1987), for comparison. The column densities and

Figure 5.3 Curves of constant brightness temperature as a function of molecular hydrogen density $n(H_2)$ and H_2CS abundance, computed from LVG model for observed transitions in TMC-1, with kinetic temperature set to 10 K. Left panel is for the ortho transitions and the right for the para transitions, as indicated in the figure. The center lines for each transition are for the observed brightness temperatures and the other two lines for 3 σ rms values. The shaded region in the left panel indicates the most probable region suggested by the LVG analysis.

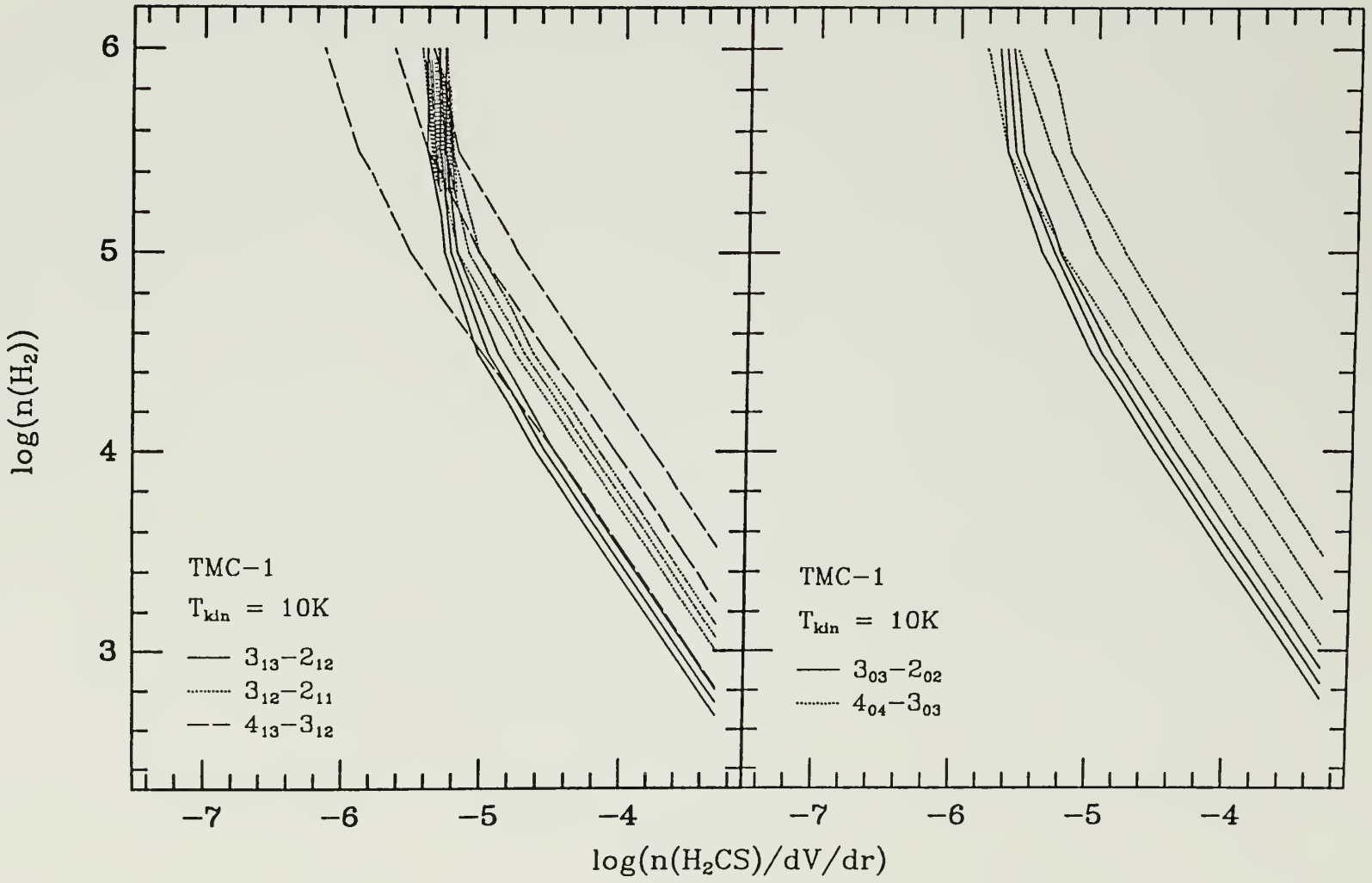
6
5
4
3
log(n(H2))
TMC−1
Tkin = 10K
3₁₃−2₁₂
3₁₂−2₁₁
4₁₃−3₁₂
TMC−1
Tkin = 10K
3₀₃−2₀₂
4₀₄−3₀₃
−7
−6
−5
−4
log(n(H2CS)/dV/dr)

ortho/para ratios found by the two procedures agree quite well. The results for a second position in this cloud, TMC-1(NH_3), have been calculated in the same way and are also listed in Table 5.3.

In Figure 5.4 we have shown the LVG model results for Orion(KL), and the shaded region in the right panel for para transitions indicates a probable locus for n(H_2) and the abundance parameter. We applied the source size ~ 30", since H_2CS is thought from the V_{LSR} values to be a constituent of the compact ridge (Blake *et al.* 1987). Although the $3_{03} - 2_{02}$ transition may be contaminated by the $3_{22} - 2_{21}$ transition ($\Delta\nu$ ~ 0.6 MHz), the constant antenna temperature curve for the $3_{21} - 2_{20}$ transition is well confined to a small range of the abundance parameter n(H_2CS)/dV/dr, so that the column density of H_2CS is well defined (Figure 5.4). The optical depths and excitation temperatures derived from the LVG analysis are included in Table 5.2 and the column densities and abundances in Table 5.3.

The column densities have also been derived by assuming optically thin emission and a rotational temperature 60 K for both para and ortho H_2CS. The rotational diagram in Figure 5.2 gives T_{rot} ~ 63 K for the $3_{03} - 2_{02}$ and $3_{21} - 2_{20}$ transitions, and we also obtained T_{rot} ~ 62 K and 60 K for para and ortho H_2CS, respectively, from the J = 7 - 6 transition data of Sutton *et al.* (1985). We derived column densities by using the $3_{21} - 2_{20}$ transition for para-H_2CS and the $3_{13} - 2_{12}$ and $3_{12} - 2_{11}$ transitions (by averaging

Figure 5.4 Same as Figure 5.3 for the observed brightness temperatures for Orion(KL). Source size of 30" has been assumed and kinetic temperature hasbeen set to 100 K.

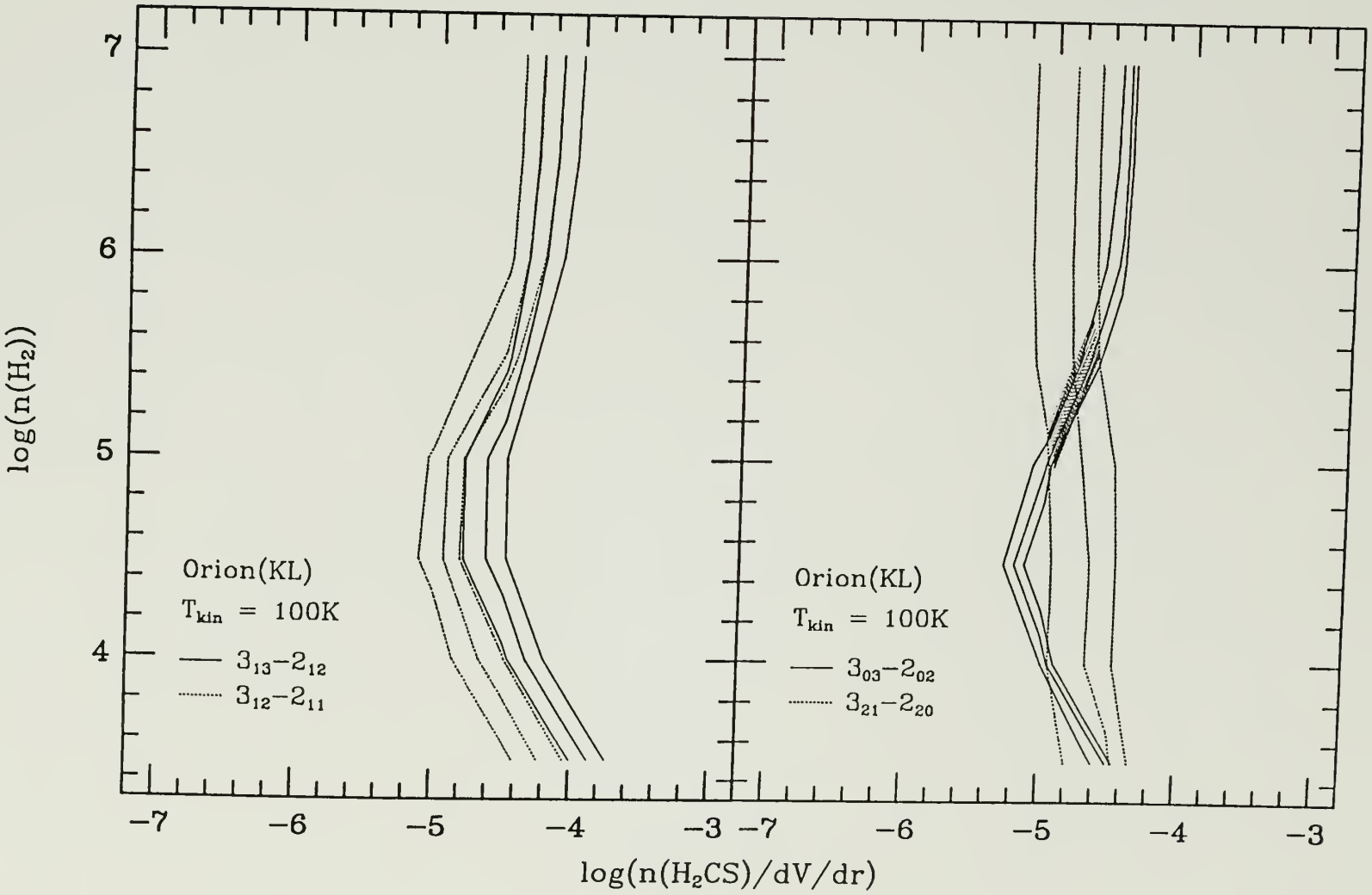
log(n(H2))
log(n(H2CS)/dV/dr)
Orion(KL)
Tkin = 100K
313–212
312–211
Orion(KL)
Tkin = 100K
303–202
321–220

TABLE 5.2

Excitation Temperatures and Optical Depths

Derived from the LVG Analysis

T_{kin} (K) =	10[a]		20[b]		100[c]	
Transition	T_{ex} (K)	Tau	T_{ex} (K)	Tau	T_{ex} (K)	Tau
$3_{03} - 2_{02}$	4.6	0.22	6.2	0.17	79.4	0.03
$4_{04} - 3_{03}$	4.2	0.12	5.3	0.13	26.2	0.12
$3_{13} - 2_{12}$	6.0	0.31	8.5	0.22	63.4	0.09
$3_{12} - 2_{11}$	5.0	0.31	7.0	0.22	37.7	0.12
$4_{13} - 3_{12}$	4.1	0.20	5.6	0.21	20.1	0.34

[a] For TMC-1 data; at $n(H_2) = 10^5$ cm^{-3}, and $n(para\text{-}H_2CS)/dV/dr = 1.6 \times 10^{-6}$ cm^{-3} $(km\ s^{-1}\ pc^{-1})^{-1}$ and $n(ortho\text{-}H_2CS)/dV/dr = 5 \times 10^{-6}$ cm^{-3} $(km\ s^{-1}\ pc^{-1})^{-1}$.

[b] For Orion(3N1E) data; at $n(H_2) = 10^5$ cm^{-3}, and $n(para\text{-}H_2CS)/dV/dr = 1.6 \times 10^{-6}$ cm^{-3} $(km\ s^{-1}\ pc^{-1})^{-1}$ and $n(ortho\text{-}H_2CS)/dV/dr = 5 \times 10^{-6}$ cm^{-3} $(km\ s^{-1}\ pc^{-1})^{-1}$.

[c] For Orion(KL) data; at $n(H_2) = 10^5$ cm^{-3}, and $n(para\text{-}H_2CS)/dV/dr = 10^{-5}$ cm^{-3} $(km\ s^{-1}\ pc^{-1})^{-1}$ and $n(ortho\text{-}H_2CS)/dV/dr = 3 \times 10^{-5}$ cm^{-3} $(km\ s^{-1}\ pc^{-1})^{-1}$.

TABLE 5.3

H_2CS Abundances

Source	N(para) ($\times 10^{13}$ cm^{-2})	N(ortho) ($\times 10^{13}$ cm^{-2})	$\frac{N(ortho)}{N(para)}$	$f(H_2CS)$[a]
		LVG Model Results		
TMC-1	0.54 ± 0.06	0.97 ± 0.04	1.8 ± 0.3	2 (-9)
TMC-1(NH_3)	0.29 ± 0.04	0.49 ± 0.06	1.7 ± 0.4	8 (-10)
Orion(KL)	17 ± 2	30 ± 4	1.8 ± 0.5	2-5 (-9)
Orion(3N1E)	0.73 ± 0.04	2.2 ± 0.3	3.0 ± 0.6	4 (-10)
		Results by Assuming Optically Thin Emission		
TMC-1	0.85 ± 0.06	1.6 ± 0.2	1.9 ± 0.4	3 (-9)
TMC-1(NH_3)	0.54 ± 0.12	0.71 ± 0.17	1.3 ± 0.6	1 (-9)
L134N	——	0.23 ± 0.05	——	~ 5 (-10)[b]
L134N(SO)	——	≤0.26	——	≤ 5 (-10)[b]
Orion(KL)	27 ± 13	45 ± 6	1.7 ± 1.0	2-7 (-9)
Orion(3N1E)	0.91 ± 0.09	2.5 ± 0.3	2.8 ± 0.6	5 (-10)
NGC7538(N)	0.86 ± 0.10	2.8 ± 0.4	3.3 ± 0.8	5 (-10)
NGC7538(S)	1.6 ± 0.2	6.3 ± 0.5	3.9 ± 0.8	1 (-9)

[a] Fractional abundance of H_2CS relative to H_2. Hydrogen total column densities $N(H_2) \sim 10^{22}$ cm^{-2} for TMC-1 (Irvine *et al.* 1987;

(Continued on next page)

TABLE 5.3

(Continued)

Friberg and Hjalmarson 1989); ~ 1-3 x 10^{23} cm^{-2} for Orion(KL) (Johansson *et al.* 1984; Blake *et al.* 1987; Irvine, Goldsmith, and Hjalmarson 1987); ~ 0.6-1 x 10^{23} cm^{-2} for Orion(3N1E) (Smith *et al.* 1979); ~ 8.2 x 10^{21} cm^{-2} for L134N (Swade 1987; assuming $N(C^{18}O)/N(H_2) = 1.7 \times 10^{-7}$); ~ 8 x 10^{22} cm^{-2} for NGC7538(N) and (S) (Campbell and Thompson 1984).

[b] Ortho-to-para ratio of 1.5:1 was assumed.

Note: Error values in LVG results are either 1 σ values or most probable regions crossed by the observed brightness temperatures, while those in results derived by assuming optically thin emission are 1 σ values.; Rotational temperature of 5 K has been assumed for TMC-1 and L134N, 60 K for Orion(KL), and 15 K for Orion(3N1E) to derive the abundances from the observed integrated antenna temperatures in the optically thin case.

their line strengths) for ortho-H_2CS, and the results are consistent with those found from the LVG analysis (see Table 5.3).

For the Orion(3N1E) position, we have assumed that the source fills the telescope beam and a kinetic temperature of 20 K (cf. Goldsmith *et al.* 1986; Wilson and Walmsley 1989) for the model calculation. The optical depths and excitation temperatures derived from the LVG analysis are included in Table 5.2 and column densities in Table 5.3, in which we also include the column densities derived by assuming optically thin emission and a rotational temperature of 15 K.

The optical depths for the transitions observed in Orion seem to be very small, as given in Table 5.2. Abundances derived from the LVG analysis for both Orion(KL) and Orion(3N1E) agree quite well with those derived by assuming optically thin emission (within a factor of 2), and the ortho-to-para ratios are very similar.

An ortho-H_2CS column density in L134N has been derived assuming optically thin emission and of a rotational temperature of 5 K (Swade 1987); we assumed an ortho-to-para ratio of 1.5 to derive the total column density, because our observations were limited to one transition.

We include in Table 5.3 data for NGC7538(N) and (S) derived using the optically thin approximation and assuming a rotational temperature of 20 K (Snell and Wootten 1984). The NGC7538 molecular cloud is a very active star-forming region and shows a very complicated structure, including OH and H_2O masers,

high-velocity outflows and several IR sources (e.g. Wynn-Williams, Werner, and Wilson 1974; Werner *et al.* 1979; Campbell and Thompson 1984; Kameya *et al.* 1989; and see referneces therein). The resolution of our H_2CS observations is too poor to discern any relationships with smaller scale structures.

5.5 Discussion

The cold dark clouds TMC-1 and L134N have similar temperature, density, and mass, but have some interesting chemical differences. Carbon-rich species and CS and HCS^+ are more prominent in TMC-1 than in L134N, while SO and SO_2 are higher in L134N, which may result from, for example, different gas phase elemental abundances or from differing cloud ages (Irvine, Goldsmith, and Hjalmarson 1987). This pattern is reflected in our present results.

We derive a total column density $N(H_2CS) \sim 1 - 2 \times 10^{13}$ cm^{-2} for the TMC-1 cyanopolyyne peak and the ammonia peak, which corresponds to a fractional abundance of H_2CS relative to H_2, $f(H_2CS) \sim 1 - 2 \times 10^{-9}$ for $n(H_2) \sim 10^{22}$ cm^{-2} (see references in Table 5.3). The H_2CS abundance in L134N is about a factor of 5 less than that in TMC-1. The result for TMC-1 agrees quit well with the prediction of "pseudo-time-dependent" models (Herbst and Leung 1986a,b; Millar and Herbst 1989) at the "early time" which produces best agreement between the model and observations for many heavier organic molecules. The model predicts a lower H_2CS

abundance at steady state, which would be consistent with L134N being more chemically evolved than TMC-1.

On the other hand, Duley, Millar, and Williams (1980) have suggested grain surface formation for H_2CS and H_2S, and if carbon abundance is high, H_2CS would be expected to form instead of H_2S. Indeed, the abundances of H_2CS have been observed to be high where those of H_2S are low in L134N and TMC-1 (this paper and Minh, Irvine, and Ziurys 1989).

The initial ortho-to-para ratios are expected to be the statistical value 3, since gas-phase (or grain-surface) formation reactions release large reaction heats compared to the energy difference between the lowest ortho and para states (~ 15 K for H_2CS and H_2CO). We derive instead ~ 1.8 at both the TMC-1 cyanopolyyne peak and the ammonia peak, which may suggest thermalization on 10 K grains and hence an efficient interchange between the grains and the gas phase. Kahane *et al.* (1984) derived essentially the same value for H_2CO in dark clouds, although the observed lines of H_2CO are severely self-absorbed, and had to be interpreted with the aid of a radiative transfer model. It is significant that we confirm their results for the ortho-to-para ratios in cold dark clouds by using H_2CS lines which are optically thin.

In Orion(KL), we derive an ortho-to-para ratio ~ 2, which is much smaller than the statistical value 3, while KFLEL derive ~ 3 for H_2CO after correcting for the radiative transfer effects. Gardner *et al.* (1985) derive ~ 3 in Orion(KL) by using the same H_2CS

transitions as we use. Gardener *et al.*'s spectra, obtained using the Bell Lab's 7 m telescope, are fairly different compared to ours in Figure 5.1, which may result from the different beam sizes between the two telescopes. The small H_2CS ortho-to-para ratio in the Orion compact ridge cannot be explained by thermalization in the gas phase or on the grains, because the expected kinetic temperature for the Orion compact ridge is on the order of 100 K. We have examined the ortho-to-para ratio with the H_2CS J = 7 - 6 transitions observed in the spectral survey of Sutton *et al.* (1985) and derived an ortho-to-para ratio ~ 2.1 from a least square fit of the data, assuming optically thin emission. These data thus support our present result. The reason for small values is not certain. Since the outflow materials from IRc 2 are believed to be interacting with surrounding quiescent clouds in the compact ridge, our small ortho-to-para ratio may result from the non-equlibrium condition of the H_2CS excitation. The physical and chemical conditions for the compact ridge should be studied further.

For the Orion(3N1E) position, if H_2CS is thermalized on grains at ~ 20 K, we expect the ortho-to-para ratio to be ~ 2.7, which is close to the derived values of 2.8 - 3.0. We derive roughly ~ 3 - 4 for the NGC7538(N) and (S) positions.

We may conclude that the H_2CS ortho-to-para ratio is thermalized at ~ 10 K by gas-grain interactions in cold dark clouds, while it becomes the statistical value ~ 3 in warmer regions. These results thus support the idea of exchange of material between

grain surfaces and the gas phase in at least the cold clouds, which must indeed be present to prevent a nearly complete "freeze out" of gas phase molecules during expected cloud life times (e.g. Leger, Jura, and Omont 1985). It is curious that so little other evidence for this expected phenomenon exists.

CHAPTER 6

UPPER LIMITS FOR THE ETHYL CYANIDE ABUNDANCES IN TMC-1 AND L134N

6.1 Summary

We have sought interstellar ethyl cyanide via its $2_{02} - 1_{01}$ transition towards two cold, dark clouds and report upper limits of the total column densities of 3×10^{12} cm^{-2} and 2×10^{12} cm^{-2} for TMC-1 and L134N, respectively. These values are lower than previous limits. We observed the $2_{02} - 1_{01}$ transition of vinyl cyanide previously identified in TMC-1 by Matthews and Sears (1983b). The detection of vinyl cyanide and the non-detection of ethyl cyanide in TMC-1 are consistent with gas phase ion-molecule chemical models, and there is thus no necessity of invoking grain surface synthesis for vinyl cyanide in cold clouds.

6.2 Introduction

Grain surface reactions have been sometimes suggested to play an important role in the formation of gas-phase interstellar molecules (e.g. Millar 1982). Although there are a number of serious uncertainties in the grain surface reaction schemes, observations between 3 and 12 μm have identified several molecules in grain mantles (cf. Tielens and Allamandola 1987) which are

typically highly saturated. Large abundances of NH_3, HDO, HCN, and H_2S in the Orion hot core have also been regarded as an indication of grain mantle evaporation (Blake *et al.* 1987; Minh *et al.* 1989, see also Chapter 3).

Irvine and Hjalmarson (1984) and Blake *et al.* (1987) have pointed out large abundances of highly saturated molecules such as ethyl cyanide (CH_3CH_2CN) and vinyl cyanide (CH_2CHCN) in the Orion hot core, and suggested that they might result from hydrogenation of HC_3N on grain surfaces. Ion-molecule processes leading to the formation of CH_3CH_2CN are highly endothermic and proceed quite slowly (Herbst, Adams, and Smith 1983). The hydrogenation of HC_3N may proceed efficiently on the grain surfaces to form vinyl cyanide and ethyl cyanide, especially since there is no rearrangement in the CCCN frame. Blake *et al.* suggest that the observed ratios of $[HC_3N]/[CH_2CHCN]$ and $[HC_3N]/[CH_3CH_2CN]$ in the Orion extended ridge and the hot core indicate that the hydrogenation process prefers to saturate any cyanoacetylene deposited on the grain surface completely.

A detection of vinyl cyanide in the cold dark cloud TMC-1 (Matthews and Sears 1983) raises an interesting question. If vinyl cyanide has formed on the grain surfaces by hydrogenation of HC_3N and then desorbed to the gas-phase, why has ethyl cyanide not been detected in TMC-1 ? Grain surface molecules tend to be saturated, which would lead to an abundance ratio $[CH_3CH_2CN]/[CH_2CHCN] > 1$, as is the case in the Orion hot core. In this Chapter, we report good

upper limits for the ethyl cyanide abundance in TMC-1 and L134N and conclude that ion-molecule reactions may explain observed abundances of vinyl cyanide in cold, dark clouds.

6.3 Observations and Results

The observations were made in 1989 January, using the 43 m telescope of the NRAO for the $2_{02} - 1_{01}$ transitions of ethyl cyanide and vinyl cyanide. The half-power beam width was 1.5 arcminutes, and the beam efficiency (η_B) 0.40 at the observing frequency of 18 GHz. The temperature scale was determined using a noise diode and is given in terms of antenna temperature T_A. We approximate the brightness temperature by the main-beam brightness temperature T_{MB}, which is defined by $T_{MB} = T_A/\eta_B$. The maser receiver gave a system temperature of typically 70 K. The 1024 channel autocorrelation spectrometer was used with a spectral resolution of 9.8 kHz, and frequency-switching was employed. The observed line frequencies and positions are included in the notes of Table 6.1.

The column densities in the last column of Table 6.1 were determined using the "standard" equation (Irvine, Goldsmith, and Hjalmarson 1987), assuming statistical relative intensities for the hyperfine components, optically thin emission, and equilibrium at a rotational temperature of 5 K for both TMC-1 and L134N (cf. Matthews and Sears 1983b; Swade 1987). A correction for the cosmic background radiation has been included. For a Boltzmann population

TABLE 6.1

A Summary of Observations[a]

Molecule	Transition		T_A (mK)	ΔV (km s^{-1})	V_{LSR} (km s^{-1})	$\int T_A dV$ (mK km s^{-1})	N_{column} (cm^{-2})
			TMC-1				
CH_3CH_2CN	2_{02}-1_{01}	F=3-2	≤ 14[b]	—	—	—	≤ 3.4(12)[c]
CH_2CHCN	2_{02}-1_{01}	F=3-2	43	0.70	5.5	26	6.8(12)
		2-1	29	0.39	5.6	15	
			L134N				
CH_3CH_2CN	2_{02}-1_{01}	F=3-2	≤ 12[b]	—	—	—	≤ 2.2(12)[d]
CH_2CHCN	2_{02}-1_{01}	F=3-2	≤ 33[b]	—	—	—	≤ 4.2(12)[d]

[a] Spectral resolution is 9.8 kHz.

[b] 3 σ upper limit.

[c] 3 σ value and ΔV = 0.7 km s^{-1} were used.

[d] 3 σ value and ΔV = 0.5 km s^{-1} were used.

NOTE. - Position; TMC-1: RA(1950) = $4^h38^m38^s.6$, Dec(1950) = $25^\circ35'45"$; L134N: RA(1950) = $15^h51^m30^s.0$; Dec(1950) = $-2^\circ43'31"$.

Rest frequency; 17.8910 GHz for the CH_3CH_2CN (2_{02} - 1_{01}, F = 3 - 2) line (Lovas 1982); 18.966614 GHz and 18.966534 GHz for CH_2CHCN (2_{02} - 1_{01}) F = 3 - 2 and F = 2 - 1, respectively (Gerry, Yamada, and Winnewisser 1979).

distribution the total column density in dark clouds is rather insensitive to the assumed rotational temperature for values in the range 5 - 10 K (the latter being the approximate kinetic temperature in these sources).

Morever, since the dipole moments and molecular constants of ethyl cyanide and vinyl cyanide are quite similar (Poynter and Pickett 1984), we expect that the ratio of these column densities and hence the upper limit on CH_3CH_2CN relative to CH_2CHCN should be quite accurate. The abundances ratios of ethyl cyanide and vinyl cyanide relative to HC_3N are listed in Table 6.2 towards TMC-1, L134N and Orion(KL), including the results of previous publications.

However, the absolute abundances may be slightly affected by the existence of both a- and b-components of the electric dipole moment (μ) for both ethyl and vinyl cyanide. The existence of b-type transitions tends to drain the population from states with $K_a \geq 1$ into lower K-ladders, tending to produce a non-equilibrium population distribution. However, the abundance ratio of these two species is expected to remain essentially unchanged since both μ_a and μ_b are very similar.

Matthews and Sears (1983a) obtained an upper limit on the abundance of CH_3CH_2CN ($\leq 5 \times 10^{12}$ cm^{-3}) by observing its $1_{10} - 2_{11}$ transition and assuming an LTE population distribution. For the reasons given in the preceding paragraph, we think their result is somewhat uncertain since transitions in the $K_a = 1$ ladder were used.

TABLE 6.2

Abundance Ratios

Source	$\frac{[CH_3CH_2CN]}{[HC_3N]}$	$\frac{[CH_2CHCN]}{[HC_3N]}$	$\frac{[HC_3N]}{[H_2]}$	References
TMC-1	≤ 0.02	0.05	1 (-8)	1, 2
L134N	≤ 0.4	≤ 0.8	7 (-10)	3
Orion hot core	6.5	1.0	2 (-9)	2, 4

References: (1) Irvine and Schloerb (1984), (2) Irvine *et al.* (1985), (3) Swade (1987), (4) Blake *et al.* (1987)

The vinyl cyanide abundance obtained by Matthews and Sears (1983b) is about a factor of two less for TMC-1 than that in Table 6.1. The reason for this difference is unclear, but conceivably is related to the improved efficiency of the 43 m antenna in recent years (R. Maddalena, private communication).

6.4 Discussion

The large enhancements of ethyl cyanide and vinyl cyanide in the Orion hot core relative to the quiescent ridge have been interpreted as indicating that hydrogenation of HC_3N on grain surfaces must be efficient (Blake *et al.* 1987). Although the gas-phase reactions leading to the formation of HC_3N are still controversal (Herbst 1988), the large observed abundance of HC_3N in TMC-1 (Irvine and Schloerb 1984) might be expected to produce large abundances of vinyl cyanide and ethyl cyanide after "freezing out" on the grain mantles in TMC-1. Since grain surface molecules tend to be saturated, ethyl cyanide would probably be more abundant than vinyl cyanide, and this is the case for the Orion hot core. Curiously enough, only vinyl cyanide has been detected in TMC-1 (in the gas phase), and the present upper limit for the ethyl cyanide abundance is much less than that for the Orion hot core relative to vinyl cyanide (Table 6.2). Since the molecular weights of ethyl cyanide and vinyl cyanide are very similar, desorption processes should not be so different between these two species. Then we may

have to conclude that the vinyl cyanide observed in TMC-1 has not formed on grain surfaces.

Millar and Freeman (1984) have suggested that reactions of $C_3H_5^+$ with N followed by dissociative electron recombination could lead to the formation of vinyl cyanide, and their prediction agrees well with the observed abundance. But gas-phase reactions for the formation of ethyl cyanide are thought to be quite endothermic (Herbst, Adams, and Smith 1983). Therefore, purely gas-phase reactions are sufficient to explain the observed abundance of vinyl cyanide and the failure to detect ethyl cyanide in TMC-1. Moreover, since HC_3N is quite abundant in TMC-1 and would be expected to stick to grains in cold clouds and be hydrogenated, it appears that desorption processes are inefficient in TMC-1, at least for heavy molecules like CH_3CH_2CN and CH_2CHCN. This result is quite different than that obtained for H_2CS and H_2CO, for which the ortho/para ratio in dark clouds suggests efficient interchange between the grains and the gas phase (Minh, Irvine, and Brewer 1989; Kahane *et al.* 1984).

CHAPTER 7

OBSERVATIONS OF INTERSTELLAR $HOCO^+$: ABUNDANCE ENHANCEMENTS TOWARDS THE GALACTIC CENTER

7.1 Summary

A survey of the 4_{04} - 3_{03} and 1_{01} - 0_{00} transitions of $HOCO^+$ has been made toward several molecular clouds. The $HOCO^+$ molecule was not observed in any sources except Sgr B2 and Sgr A. The 5_{05} - 4_{04} and 4_{14} - 3_{13} transitions were also detected toward Sgr B2. The results indicate that gas phase CO_2 is not a major carbon reservoir in typical molecular clouds. In Sgr B2, the $HOCO^+$ antenna temperature exhibits a peak ~ 2 arcmin north of the Sgr B2 central position (Sgr B2[M]) and the 4_{04} - 3_{03} line emission is extended over a ~ 10′ x 10′ region. The column density of $HOCO^+$ at the northern peak in Sgr B2 is ~ 3×10^{14} cm^{-2}, and the fractional abundance relative to H_2 $\geq$ 3×10^{-10}, which is about two orders of magnitude greater than recent predictions of quiescent cloud ion-molecule chemistry.

7.2 Introduction

Herbst *et al.*(1977) have suggested that the abundances of molecules which lack permanent electric dipole moments and hence

rotational transitions in the millimeter spectral region, but which are important to the chemistry of the interstellar medium, may be estimated from observations of their protonated ions. An example of this approach is the investigation of molecular nitrogen from studies of its protonated form, N_2H^+ (Turner and Thaddeus 1977; Linke, Guélin, and Langer 1983).

The $HOCO^+$ molecule, the protonated form of CO_2, was first identified in the rich molecular cloud Sgr B2 by Thaddeus, Guélin, and Linke (1981), who determined the molecular rotational constants accurately from 3 harmonically related lines. The subsequent laboratory detection of this molecule by Bogey, Demuynck, and Destombes (1984) has confirmed this identification and the values of the rotational constants. The dipole moment of $HOCO^+$ is estimated to be 2 Debyes (Green *et al.* 1976). According to Herbst *et al.* (1977), $HOCO^+$ can be formed in molecular clouds via a standard ion-molecule reaction, transfer of a proton from H_3^+ to CO_2. Therefore, $HOCO^+$ might be widely distributed in interstellar sources if CO_2 were relatively abundant. Since only ~ 10 % of the cosmic abundance of carbon is contained in CO (Irvine and Knacke 1988), and simple hydrocarbons such as CH_4 are even less abundant (Knacke *et al.* 1985), CO_2 might be an important reservoir of interstellar carbon, and an observational determination of its abundance in molecular clouds is quite important.

The $HOCO^+$ ion has heretofore been observed in only one interstellar cloud, Sgr B2 (Thaddeus, Guélin and Linke 1981;

Cummins, Linke, and Thaddeus 1986), which is an extremely large giant molecular cloud with high mass star formation. The 4_{04} - 3_{03} transition of $HOCO^+$ at 85.6 GHz and several higher J transitions were readily detected toward Sgr B2(OH).(No other positions were observed in the cloud). If the chemical abundances in other clouds are similar to Sgr B2, emission lines of $HOCO^+$ should be detectable. Consequently, we conducted a search for $HOCO^+$ toward a variety of interstellar sources, and also mapped the 4_{04} - 3_{03} line over Sgr B2. The results of this study are presented here.

7.3 Observations

Observations of the 1_{01} - 0_{00} transition of $HOCO^+$ were taken with the NRAO 43 m telescope and K-band maser during January 1987. Telescope parameters are included in Table 7.1. The temperature scale was determined using a noise diode and is given in terms of antenna temperature T_A. The 1024 channel autocorrelation spectrometer was used, and either frequency - switching or beam - switching was employed.

Observations of the 4_{04} - 3_{03}, 4_{14} - 3_{13}, 4_{13} - 3_{12}, and 5_{05} - 4_{04} transitions were made using the FCRAO 14 m telescope between October 1986 and October 1987. Telescope parameters are included in Table 7.1. The receiver and spectrometers are described in Schloerb, Snell and Young (1983). The temperature scale was

TABLE 7.1

Telescope Parameters

Transition $J_{K_a K_c} - J'_{K'_a K'_c}$	Rest freq.[a] (GHz)	Telescope	HPBW[b] (arcsec)	η_A[c]	η_B[d]
$1_{01} - 0_{00}$	21.38280	NRAO 43 m	84	0.23	0.29
$4_{04} - 3_{03}$	85.53068	FCRAO 14 m	60	0.47	0.56
$4_{14} - 3_{13}$	85.231	FCRAO 14 m	60	0.47	0.56
$4_{13} - 3_{12}$	85.831	FCRAO 14 m	60	0.47	0.56
$5_{05} - 4_{04}$	106.91301	FCRAO 14 m	48	0.44	0.52

[a] from Bogey, Demuynck, and Destombes (1984)

[b] half power beam width

[c] aperture efficiency

[d] beam efficiency

determined by the standard chopper wheel method, and is given in terms of T_A^*. Observations were made by position switching.

Main beam brightness temperature T_R is then defined for both telescopes by $T_R = T_A/\eta_B$ or T_A^*/η_B, where η_B is the beam efficiency.

7.4 Results

7.4.1 Galactic Center Region

A study of a number of molecules in Sgr B2 by Goldsmith *et al.*(1987) suggests that the column densities of different species show major variations between two locations of local maxima: Sgr B2(M) at RA(1950) = $17^h44^m10^s.5$; DEC(1950) = - 28°22'05", and Sgr B2(N), ~ 45 arcsec north from Sgr B2(M). For example, SO is strongly peaked near Sgr B2(M) and OCS is concentrated around Sgr B2(N).

In contrast, our observations of $HOCO^+$ in the 4_{04} - 3_{03} transition show a peak at 2 arcmin north from Sgr B2(M), a position we shall refer to as Sgr B2(2N), with a peak intensity of T_A^* = 0.82 K. The spectra observed toward 0, 1, 2, and 3 arcmin north from Sgr B2(M) are shown in Figure 7.1. In all, we detected $HOCO^+$ in a region extended over 10' x 10'. The observed line parameters are given in Table 7.2, which also includes the integrated intensity of the CH_3CCH J = 5 - 4 transition (over all K components), simultaneously observed. Figure 7.2 shows a velocity versus

Figure 7.1 Spectra at 85.5 GHz obtained toward 0, 1, 2, and 3 arcmin north from Sgr B2(M). Spectral resolution is 1 MHz. The Sgr B2(M) position is RA(1950) = $17^h44^m9^s.5$ and Dec(1950) = $-28^\circ22'20''$. The ordinate is corrected antenna temperature, T_A^*. The velocity scale assumes the rest frequency of the $4_{04} - 3_{03}$ transition of $HOCO^+$ (Table 7.1).

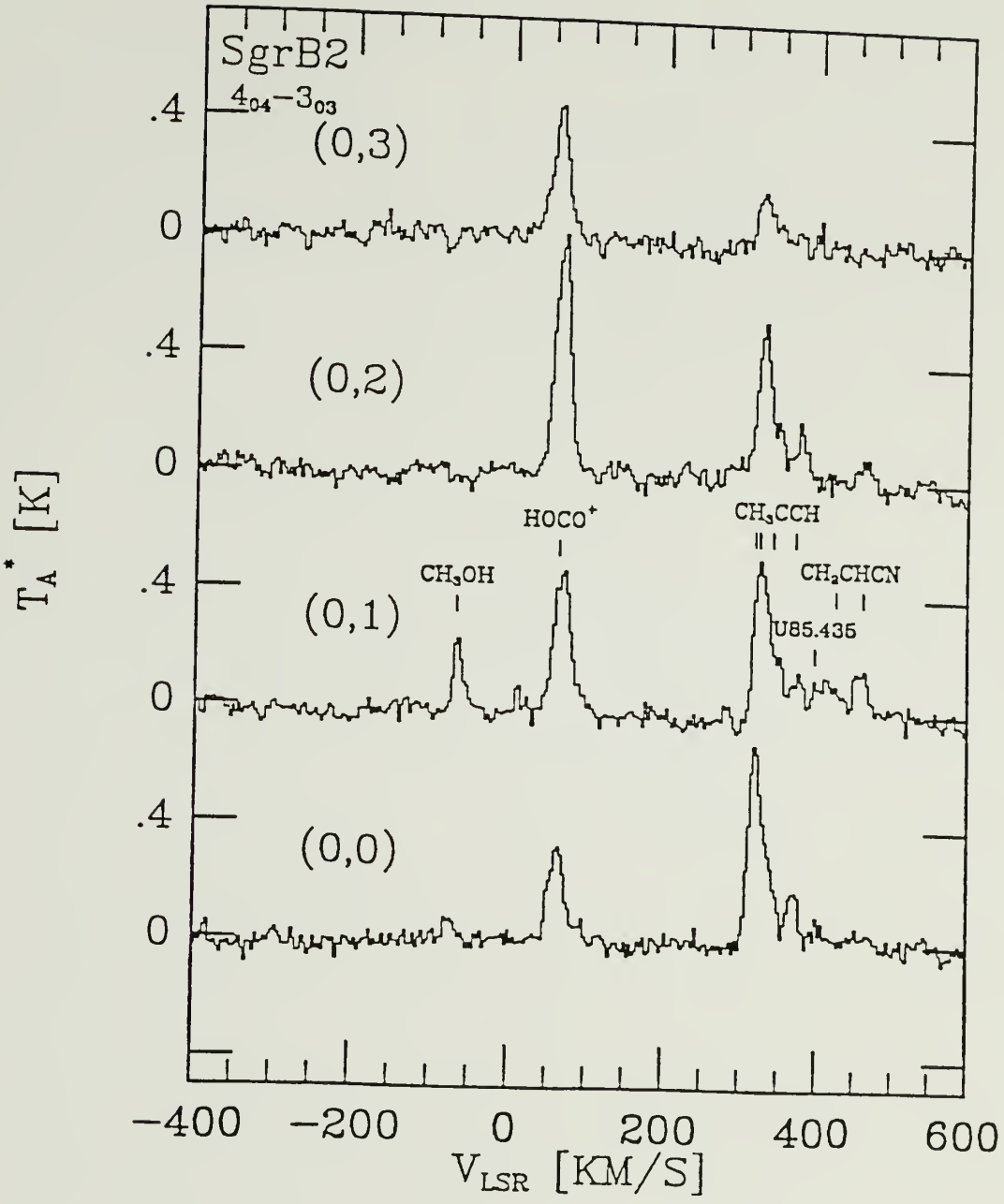
SgrB2
$4_{04}-3_{03}$
(0,3)
(0,2)
(0,1)
(0,0)
.4
0
HOCO+
CH3CCH
CH3OH
CH2CHCN
U85.435
T_A^* [K]
−400
−200
0
200
400
600
V_{LSR} [KM/S]

TABLE 7.2

Observed Parameters of the $4_{04} - 3_{03}$ transition at Sgr B2

Offset		T_A^*	ΔV	V_{LSR}	$\int T_A^* dV$	$\int T_A^*(CH_3CCH)dV$
$\Delta\alpha$	$\Delta\delta$	(K)	(km s^{-1})	(km s^{-1})	(K km s^{-1})	(K km s^{-1})
0′	0′[a]	0.33	27.3	63.8	9.0	24.7
0	1	0.48	27.4	70.8	13.0	23.9
0	2	0.82	24.7	67.3	20.2	20.8
0	3	0.46	27.3	60.3	12.6	5.9
0	4	0.25	20.1	60.3	5.0	1.0
0	5	0.11	12.6	53.2	1.3	3.0
0	-1	0.22	25.2	49.7	5.4	14.0
0	-2	0.23	24.9	60.3	5.7	10.2
0	-3	0.23	18.1	46.2	4.1	7.6
0	-4	0.14	24.7	53.2	3.4	6.0
1	0	0.25	23.2	56.7	5.9	11.6
1	1	0.33	17.8	60.3	5.9	10.7
1	2	0.70	23.3	60.2	16.3	17.0
1	3	0.37	27.9	56.7	10.3	3.7
-1	0	0.40	33.6	60.2	13.1	6.1
-1	1	0.51	30.5	67.3	15.7	9.5
-1	2	0.70	24.3	63.8	16.9	8.5
-1	3	0.41	26.2	56.7	10.8	4.7
2	2	0.28	21.8	60.3	6.2	3.7
3	2	0.21	22.3	56.7	4.7	5.7
4	2	0.24	17.3	53.2	4.2	4.5
5	2	0.24	17.9	49.7	4.3	2.4
6	2	0.13	9.7	49.7	1.3	1.8
-2	2	0.35	22.7	60.3	7.8	2.3
-3	2	0.25	21.4	42.7	5.5	3.0
-4	2	0.25	18.1	53.2	4.5	6.8
-5	2	0.18	20.5	56.7	3.7	2.6

[a] RA(1950) = $17^h44^m9^s.5$; DEC(1950) = - $28°22'20"$

Figure 7.2 Spatial-velocity map of $HOCO^+$ antenna temperature (T_A^*) for the $4_{04} - 3_{03}$ line along the N-S direction. The (0, 0) position is given in Figure 7.1. The contour levels are 0.3, 0.4, 0.5, 0.6, and 0.7 K.

6
4
2
0
−2
−4
−6
Δδ [arcminute]
20
40
60
80
100
v_{LSR} [km s^{-1}]

declination map along the N-S direction. There appears to be an increase in the peak velocity around the (2N) position, as well as an extended weak emission at velocities in the range of 40 - 80 km s^{-1}.

The 5_{05} - 4_{04} transition has been observed toward Sgr B2(M) and (2N), and also shows an enhancement at the (2N) position; line parameters are included in Table 7.3. In addition, the 4_{14} - 3_{13} and 4_{13}-3_{12} transitions of the K_a = 1 ladder were searched for at Sgr B2(M) and (2N). The frequencies of these transitions differ by only ≈ 300 MHz from the 4_{04} - 3_{03} transition. The 4_{14} - 3_{13} transition was detected at Sgr B2(2N), and the spectra observed toward Sgr B2(M) and (2N) are shown in Figure 7.3. The U-line at 85.231 GHz detected by Cummins, Linke, and Thaddeus (1986) seems to be the 4_{14} - 3_{13} transition of $HOCO^+$. The 4_{13} - 3_{12} transition was not detected down to a 3 σ limit of T_A^* = 60 mK.

The 4_{04} - 3_{03} and 5_{05} - 4_{04} transitions have been observed toward Sgr A (NH_3A), and their line parameters are included in Table 7.3. The 5_{05} - 4_{04} transition seems to be stronger than the 4_{04} - 3_{03} transition although the signal-to-noise ratio is not as good.

7.4.2 Other Sources

$HOCO^+$ was searched for via its 4_{04} - 3_{03} and 1_{01} - 0_{00} transitions toward several other molecular clouds, including active star formation regions such as Orion A and W51, and cold dark clouds

TABLE 7.3

A Summary of the $HOCO^+$ Survey

Source	R.A.(1950)	Decl.(1950)	ΔV [a] ($km\ s^{-1}$)	T_{rot} [a] (K)	Size [b] (pc)
W3(OH)	$2^h23^m16^s.8$	$61°38'57''$	6.0	20	1.0
TMC-1	4 38 38.6	25 35 45	1.0	6	0.2
TMC-2A	4 28 54.0	24 26 27	1.0	6	0.2
Ori-A(KL) ..	5 32 46.8	- 5 24 25	3.0	25	0.7
	5 32 51.0	- 5 20 20	2.5	25	0.7
IC443B	6 14 15.0	22 26 50	10.0	15	0.5
NGC2264	6 38 25.0	9 32 29	2.0	7	0.9
L134N	15 51 32.0	- 2 40 30	0.5	5	0.3
	15 51 26.0	- 2 43 31	0.5	5	0.3
ρ Oph A	16 23 25.0	-24 15 49	0.6	7	0.2
ρ Oph B	16 23 25.0	-24 20 40	0.4	7	0.2
W49	19 07 49.0	9 01 28	15.0	25	3.0
W51	19 21 27.0	14 24 30	10.0	25	1.5
B335	19 34 35.0	7 27 30	0.8	10	1.0
DR 21(OH) ..	20 37 14.0	42 12 00	3.0	20	0.9
Cep MC-1 ...	22 54 24.4	61 45 43	4.5	25	1.0
NGC7538	23 11 37.0	61 10 00	4.0	20	1.0
Sgr A	17 42 28.0	-29 01 30	18.7 24.3	15	8.0
Sgr B2(M) ..	17 44 09.5	-28 22 20	27.3 22.5	13.2	10.0
Sgr B2(2N) .	17 44 09.5	-28 20 20	24.7 22.7	13.4	10.0

(Continued on next page)

TABLE 7.3

(Continued)

Source	T_A^{*} [c,d] $4_{04} - 3_{03}$ / $5_{05} - 4_{04}$	T_A [c] $1_{01} - 0_{00}$	$N(HOCO^+)$ [e] (cm^{-2})	$\frac{[CO_2]}{[CO]}$ [f]	References
W3(OH)	≤ 0.04 [g]	—	≤ 4.7(12)	≤ 0.01	1, 2
TMC-1	≤ 0.05 [h]	≤ 0.03	≤ 4.3(12)	≤ 0.04	3, 4
TMC-2A	≤ 0.11 [h]	—	≤ 1.2(12)	≤ 0.01	
Ori-A(KL) ..	≤ 0.07 [i]	—	≤ 5.2(12)	≤ 0.02	5
	≤ 0.06 [i]	—	≤ 3.7(12)	≤ 0.01	5
IC443B	—	≤ 0.02	≤ 5.1(13)	≤ 0.21	
NGC2264	≤ 0.11 [h]	≤ 0.02	≤ 6.1(12)	≤ 0.01	2, 6, 9
L134N	≤ 0.06 [h]	≤ 0.04	≤ 2.8(12)	≤ 0.02	8
	—	≤ 0.03	≤ 2.1(12)	≤ 0.01	8
ρ Oph A	≤ 0.05 [i]	≤ 0.08	≤ 9.8(12)	≤ 0.10	2, 6, 9
ρ Oph B	—	≤ 0.08	≤ 6.5(12)	≤ 0.07	2, 6, 9
W49	≤ 0.04 [g]	—	≤ 1.9(12)	≤ 0.001	7
W51	≤ 0.06 [i]	—	≤ 1.9(12)	≤ 0.001	4
B335	—	≤ 0.06	≤ 7.6(12)	≤ 0.02	10
DR 21(OH) ..	≤ 0.03 [g]	≤ 0.02	≤ 1.8(12)	≤ 0.01	2, 6, 9
Cep MC-1 ...	≤ 0.03 [g]	—	≤ 3.3(12)	≤ 0.01	6
NGC7538	≤ 0.08 [g]	≤ 0.03	≤ 6.3(12)	≤ 0.01	1, 2
Sgr A	0.08 [g]	—	2.3(13)	0.006	9
	0.23 [g,j]				
Sgr B2(M) ..	0.33 [g]	—	1.2(14)	0.02	10
	0.39 [g]				
Sgr B2(2N) .	0.82 [g]	—	2.8(14)	0.06	
	0.71 [g,j]				

(Continued on next page)

TABLE 7.3

(Continued)

[a] Values of ΔV and T_{rot} are assumed, except ΔV for Sgr A and Sgr B2, and T_{rot} for Sgr B2, which were measured.

[b] Assumed to calculate the volume density of $HOCO^+$ for $[CO_2]/[CO]$.

[c] Upper limits are 3 σ.

[d] The $4_{04} - 3_{03}$ transition except for values indicated by footnote j.

[e] Assumes source fills main beam. Integrated intensities were used for Sgr A and Sgr B2.

[f] $[CO]/[H_2] \sim 8 \times 10^{-5}$ was assumed.

[g] Observed with 1 MHz resolution.

[h] Observed with 100 kHz resolution.

[i] Observed with 250 kHz resolution.

[j] The $5_{05} - 4_{04}$ transition.

References. - (1) Andersson 1985; (2) Snell and Wootten 1979; (3) Schloerb, Snell, and Young 1983; (4) Askne *et al.* 1984; (5) Turner and Thaddeus 1977; (6) Vanden Bout *et al.* 1983; (7) Scoville and Solomon 1973; (8) Swade 1987; (9) Güsten, Walmsley, and Pauls 1981; (10) Irvine, Goldsmith, and Hjalmarson 1987.

Figure 7.3 Spectra observed at 85.2 GHz (4_{14} - 3_{13}) toward Sgr B2(M) and (2N). The (0,0) position is given in Figure 7.1. The resolution is 1 MHz.

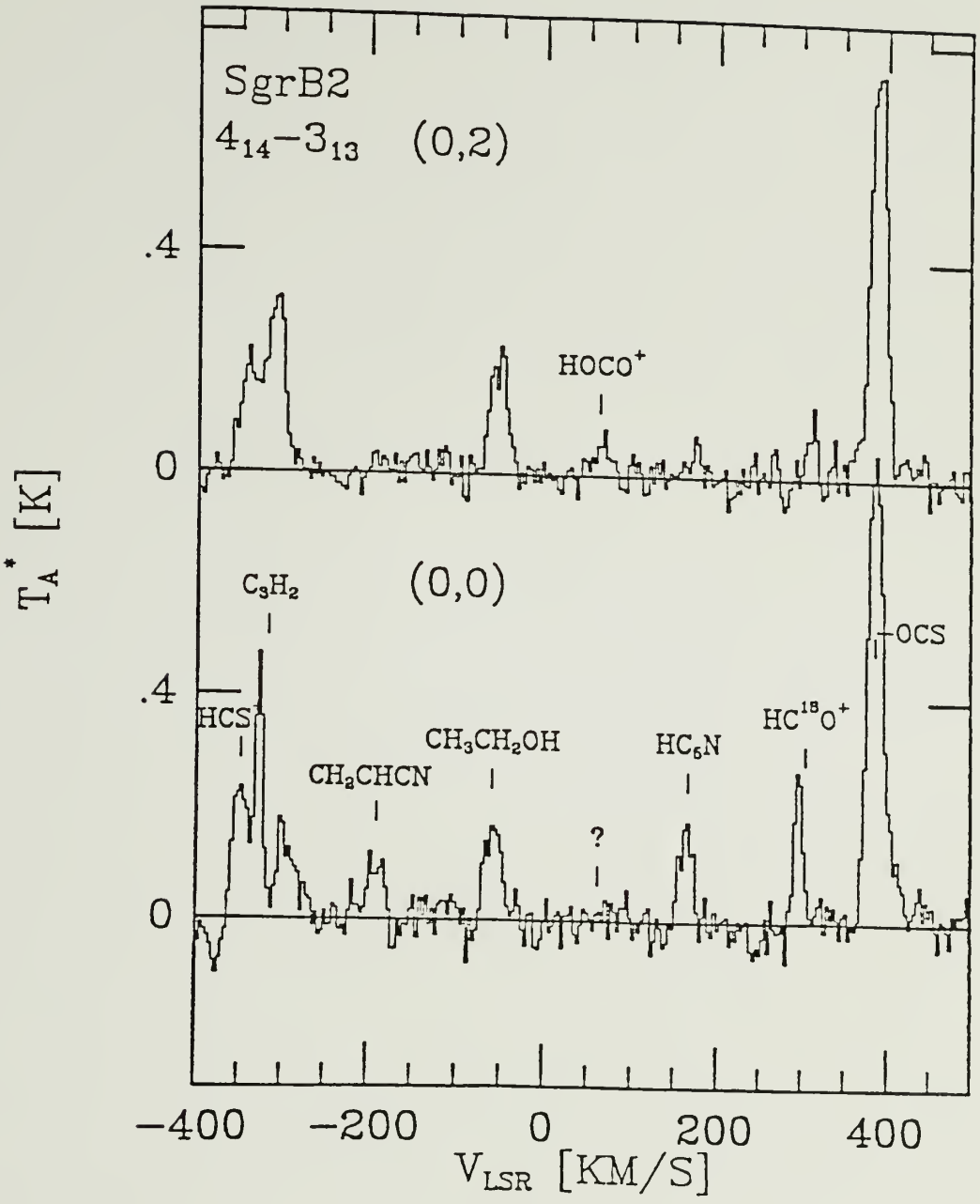
SgrB2
$4_{14}-3_{13}$ (0,2)
.4
0
$HOCO^+$
T_A^* [K]
C_3H_2
(0,0)
.4
HCS
CH_2CHCN
CH_3CH_2OH
?
HC_5N
$HC^{18}O^+$
OCS
0
−400
−200
0
200
400
V_{LSR} [KM/S]

such as TMC-1. However, no lines were detected in any of these other sources. A summary of the observations is given in Table 7.3.

7.5 Discussion

7.5.1 Column Densities and Abundances

Values and upper limits of the $HOCO^+$ column density given in Table 7.3 were determined from the following equation, assuming optically thin emission,

$$N(HOCO^+) = 2\pi \nu^2 k \Delta V T_R / h c^3 f A$$

where ν is the line frequency, f the fractional population in the upper level of the transition, ΔV the FWHP linewidth, T_R the brightness temperature assuming the source fills the main beam, and A the Einstein spontaneous emission coefficient (cf. Irvine, Goldsmith, and Hjalmarson 1987). The Einstein A coefficient for the $4_{04} - 3_{03}$ was taken to be 1.31×10^{-5} s^{-1} (Herbst *et al.* 1977). Column densities were calculated using the $4_{04} - 3_{03}$ transition for "warm" sources , and $1_{01} - 0_{00}$ for cold clouds ($T_{kin} \leq 10$ K) with the correction term for background radiation, $[1-T_{BG}/T_{EX}]^{-1}$. The fractional population of the upper level of the transition, f, is estimated using the asymmetric top partition function of $HOCO^+$, assuming a Boltzmann distribution. The rotational temperature T_{ROT}

is assumed to be equal to that found for other large dipole moment molecules and is given in the 5th column of Table 7.3. Approximate upper limits on the $[CO_2]/[CO]$ ratio, given in the last column of Table 7.3, are derived from equation (4) of Herbst *et al.* (1977). This equation results from balancing the expected major formation and destruction reactions of $HOCO^+$:

$$[CO_2]/[CO] \approx 7.7 \times 10^7 \, [HOCO^+] \, [CO]/[H_2],$$

where the square brackets signify volume density and $[CO]/[H_2]$ has been assumed to be a constant (8×10^{-5}) throughout all clouds in Table 7.2. The volume densities of $HOCO^+$ have been calculated from the assumed source sizes given in column 6 of Table 7.3.

The negative results for $HOCO^+$ in molecular clouds other than Sgr B2 and Sgr A are consistent with the small fractional abundance of $HOCO^+$ predicted by quiescent ion-molecule gas-phase chemistry. For example, Herbst and Leung (1986) predict $f(HOCO^+) \sim 10^{-11}$-10^{-12}, for a cloud with $n \sim 2 \times 10^3$ cm^{-3} and $T \sim 10$ - 50 K for their low metal model. They find $f(HOCO^+) \sim 6 \times 10^{-13}$ for a cloud of $n \sim 4 \times 10^5 cm^{-3}$ and $T \sim 50$ K. In comparison, we derive a fractional upper limit to the abundance of $HOCO^+$ of $f < 4 \times 10^{-10}$ for TMC-1, and $f < 5 \times 10^{-11}$ for Orion(KL) (quiescent component), using values of $N(H_2)$ from Irvine, Goldsmith, and Hjalmarson (1987). Such limits to the $HOCO^+$ fractional abundances typically imply $[CO_2]/[CO] < 0.01$-0.1 (see Table 7.3). Thus, CO_2 does not appear to be a major

repository for carbon in molecular clouds (usually in quiescent clouds about 10 % of the cosmic complement of carbon is in CO ; cf. van Dishoeck and Black, 1988; Irvine and Knacke, 1988).

In contrast, towards Sgr B2(2N) the column density of $HOCO^+$ is about 2.8×10^{14} cm^{-2}, derived from the rotational diagram of Figure 7.4. If we assume $N(H_2) < 10^{24}$ cm^{-2} (a likely upper limit; D.Lis, private comm. based on $C^{18}O$ and 1mm continuum data), then $f(HOCO^+) > 3 \times 10^{-10}$, which is about two orders of magnitude greater than the predictions of gas-phase ion-molecule chemistry. This abundance implies a $[CO_2]/[CO]$ ratio of > 0.06 using the model of Herbst *et al.* (1977). Although quite uncertain, this value is about two orders of magnitude larger than those estimated from models of ion-molecule chemistry ($[CO_2]/[CO] \sim 10^{-3}$; Herbst and Leung 1986). Moreover, the average $HOCO^+$ column densities over 3 x 4 arcmin in Sgr B2 are $\sim 1 \times 10^{14}$ cm^{-2} for $T_{ROT} \sim 15$ K, which implies that such high abundances exist over an extended region. One explanation of such a high $[CO_2]/[CO]$ ratio might be an oxygen to carbon abundance that is much larger than the "cosmic" value. Another possible reason might be an increase in the low energy cosmic-ray flux, which is suggested by Güsten, Walmsley, and Pauls (1981) in the galactic center region. This would increase the H_3^+ abundance and consequently produce a larger $HOCO^+$ abundance. We note, however, that the chemical abundances for both neutral and ionized species, including those containing oxygen and carbon, appear to be fairly uniform between Sgr B2 and other typical molecular clouds (Irvine,

Figure 7.4 Rotational diagrams for $HOCO^+$ observed toward Sgr B2(M), Sgr B2(2N) and Sgr A. In the ordinate (see Irvine, Goldsmith, and Hjalmarson 1987)
$I = [1.94 \times 10^3 \nu^2(GHz)/ A_{UL} g_U \eta_B] \int T_A^* dV(km\ s^{-1})$. The rotational temperature of 13.2 K at Sgr B2(M) is derived from the 4_{04} - 3_{03} and 5_{05} - 4_{04} transitions, while T_{ROT} = 13.4 K at Sgr B2(2N) is the best least square fit including also the 4_{14} - 3_{13} transition. Error bars are 3 σ.

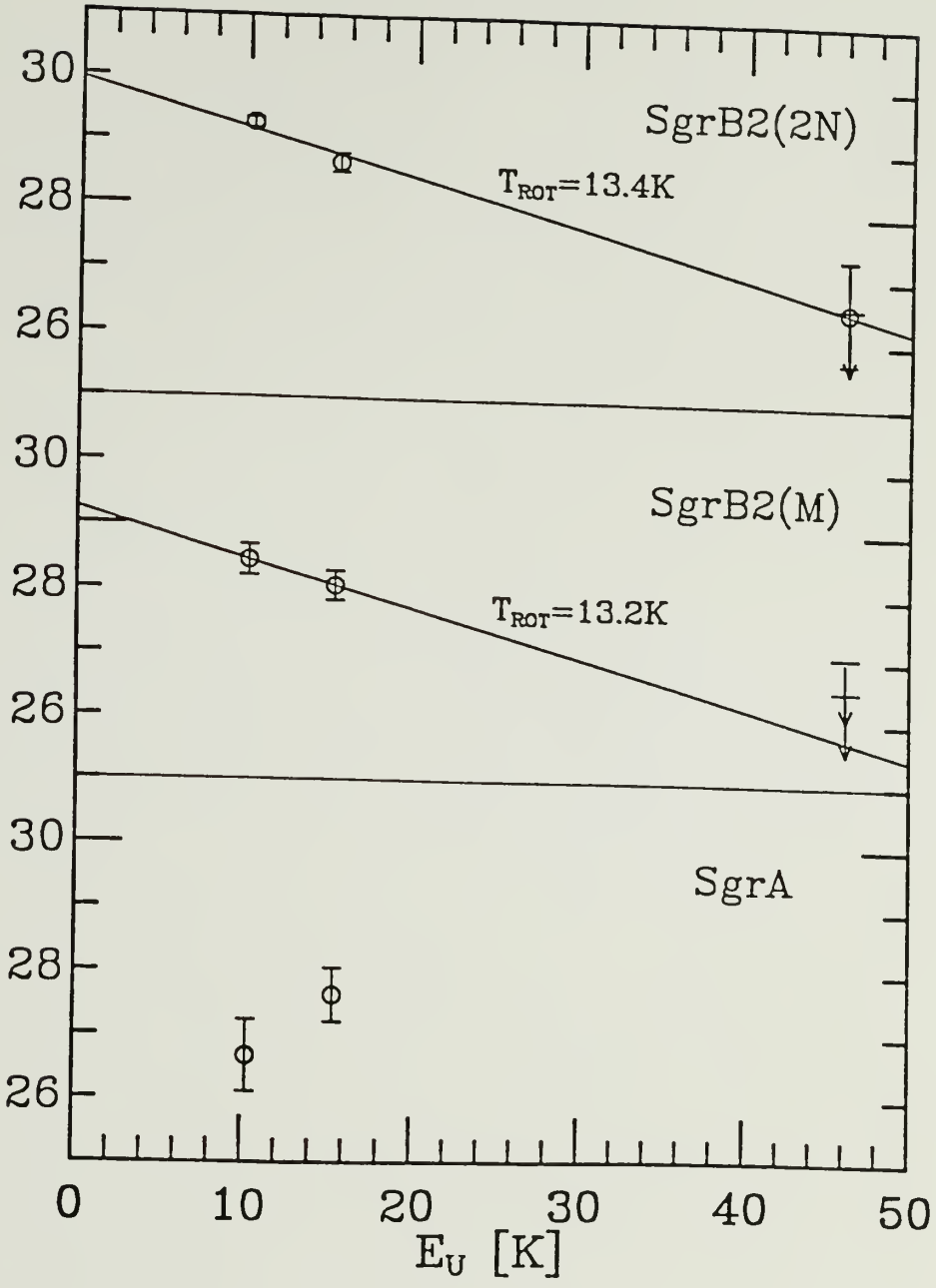
SgrB2(2N)
T_{ROT}=13.4K
SgrB2(M)
T_{ROT}=13.2K
SgrA
30
28
26
0
10
20
30
40
50
E_U [K]
$\mathcal{L}n$ I

Goldsmith, and Hjalmarson 1987). This is true for example, for both CO and HCO^+, as estimated from their ^{18}O isotopes.

7.5.2 Excitation versus Chemistry

Could the enhanced $HOCO^+$ emission be an effect of excitation rather than an abundance anomaly ? Indeed, it is interesting that $HOCO^+$ peaks at the 2N position, where HNCO is known to have an emission maximum (Churchwell *et al.* 1986), while most other known molecules tend to peak further south (Goldsmith *et al.* 1987). $HOCO^+$ is similar in structure to HNCO, both species being slightly asymmetric tops with comparable a- and b-dipole moments. It has been suggested by Churchwell *et al.* (1986) that HNCO emission in Sgr B2 is enhanced by far-infrared excitation and subsequent decay via fast b-type transitions. Perhaps such a mechanism applies to $HOCO^+$ as well as HNCO at the Sgr B2(N) position, and accounts for their enhanced emission there. However, at present there is little evidence for an embedded source at the 2N position, such as a compact HII region which might heat the dust and supply the necessary IR radiation (S.N.Vogel, private communication). Also, if we estimate the dust temperature at Sgr B2(2N) from the observed flux at 100 μm (Gatley *et al.* 1978) and 350 μm (Righini, Simon, and Joyce 1976), we find $T_{dust} \sim 16$ K, which is not particularly hot.

Perhaps the greatest argument against anamolous excitation of $HOCO^+$ mimicking an enhanced abundance is the fact that the species

appears to have quite a high concentration at positions extending over several arc minutes. As Table 7.2 shows, even at positions several arc minutes away from Sgr B2(2N) the integrated intensities do not vary more than a factor of two. Therefore, in order to invoke excitation as the cause of the enhanced $HOCO^+$ emission in Sgr B2, a mechanism would have to be found that is fairly general and could occur over extended regions. Infrared excitation is thus unlikely, although some collisional process might conceivably be possible. It is therefore most probable that the large column density of $HOCO^+$ in Sgr B2 is a result of chemistry. Why the physical and chemical conditions favor the production of this ion in this source , and not in other sources, is unknown. Further studies of $HOCO^+$ are certainly necessary in order to answer this question.

CHAPTER 8

ABUNDANCES AND CHEMISTRY OF INTERSTELLAR $HOCO^+$

8.1 Summary

We derive $HOCO^+$ column densities ~ 10^{15} cm^{-2} towards the Galactic center and $\leq 10^{12}$ cm^{-2} for cold dark clouds using a statistical equlibrium and LVG model. A map of $HOCO^+$ in its 4_{04} - 3_{03} transition has been obtained toward neutral gas clouds in Sgr A. The fractional abundance of $HOCO^+$ in the Galactic center region is found to be about three orders of magnitude larger than that predicted by quiescent ion-molecule chemistry and about an order of magnitude larger than predicted by a MHD shock model. If $HOCO^+$ traces interstellar CO_2, the implied high abundance ($[CO_2]$ ~ $[CO]$) in the Galactic center may result from the UV photolysis of grain mantles.

8.2 Introduction

The $HOCO^+$ molecule, the protonated form of CO_2, has been suggested as a tracer of interstellar CO_2 (Herbst *et al.* 1977). Although CO_2 is conceivably an important carbon and oxygen reservoir in the dense interstellar medium, determination of its abundance by radio astronomical techniques is hindered by its lack of a permanent

electric dipole moment. Searches for interstellar $HOCO^+$ have been made by Thaddeus, Guélin, and Linke (1981) and Minh, Irvine, and Ziurys (1988; Paper 1; Chapter 7). $HOCO^+$ has been detected only in the Galactic center region and appears to have quite a high concentration at positions extending over several arcminutes in Sgr B2. The large column density of $HOCO^+$ in Sgr B2 may be a result of chemistry which is peculiar to the Galactic center (Paper 1). In this Chapter we report the results of observations of $HOCO^+$ toward the Sgr A molecular cloud complex, derive $HOCO^+$ abundances using an LVG model for Sgr A and the sources in Paper 1, and discuss the chemical implications.

8.3 Observations and Results for Sgr A

Data for the $4_{04} - 3_{03}$ and $5_{05} - 4_{04}$ transitions of $HOCO^+$ were obtained in 1988 June with the Swedish-ESO 15 m diameter submillimeter wavelength telescope (SEST) on La Silla in the Chilean Andes. A cryogenic Schottky diode mixer receiver with a quasi-optical beam transporting system was employed. The relevant telescope parameters and the system temperatures are included in Table 8.1. Spectra were detected with the wide band acousto-optic spectrometer of 0.69 MHz resolution and 728 channels. Since molecular line emission observed toward Sgr A is well confined and elongated along the Galactic plane, data were obtained by double beam switching with the beam separation being approximately 12′ on

TABLE 8.1

Telescope Parameters at SEST [a]

Parameters	86 GHz	110 GHz
Aperture Efficiency	0.63 ± 0.04	0.58 ± 0.04
Main Beam Efficiency	0.73 ± 0.04	0.68 ± 0.04
HPBW (arcsec)	55.6 ± 1	43.5 ± 1
System Temperature (K SSB)[b]	~ 340	~ 380

[a] From Booth *et al.* (1989).

[b] From present observations.

the sky. The basic calibration was accomplished by the standard chopper wheel method, which provides the antenna temperature, T_A^*, corrected for atmospheric attenuation and certain telescope losses. We then approximate the radiation temperature T_R by the main beam brightness temperature $T_{MB} = T_A^*/\eta_B$, where η_B is the antenna main beam efficiency.

The Sgr A region shows a complicated structure in both ionized and neutral gas, and is reviewed in detail by Oort (1977) and Brown and Liszt (1984). The Sgr A molecular complex is composed of several "condensations" of masses greater than 10^5 $M_\odot$ (Armstrong and Barrett 1984). Although these "condensations" appear to be related, the geometry and dynamics are still controversal (Brown and Liszt 1984). The molecular abundances and chemistry of the Sgr A region, however, have not been as well characterized as those of the Sgr B2 molecular cloud complex. The total column density toward the Sgr A molecular complex is about a factor of 10 less than that toward the Sgr B2 complex.

A map of T_A^* for the $HOCO^+$ 4_{04} - 3_{03} transition was obtained on a 1' grid, totaling 150 points which are indicated as dots beneath the contour map in Figure 8.1a. Figure 8.1b shows the corresponding integrated intensity map, and Figure 8.1c shows the velocity contours of the $HOCO^+$ 4_{04} - 3_{03} transition, superimposed on its integrated intensity map. The 5_{05} - 4_{04} transition was observed towards the cores of each condensation. The general structure of the $HOCO^+$ clouds is quite similar to that of NH_3

Figure 8.1a - c (a) Map of the observed antenna temperature, T_A^*, for the $HOCO^+$ 4_{04} - 3_{03} transition. Dots indicate observed points, and the cross is the position of Sgr A West. Contour levels are 0.15, 0.2, 0.25, 0.3, and 0.35 K. (b) Integrated intensity ($\int T_A^* dV$) map of the $HOCO^+$ 4_{04} - 3_{03} transition. Contour levels are 2.0, 3.5, 5.0, 6.5, and 8.0 K km s^{-1}. (c) Velocity contours of the $HOCO^+$ 4_{04} - 3_{03} transition (full lines) superimposed upon the integrated intensity map (dashed lines).

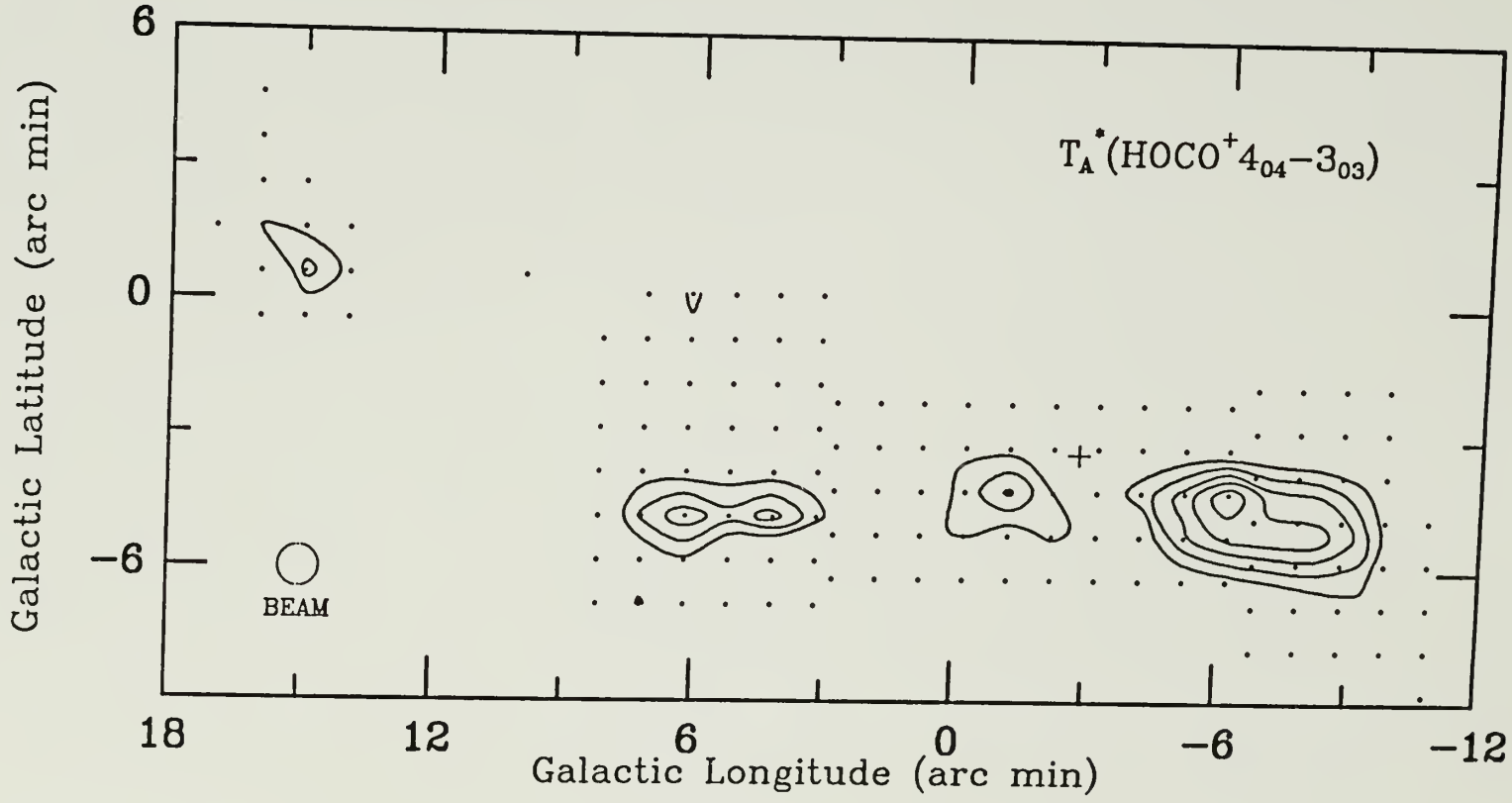
6
0
−6
Galactic Latitude (arc min)
$T_A^*(HOCO^+4_{04}-3_{03})$
V
+
BEAM
18
12
6
0
−6
−12
Galactic Longitude (arc min)

(a)

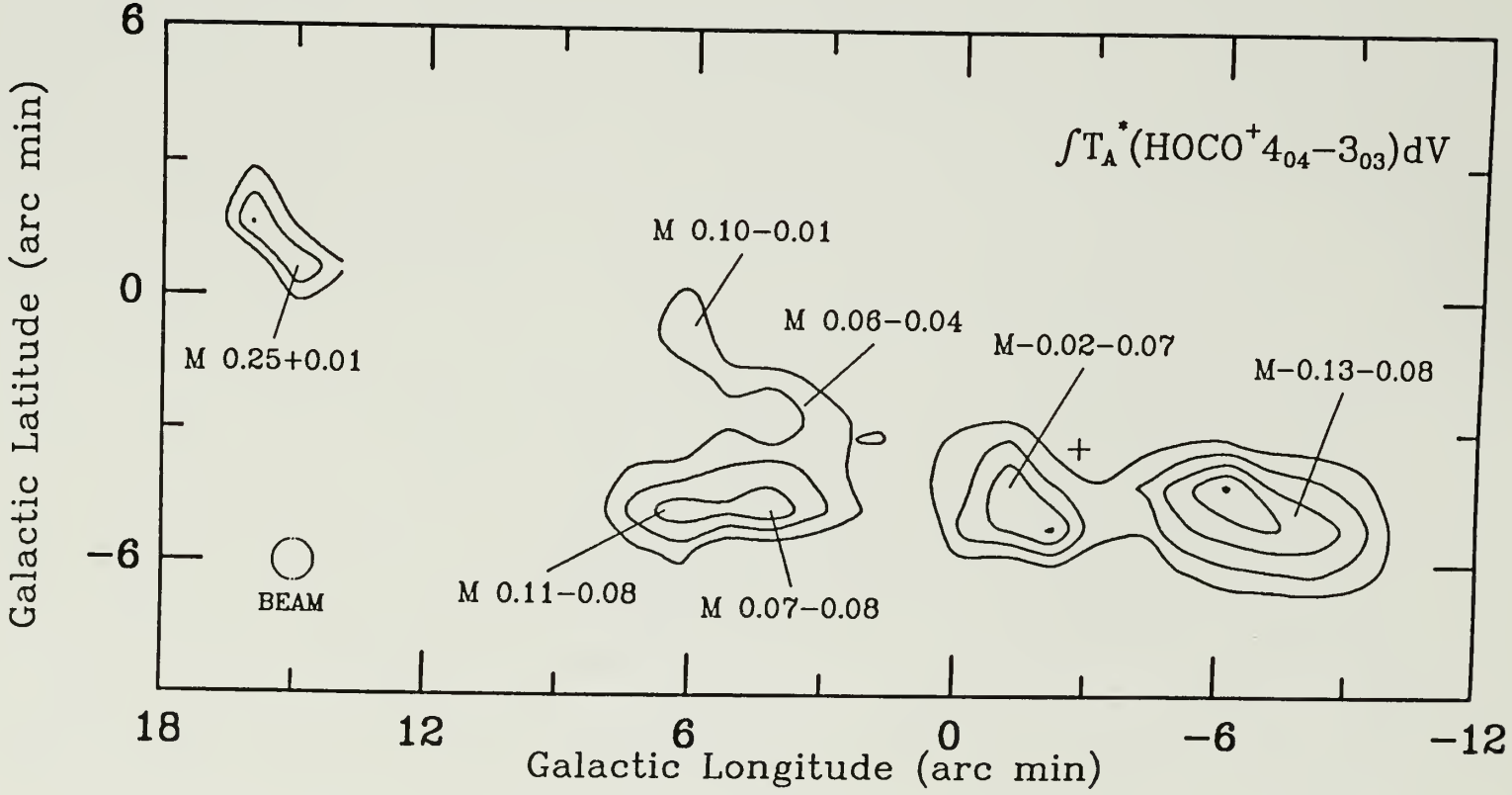
$\int T_A^*(HOCO^+4_{04}-3_{03})dV$
M 0.25+0.01
M 0.10−0.01
M 0.06−0.04
M−0.02−0.07
M−0.13−0.08
M 0.11−0.08
M 0.07−0.08
BEAM
6
0
−6
18
12
6
0
−6
−12
Galactic Latitude (arc min)
Galactic Longitude (arc min)

(b)

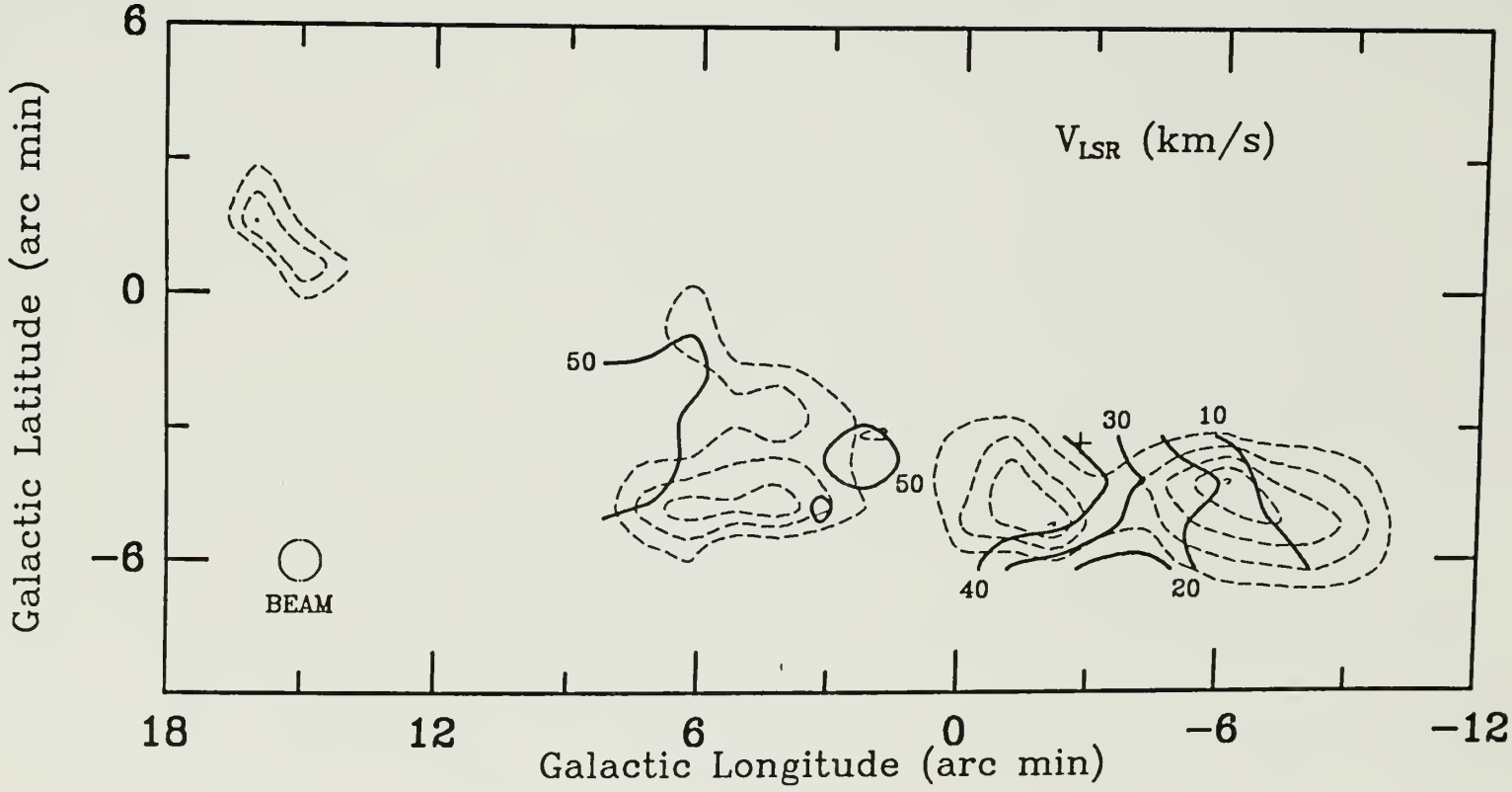
6
0
−6
Galactic Latitude (arc min)
V_{LSR} (km/s)
50
50
30
10
40
20
BEAM
18
12
6
0
−6
−12
Galactic Longitude (arc min)

(c)

(Güsten, Walmsley, and Pauls 1981). The clouds M-0.13-0.08 and M-0.02-0.07 seem to be merging or overlapped in the line of sight, as is also shown in the velocity map of Figure 8.1c. The region of positive longitudes shows a fairly uniform velocity in the range 40 - 50 km s^{-1}, while the negative longitude region shows an apparent velocity gradient from V_{LSR} ~ 10 km s^{-1} to ~ 50 km s^{-1} along the Galactic plane.

In Table 8.2, we summarize the $HOCO^+$ observations towards the cores of the condensations observed in ammonia by Güsten, Walmsley, and Pauls (1981) (see Figure 8.1b). Data towards the condensation M-0.13-0.08 are given at the location of the strongest emission of the $HOCO^+$ 4_{04} - 3_{03} transition, which is offset (Δl, Δb) = (1.4', 0.4') from the nominal position implied by the name.

8.4 Excitation of $HOCO^+$

We have used an LVG model to solve the statistical equilibrium and radiative transfer equations for $HOCO^+$. The model is described in Appendix A. $HOCO^+$ is an asymmetric top with a $^1\Sigma$ ground electronic state. It has both a- and b-components of its electric dipole moment (molecular constants are given in Bogey, Demuynck, and Destombes 1984). We included in the calculation a total of 72 levels up to energies of ~ 200 K above the ground state in the K_a = 0, 1, and 2 ladders. We have used HNCO collisional de-excitation rates (S. Green, private communication) for those of $HOCO^+$ as a

TABLE 8.2

Summary of the $HOCO^+$ Observations[a,b] for the Sgr A Molecular Cloud

Position	Freq.[c] (GHz)	T_A^* (K)	$\int T_A^* dV$ (K km s^{-1})	V_{peak} (km s^{-1})	ΔV (km s^{-1})
M-0.13-0.08	85	0.39 ±.02[d]	8.2	18	17
	106	0.34 ±.03	6.5	21	18
M-0.02-0.07	85	0.26 ±.05	6.3	45	24
	106	0.23 ±.02	6.0	50	24
M 0.06-0.04	85	0.13 ±.05	2.3	45	15
	106	0.12 ±.02	1.1	50	9
M 0.07-0.08	85	0.27 ±.06	6.1	50	25
	106	0.18 ±.02	3.8	48	20
M 0.10-0.01	85	0.18 ±.05	3.9	47	19
	106	0.11 ±.02	2.6	46	20
M 0.11-0.08	85	0.29 ±.06	5.9	45	19
	106	0.25 ±.02	5.8	48	22
M 0.25+0.01	85	0.22 ±.04	5.0	33	25
	106	0.23 ±.02	5.0	36	21

[a] At the cores of each condensation.

[b] Spectral resolution is 0.69 MHz.

[c] 85. 53068 GHz for the $4_{04} - 3_{03}$ transition and 106.91336 GHz for the $5_{05} - 4_{04}$ transition (Bogey, Demuynck, and Destombes 1984).

[d] 1 σ uncertainty.

first approximation, since $HOCO^+$ and HNCO have similar molecular constants and structures. The collisional de-excitation rates are fairly insensitive to kinetic temperature and ΔJ. The HNCO excitation has been modelled in Sgr B2 by Churchwell *et al.* (1986), and we might expect that the general features of the $HOCO^+$ excitation would be similar to that for HNCO. Our main purpose for the LVG analysis is to check the effect of the fast b-type transitions and background radiation on the excitation of $HOCO^+$; this should allow us to calculate its abundance more accurately that was done in Paper 1, which assumed optically thin emission and a Boltzmann population distribution. In Figure 8.2, we have shown fractional abundances for each J level in the $K_a = 0$ ladder for several Boltzmann distributions and for the LVG analysis results. The fast b-type transitions drain the populations in $K_a \geq 1$ levels to the $K_a = 0$ ladder, and consequently enhance the populations of the $K_a = 0$ ladder. This enhancement of $K_a = 0$ ladder populations may partly result in the extended emission of the $HOCO^+$ $4_{04} - 3_{03}$ transition observed towards Sgr B2 and Sgr A.

In Figure 8.3, we have plotted the antenna brightness temperature (T_R), the optical depth (Tau), and the excitation temperature (T_{ex}) as functions of the apparent background radiation temperature (T_{rad}), as calculated from the LVG model for the $4_{04} - 3_{03}$ and $5_{05} - 4_{04}$ transitions. $T_{ex} \sim T_{rad}$ for $n(H_2) \leq 10^4$ cm^{-3} and $T_{kin} \geq T_{ex} \geq T_{rad}$ for $n(H_2) > 10^4$ cm^{-3}, as shown in the bottom panel of Figure 8.3. The antenna temperatures for the $K_a = 0$

Figure 8.2 Fractional populations of each J level in the $K_a = 0$ ladder of $HOCO^+$. Left panel is for Boltzmann distributions, middle for LVG calculations with volumn density $n(H_2) = 10^4$ cm^{-3}, and right for LVG calculations with $n(H_2) = 10^5$ cm^{-3}. Temperatures are indicated in the figure. No background radiation is included.

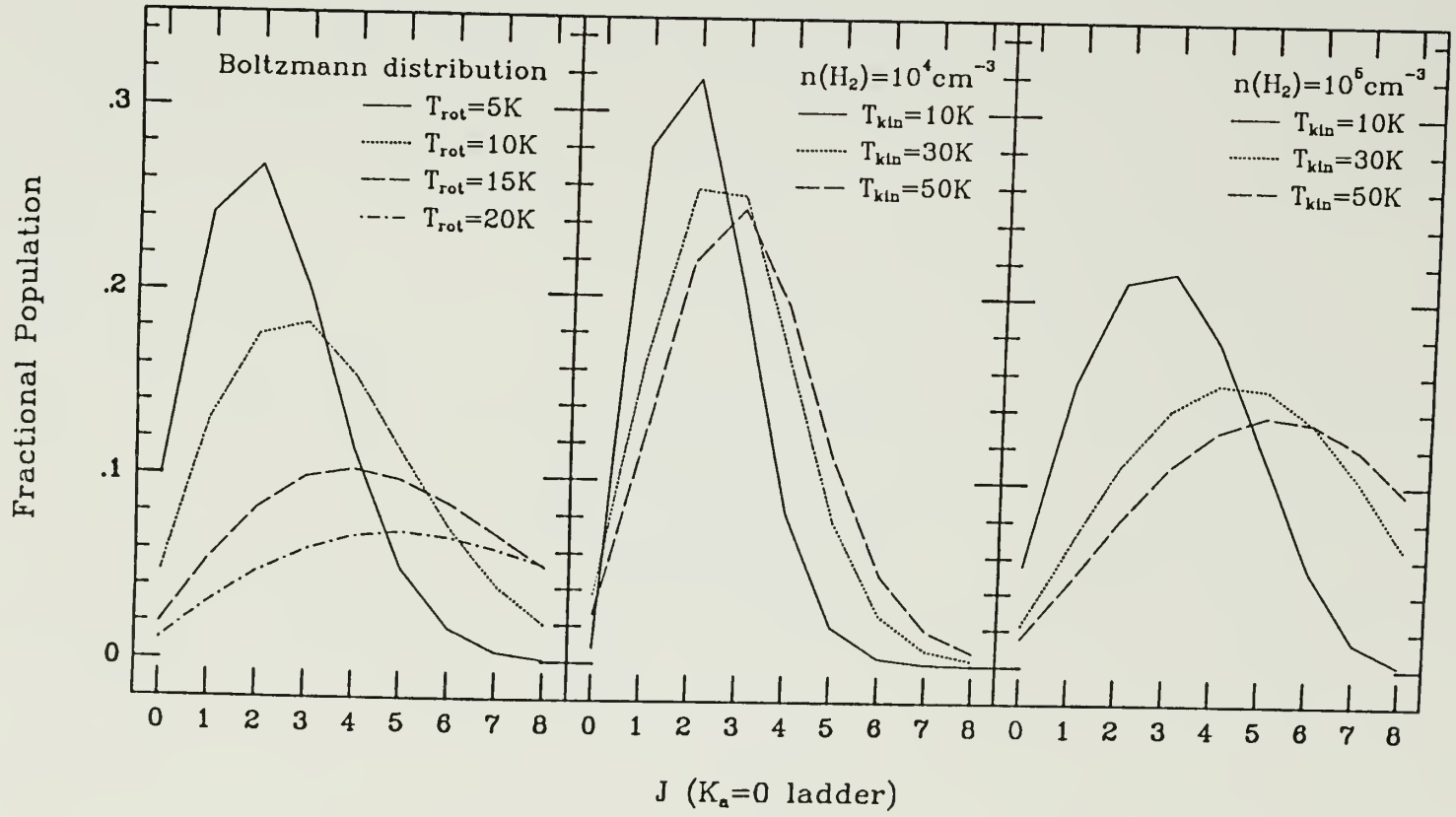
Boltzmann distribution
T_{rot}=5K
T_{rot}=10K
T_{rot}=15K
T_{rot}=20K
$n(H_2)=10^4 cm^{-3}$
T_{kin}=10K
T_{kin}=30K
T_{kin}=50K
$n(H_2)=10^5 cm^{-3}$
T_{kin}=10K
T_{kin}=30K
T_{kin}=50K
Fractional Population
.3
.2
.1
0
0 1 2 3 4 5 6 7 8
J (K_a=0 ladder)

Figure 8.3 Sample of the LVG analysis results for the antenna brightness temperature (T_R) for the two observed $HOCO^+$ transitions, the optical depth (Tau), and the excitation temperature (T_{ex}), as functions of the apparent background radiation temperature (T_{rad}).

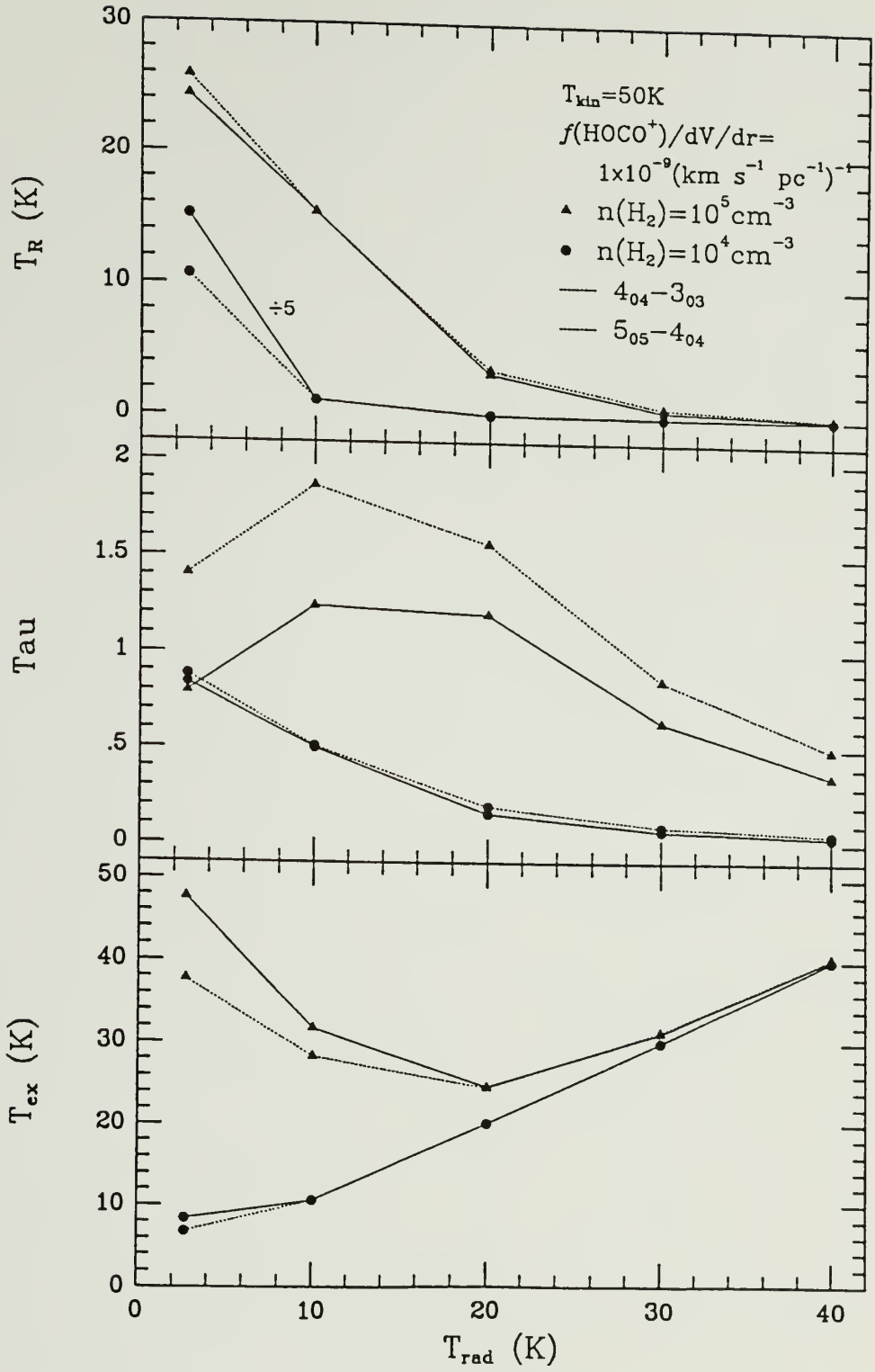
T_{kin}=50K
$f(HOCO^+)/dV/dr$=
1×10^{-9}(km s^{-1} pc^{-1})$^{-1}$
$n(H_2)=10^5 cm^{-3}$
$n(H_2)=10^4 cm^{-3}$
$4_{04}-3_{03}$
$5_{05}-4_{04}$
÷5
T_R (K)
Tau
T_{ex} (K)
T_{rad} (K)
30
20
10
0
2
1.5
1
.5
0
50
40
30
20
10
0
0
10
20
30
40

ladder transitions decrease quickly as T_{rad} increases (upper panel of Figure 8.3), because the excitation temperatures between the K_a ladders equilibrate to T_{rad}, which increases the populations in the $K_a \geq 1$ ladders, as was discussed by Churchwell *et al.* (1986), and the antenna brightness temperature is proportional to the difference between the excitation temperature and the background radiation temperature.

Churchwell *et al.* (1986) suggest that the strength of the HNCO lines observed in the center of Sgr B2 can be explained best if the excitation includes the effect of a 10 K radiation field with a beam filling factor ~ 0.8 and a 70 K field with a beam filling factor of ~ 0.2, which results in 15 % of the total HNCO column density in $K_a \geq 1$ ladders (see discussion in the reference). We also apply a 10 K radiation field but with a beam filling factor 1 in the $HOCO^+$ LVG analysis for Sgr B2(M) and (2N). If a 70 K radiation field with a beam filling factor 0.2 is included for the model of Sgr B2(M), then the column density is expected to increase by ~ 10 %. In Sgr A, the infrared surface brightness intensities peak around Sgr A (West) at 30 μm, show a double-lobed structure at 50 μm and 100 μm (Becklin, Gatley, and Werner 1982), and peak at the center of M-0.13-0.08 at 540 μm (Hildebrant *et al.* 1979). Therefore, hot grains (T_{dust} ~ 40 K; Gatley *et al.* (1977); Dent *et al.* (1982)) dominate around Sgr A (West), while the neutral gas clouds which we have observed may be more closely related to relatively cool dust grains. We derive a dust color temperature of ~ 20 K at the center

of M-0.13-0.08 from 100 μm and 540 μm data (the energy differences corresponding to the inter-ladder b-type transitions are $\Delta E(K_a = 0\text{-}1)$ ~ 390 μm and $\Delta E(K_a = 1\text{-}2)$ ~ 130 μm). The apparent radiation temperature depends on the actual energy density of the region, which is less than the grain color temperature, and we assume an apparent radiation temperature of 10 K as a lower limit for Sgr A (M-0.13-0.08). Constant brightness temperature curves calculated from the LVG model for the Galactic center sources are shown in Figure 8.4a to c for the observed antenna temperatures of the 4_{04} - 3_{03} and 5_{05} - 4_{04} transitions and corresponding 3 σ values. Similar curves corresponding to the observed upper limits for the 1_{01} - 0_{00} and 4_{04} - 3_{03} transitions for TMC-1 (3 σ) are indicated in Figure 8.4d.

We have used kinectic temperatures of 50 K and 10 K for the Galactic center clouds and for the cold dark clouds, respectively. Churchwell and Hollis (1983) derive an almost constant kinetic temperature T_{kin} ~ 50 K across Sgr B2 with CH_3CCH data. In Sgr A, Güsten, Walmsley, and Pauls (1981) derive T_{kin} ~ 50 - 120 K, while Morris *et al.* (1983) derive T_{kin} ~ 30 - 60 K, using NH_3 lines. The $HOCO^+$ LVG analysis shows that the excitation is dominated by radiation processes not collisional processes, and we also use T_{kin} ~ 50 K for Sgr A. T_{kin} ~ 10 K may be a typical value for cold, dark clouds (Irvine, Goldsmith, and Hjalmarson 1987), and we use this value for TMC-1 and L134N in the LVG analysis.

Figure 8.4a - d Constant brightness temperature curves calculated from the LVG models which match the observations of the 4_{04} - 3_{03} and 5_{05} - 4_{04} transitions of $HOCO^+$. Calculations for Sgr A and Sgr B2 include the effect of a 10 K radiation field. Each center line is for the observed antenna temperature (T_A^*/η_B) and the other two lines for corresponding 3 σ values. (a) Sgr A (M-0.13-0.08). Contours are 0.46, 0.53, and 0.61 K for the 4_{04} - 3_{03} line, and 0.39, 0.50, and 0.62 K for the 5_{05} - 4_{04} line. (b) Sgr B2(2N). 1.30, 1.46, and 1.62 for the 4_{04} - 3_{03} line, and 1.23, 1.37, and 1.51 for the 5_{05} - 4_{04} line. (c) Sgr B2(M). 0.46, 0.59, and 0.72 for the 4_{04} - 3_{03} line, and 0.63, 0.75, and 0.87 for the 5_{05} - 4_{04} line. (d) TMC-1. 0.09 for the 4_{04} - 3_{03} line and 0.10 for the 1_{01} - 0_{00} line.

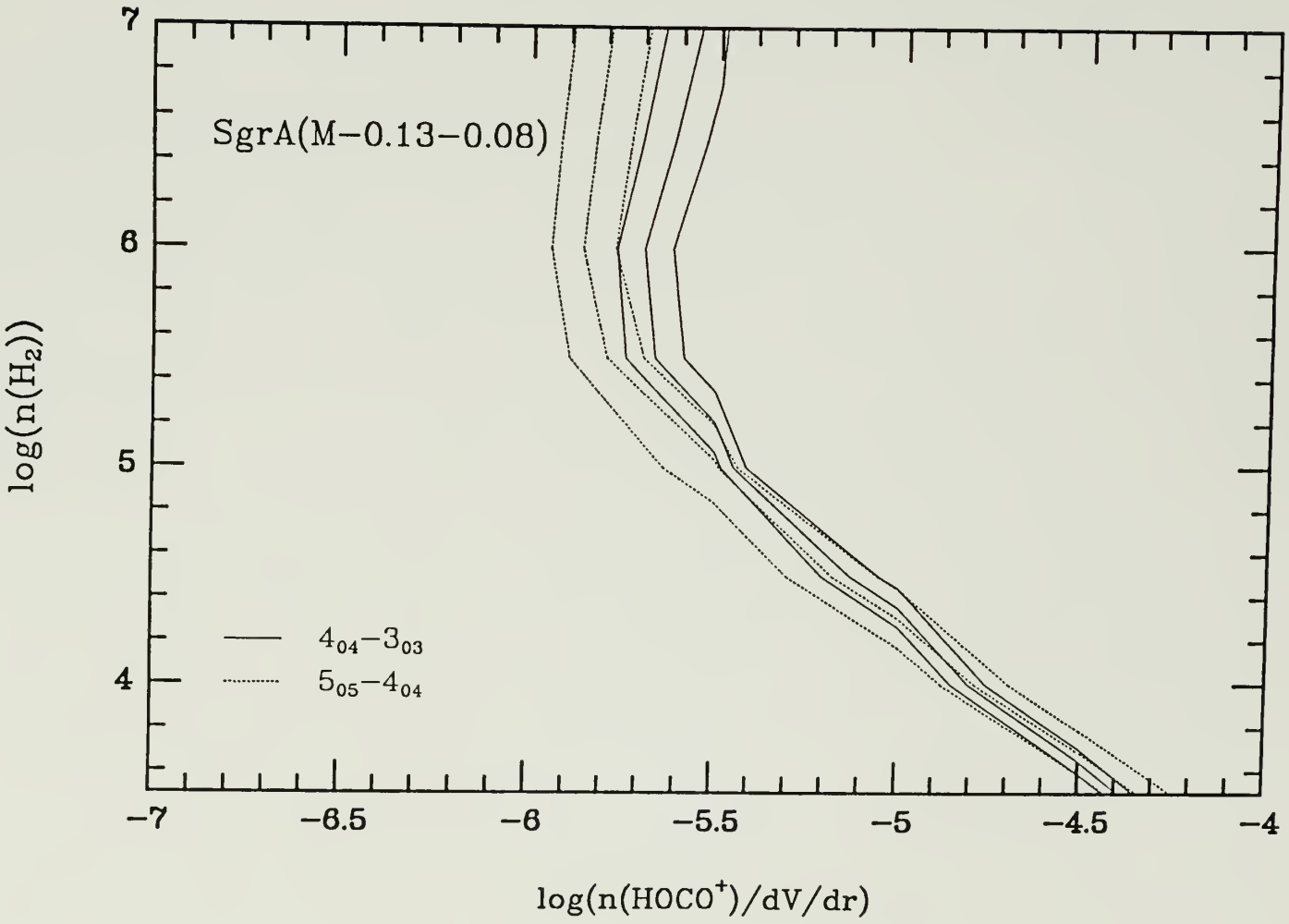
SgrA(M−0.13−0.08)
$4_{04}-3_{03}$
$5_{05}-4_{04}$
log(n(H2))
log(n(HOCO+)/dV/dr)
7
6
5
4
−7
−6.5
−6
−5.5
−5
−4.5
−4

(a)

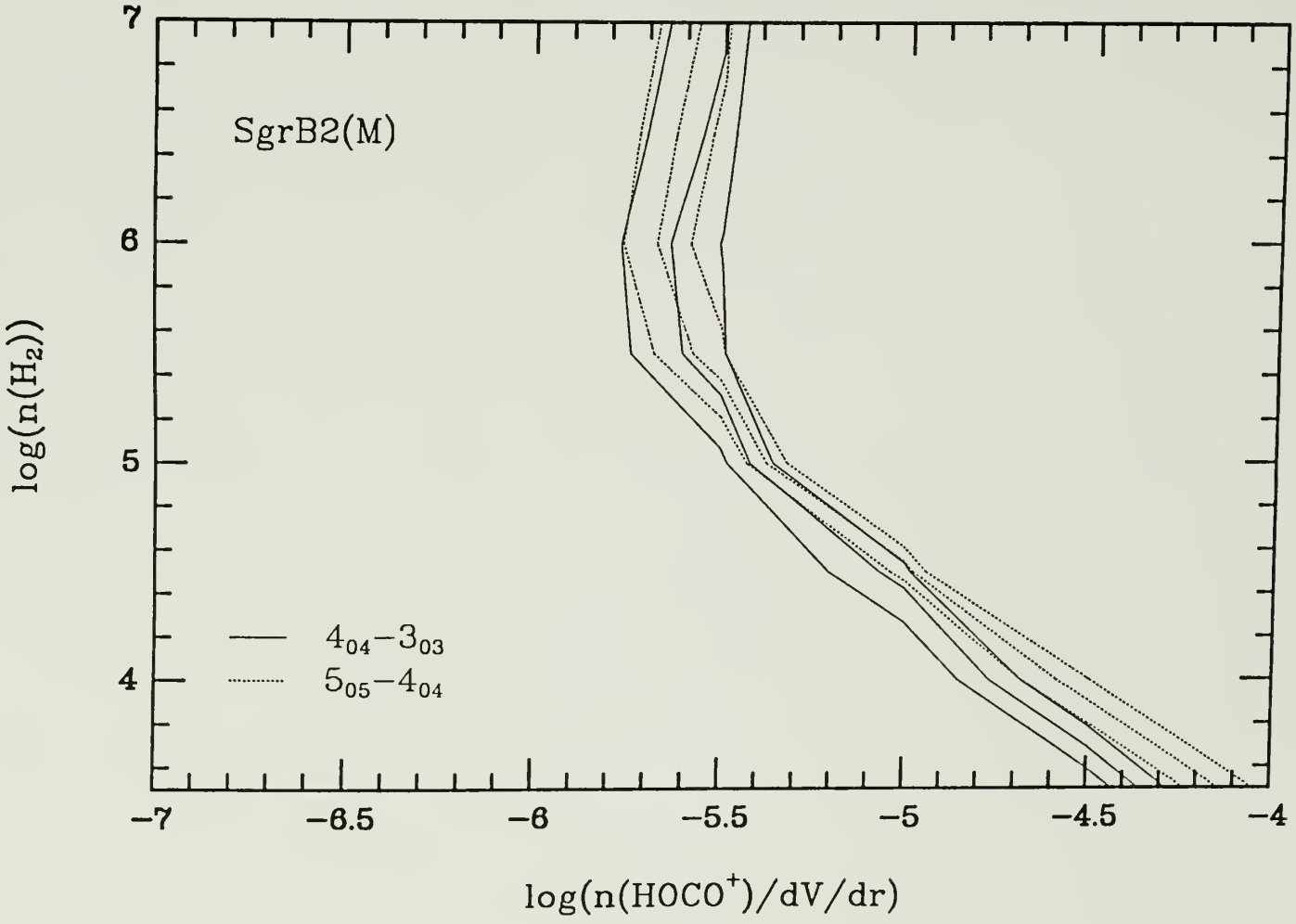
SgrB2(M)
$4_{04}-3_{03}$
$5_{05}-4_{04}$
log(n(H₂))
log(n(HOCO⁺)/dV/dr)
7
6
5
4
−7
−6.5
−6
−5.5
−5
−4.5
−4

(b)

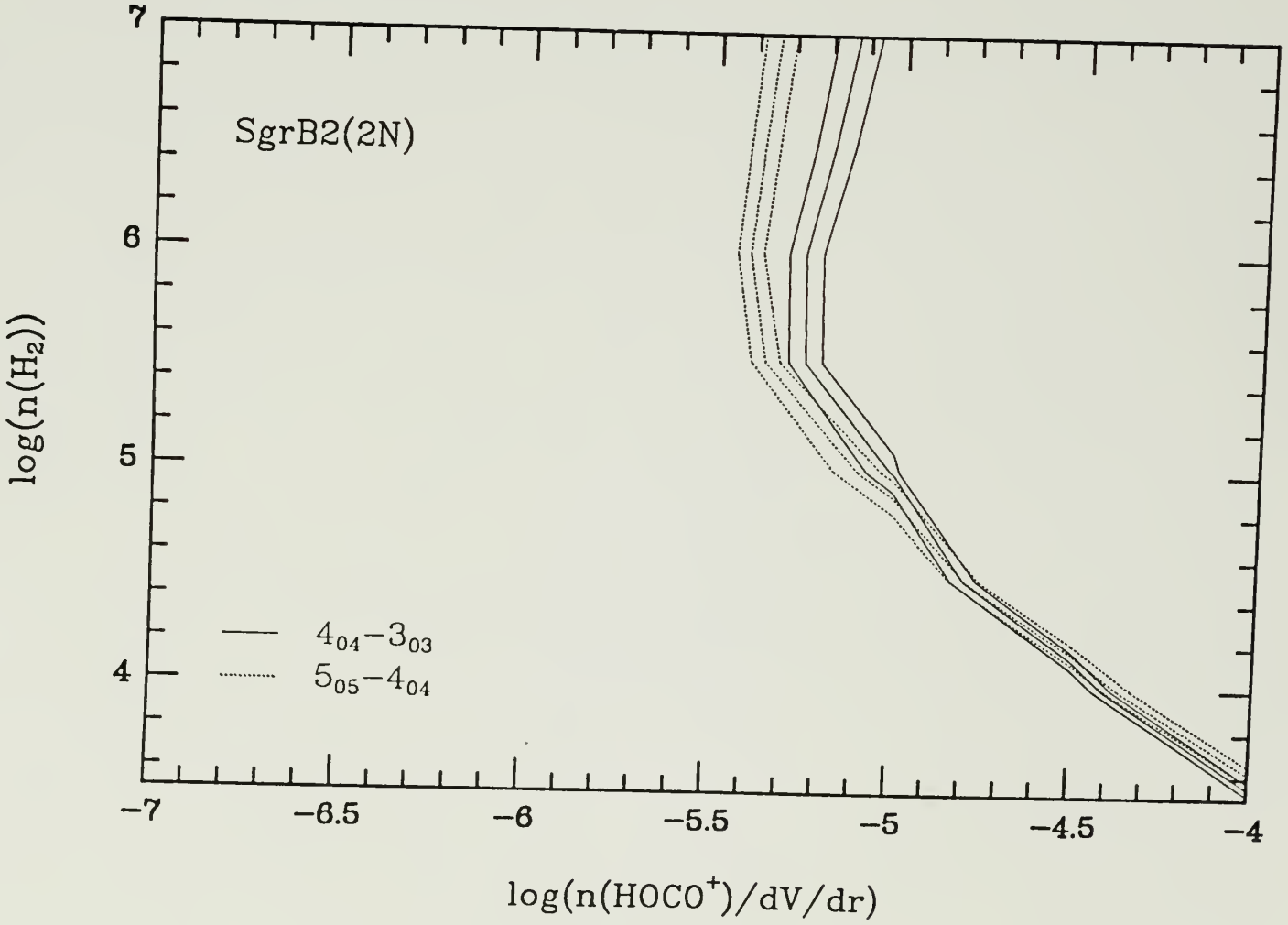
SgrB2(2N)
7
6
5
4
−7
−6.5
−6
−5.5
−5
−4.5
−4
log(n(H2))
log(n(HOCO+)/dV/dr)
4 04 − 3 03
5 05 − 4 04

(c)

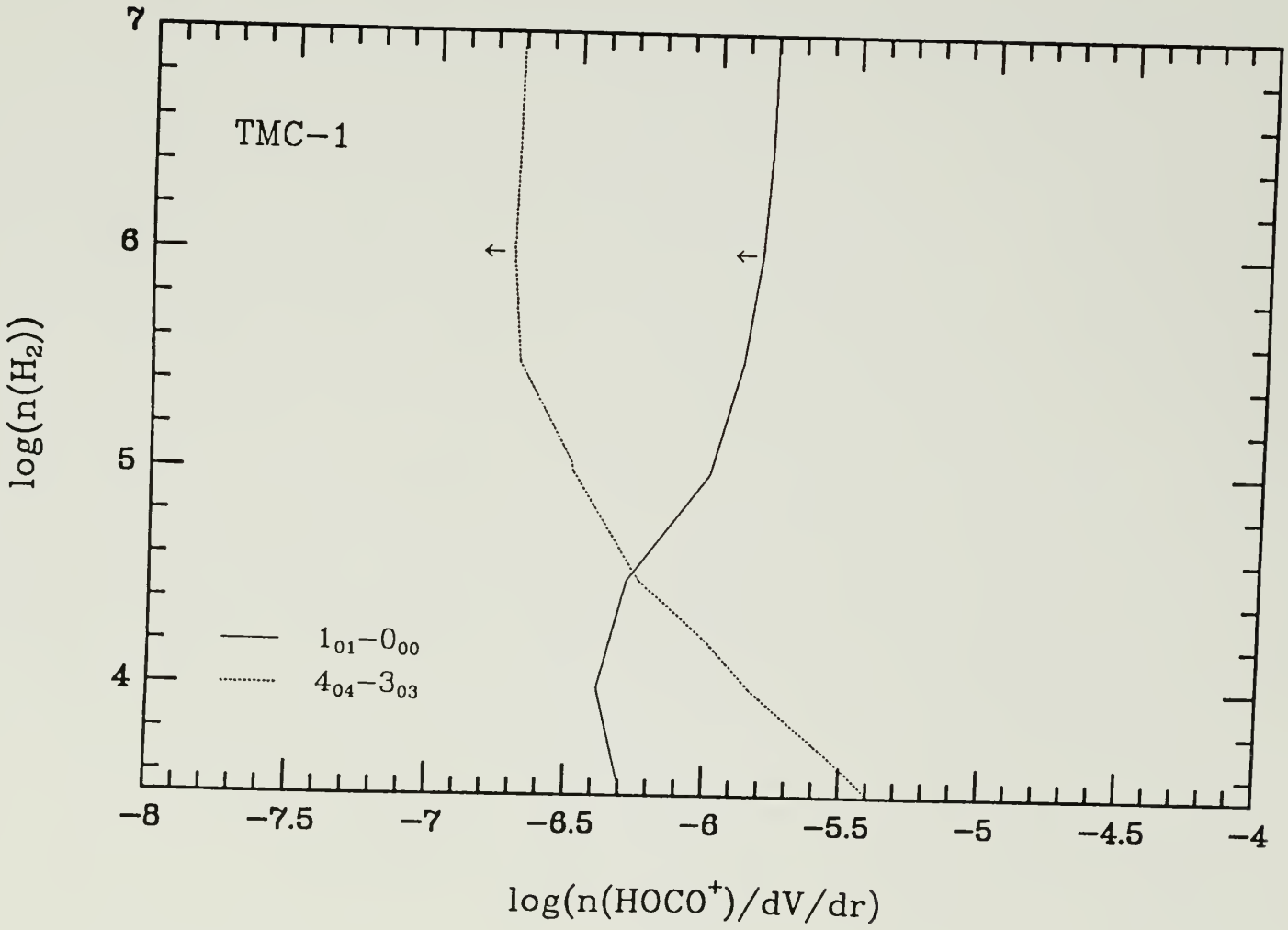
TMC−1
$1_{01}-0_{00}$
$4_{04}-3_{03}$
log(n(H₂))
log(n(HOCO⁺)/dV/dr)
7
6
5
4
−8
−7.5
−7
−6.5
−6
−5.5
−5
−4.5
−4

(d)

Since our two observed transitions typically do not well constrain both $n(H_2)$ and the abundance of $HOCO^+$ in the sources studied, we pick a range of values for $n(H_2)$ based on data for other molecules. The density distribution of the Sgr B2 molecular cloud has been modelled recently by Lis (1989), who derives $n(H_2) \sim 6 \times 10^5$ cm^{-3} for the core component at the center with a radial exponent -2, which gives $n(H_2) \sim 4 \times 10^4$ cm^{-3} at 2 arcminute north. In Sgr A (M-0.13-0.08), $n(H_2) \sim 1 \times 10^5$ cm^{-3} has been derived from the H_2CO analysis by Güsten and Henkel (1983), and $\sim 0.2 - 1 \times 10^5$ cm^{-3} from virial masses by Armstrong and Barrett (1987). We use $n(H_2) \sim 0.5\text{-}5 \times 10^5$ cm^{-3} for Sgr B2(M), and $1\text{-}5 \times 10^4$ cm^{-3} for Sgr B2(2N) and the core of M-0.13-0.08, the peak position for the $4_{04} - 3_{03}$ transition observed in Sgr A. For the cold dark clouds TMC-1 and L134N, we use the maximum upper limits determined from the 3 σ values for the two observed $HOCO^+$ transitions, $4_{04} - 3_{03}$ and $1_{01} - 0_{00}$ (see Figure 8.4d). The calculated results are normalized to a velocity gradient dV/dr = 1 km s^{-1} pc^{-1}, and the abundances derived from this LVG analysis are given in Table 8.3. Note that the Sgr A position in Table 8.3 is the peak of the $HOCO^+$ $4_{04} - 3_{03}$ emission (offset $(\Delta l, \Delta b) = (1.4', 0.4')$ from the nominal position of M-0.13-0.08), while that in Paper 1 is offset $\sim 2'$ from this peak position toward Sgr A(West). The $HOCO^+$ column density in Sgr A has been increased by a factor of ~ 50 relative to that in Paper 1, which results from the difference in line intensity between the two

TABLE 8.3

Abundances of $HOCO^+$

Source[a]	$N(HOCO^+)$ (cm^{-2})	$\frac{f(HOCO^+)}{dV/dr}$ [b] ($km\ s^{-1} pc^{-1})^{-1}$	$\frac{[HOCO^+]}{[H_2]}$ [c]	$\frac{[HOCO^+]}{[HCO^+]}$ [d]	$\frac{[CO_2]}{[CO]}$ [e]
SgrA	0.3-1.0 (15)	4(-10)	8(-9)	3	1
SgrB2(2N)	0.9-3.1 (15)	5(-10)	4(-9)	4	0.6
SgrB2(M)	≥ 1.4 (14)	≥ 4(-12)	≥ 1(-10)	≥ 0.1	≥ 0.3
TMC-1	≤ 1.1 (12)	—	≤ 1(-10)	≤ 1(-2)	≤ 3(-2)
L134N	≤ 1.0 (12)	—	≤ 1(-10)	≤ 1(-2)	≤ 3(-2)

Numbers in parentheses are powers of 10.

[a] For Sgr A at the peak position of the $HOCO^+$ 4_{04} - 3_{03} emission: Offset (Δl,Δb) = (1.4′, 0.4′) from the core of the M-0.13-0.08 condensation ; Other positions given in Paper 1.

[b] Fractional abundance of $HOCO^+$ divided by velocity gradient, derived by the LVG analysis.

[c] SgrA: $N(H_2) \sim 7.8 \times 10^{22}$ cm^{-2} (from $N(^{13}CO) \sim 2.7 \times 10^{17}$ cm^{-2} at the core of M-0.13-0.08 (Armstrong and Barrett 1987), $[^{12}CO]/[^{13}CO] \sim 23$ (Penzias 1980), and $[^{12}CO]/[H_2] \sim 8 \times 10^{-5}$); Sgr B2(M): $N(H_2) \sim 1.3 \times 10^{24}$ cm^{-2} (Lis 1989); SgrB2(2N): $N(H_2) \sim 5.0 \times 10^{23}$ cm^{-2} (from

(Continued on next page)

TABLE 8.3

(Continued)

$C^{18}O$: Lis 1989); TMC-1: $N(H_2) \sim 1 \times 10^{22}$ cm^{-2} (Irvine *et al.* 1987; Friberg and Hjalmarson 1989); L134N: $N(H_2) \sim 8.2 \times 10^{21}$ cm^{-2} (Swade 1987).

[d] SgrA: $N(HCO^+) \sim 2.8 \times 10^{14}$ cm^{-2} (at the core of M-0.13-0.08 from the unpublished data of $HC^{13}O^+$ of Minh and Irvine, and $[HCO^+]/[H^{13}CO^+] \sim 23$); SgrB2(M): $N(HCO^+) \sim 1.3 \times 10^{15}$ cm^{-2} (from the unpublished $HC^{18}O^+$ data of Minh and Irvine, assuming $[HCO^+]/[HC^{18}O^+] \sim 230$); SgrB2(2N): $N(HCO^+) \sim 4.7 \times 10^{14}$ cm^{-2} (same as for SgrB2(M)); TMC-1 and L134N: $N(HCO^+) \sim 8 \times 10^{13}$ cm^{-2} (Irvine, Goldsmith, and Hjalmarson 1987).

[e] From the equation of Herbst *et al.* (1977) (see also Paper 1).

observed positions (about a factor of 5) and the inclusion of the background radiation effect (about a factor of 10).

8.5 Discussion

8.5.1 $HOCO^+$ Abundances

We derive fractional abundances of $HOCO^+$ relative to H_2 of $f(HOCO^+) \geq 1 \times 10^{-9}$ in the Galactic center, which is about three orders of magnitude greater than predicted by quiescent ion-molecule gas-phase chemistry (Herbst and Leung 1986). The non-detection of $HOCO^+$ in the "typical" molecular clouds outside the Galactic center (Paper 1) may indicate that the $HOCO^+$ chemistry in the Galactic center is unique, although better rms values should be obtained for other sources.

If the Galactic center environment produces an unusual chemistry, this may be particularly prominent in Sgr A. The distribution of $HOCO^+$ looks quite similar to that of NH_3 (Güsten, Walmsley, and Pauls 1981) and HNCO (Armstrong and Barrett 1984). The fractional abundances of $HOCO^+$ in Sgr A appear to be in the range 1-10 x 10^{-9} relative to H_2, for values of $n(H_2)$ derived from the $N(^{13}CO + C^{18}O)$ map of Armstrong and Barrett (1984) (assuming $[^{12}CO]/[^{13}CO] \sim 23$ (Penzias 1980); $[CO]/[H_2] \sim 8 \times 10^{-5}$), with the largest values ($\sim 10^{-8}$) for the centers of M-0.13-0.08 (Table 8.3) and M 0.11-0.08. In the third column of Table 8.3 we include

$f(HOCO^+)/dV/dr$ values derived in the model calculations. If we apply an estimated source size (~ 7 - 10 pc for M-0.13-0.08 from Figure 8.1) and the $HOCO^+$ line width (~ 17 km s^{-1}), we obtain dV/dr ~ 2 km s^{-1} pc^{-1}, which gives $f(HOCO^+) \sim 10^{-9}$. Although this value is about a factor of 10 less than that found by comparing the column density of $HOCO^+$ with the H_2 column density derived from other molecular data, it is still in the range we mentioned above. The model calculations, moreover, employ a simplfied radiative transfer analysis (cf. Irvine *et al.* 1985), and the actual dV/dr in the region is quite uncertain; in addition, there may be an uncertain scaling factor in the collisional cross sections of $HOCO^+$ which were assumed to be the same as those of HNCO. Therefore we believe the fractional abundance derived by comparing the column density with other molecular data is more reliable than that found from the *in situ* $HOCO^+$ abundance in the model calculations.

Since upper limits for the $HOCO^+$ abundance in the cold dark clouds TMC-1 and L134N are much larger than the abundance predicted by quiescent ion-molecule chemistry (e.g. Herbst and Leung 1986), it is difficult to test the chemical models for $HOCO^+$. However, the fractional abundances for cold dark clouds are less by about a factor of 10 than those for the Galactic center clouds. Therefore, we expect that the formation processes of $HOCO^+$ must be efficient in the Galactic center region.

8.5.2 Chemistry related to $HOCO^+$

Herbst *et al.* (1977) have suggested that $HOCO^+$ traces interstellar CO_2, and using major formation and destruction processes suggested that an abundance ratio $[HOCO^+]/[CO_2] \sim 10^{-5}$ (Herd, Adams, and Smith 1989) would be typical in molecular clouds. This implies a high abundance of CO_2 in the Galactic center. Pineau des Forêts, Roueff, and Flower (1989; hereafter PRF), however, suggested that the endothermic reaction $HCO^+ + O_2$ can form $HOCO^+$ in MHD shocks; in this case, $HOCO^+$ does not trace CO_2.

The chemical abundances in a shocked region largely depend on the initial abundances and shock conditions. The abundance ratios of $[HOCO^+]/[HCO^+]$ and $[CO_2]/[CO]$ are increased in the MHD shock model of PRF relative to preshock values by four and three orders of magnitude, respectively, (to ~ 0.1 for both ratios), by adding the reaction $HCO^+ + O_2 \rightarrow HOCO^+ + O$. The observed abundance ratio of $[HOCO^+]/[HCO^+]$ in the Galactic center clouds is, however, about an order of magnitude larger still (Table 8.3). In addition, the $HOCO^+$ $4_{04} - 3_{03}$ line has been observed to be fairly extended in Sgr B2 (Paper 1) and Sgr A (Figure 8.1). Although shocks may be prevalent in the Galactic center, it is not certain that the whole neutral gas complex has been in MHD shocks, which occupy relatively thin slabs (linear dimension $\leq$ 0.2 pc; PRF). Therefore it may be difficult to explain the overall $HOCO^+$ abundance throughout the Galactic center clouds as a result of MHD shocks.

Another possible pathway for the formation of CO_2 is grain surface reactions. Grain-surface reactions alone form primarily simple, saturated hydrides, but UV photolysis may convert these into various other components. H_2O ice is the most abundant molecule in grain mantles, and UV photolysis of H_2O has been suggested to lead to the formation of CO_2, H_2CO, and CH_3OH by reaction between photolysis products and neighboring simple species such as CO (cf. Tielens and Allamandola 1987; and see references therein), which itself has been identified as a major constituent in grain mantles (> 20 % of H_2O toward NGC7538/IRS9 and Elias 16; see references in Grim and Greenberg 1987). This conjecture is supported by laboratory data: When a mixture of CO and H_2O is irradiated by UV radiation, an observable amount of CO_2 is formed (Greenberg 1989). Inside a dense and quiescent cloud, this process may not be important because of a lack of UV photons, but in typical star-forming regions UV photons generated by newly formed stars could both process icy mantle material and warm up the grains to a high temperature, resulting in the evaporation of the grain mantles. In a region like the hot core component of Orion(KL), grain-related processes induced by radiative heating from the luminous IRc 2 are prominent, but the high density and temperature of the hot core leads to a low fractional ionization, which results in very inefficient ion-molecule chemistry (Blake *et al.* 1987). Since $HOCO^+$ forms mainly by the ion-molecule reaction between H_3^+ and CO_2, it is not certain whether the non-detection of $HOCO^+$ toward

Orion(KL) (Paper 1) indicates a small CO_2 abundance or inefficient ion-molecule chemistry of the region. In the Galactic center, however, the strong activities and shocks can generate a large abundance of UV photons in the extended region, which may result in effective UV photolysis of grain mantles and, consequently, a large abundance of CO_2 and hence of $HOCO^+$ in the extended region.

The grain surface chemical models are still in a formative stage, and UV photolysis processing is quite uncertain, partly because the UV photon density is not well known. Here we simply suggest an alternate route to explain the putative CO_2 abundance and consequently the $HOCO^+$ abundance in the Galactic center. The gas-phase reactions leading to formation of $HOCO^+$ and CO_2 should also be studied further.

CHAPTER 9

CONCLUSIONS

9.1 Summary

We have carried out radio observations for the interstellar molecules H_2S, H_2CS, ethyl cyanide (CH_3CH_2CN), and $HOCO^+$, the chemistry of which might be related to grain processes, either directly or indirectly. Abundances of these species and chemical implications for gas phase processes and grain-related processes have been discussed in each chapter, and here we summarize the conclusions.

In Chapters 2 - 4, we report the results for H_2S observed towards the cold dark clouds L134N and TMC-1 (Chapter 2), OMC-1 (Chapter 3), and other star-forming regions (Chapter 4). The fractional abundances of H_2S have been observed to be $\sim 10^{-9}$ relative to H_2 towards L134N and quiescent warm clouds such as the Orion extended ridge, and $\sim 10^{-8}$ - 10^{-9} towards several active star-forming regions. On the other hand, its abundance is enhanced by a factor of 1000 in the Orion hot core and the plateau. We conclude that H_2S may be evaporating from the grain mantles in the hot core. Even in the cold dark clouds, gas phase reactions may not be able to produce the observed abundances, so that grain surface reactions may be ultimately responsible for the gas phase

H_2S abundances. For these reasons H_2S may be a good candidate to trace grain processes.

Our results for H_2CS ortho-to-para ratios (Chapter 5) and ethyl cyanide abundances (Chapter 6) may contradict each other concerning the role of grains in dark cloud chemistry. The ortho-to-para ratio of ~ 1.8 for H_2CS in TMC-1 seems to indicate thermalization on ~ 10 K grain surfaces and imply continuous interactions between gas and grains: i.e. continuous adsorption and desorption. On the other hand, the upper limit on the abundance of ethyl cyanide in TMC-1 may suggest that desorption processes are quite inefficient in cold dark clouds and the hydrogenation of HC_3N on grain surfaces does not affect the gas phase abundances. Perhaps the difference between these results is related to the larger molecular weight of CH_3CH_2CN relative to H_2CS, and a consequent lower desorption probability.

In Chapters 7 and 8, we have presented the results for $HOCO^+$. We derive $HOCO^+$ fractional abundances ~ 10^{-8} - 10^{-9} relative to molecular hydrogen towards the Galactic center sources Sgr A and Sgr B2, which are about three orders of magnitude larger than those predicted by quiescent ion-molecule chemistry and about an order of magnitude larger than predicted by a MHD shock model. If $HOCO^+$ traces interstellar CO_2, the high abundance of the latter ($[CO_2]$ ~ $[CO]$) in the Galactic center may result from the UV photolysis of grain mantles. On the other hand, the $HOCO^+$ 4_{04} - 3_{03} line has not been detected in our survey of other Galactic sources. Therefore,

gas phase CO_2 seems not to be an important carbon and oxygen reservoir in typical molecular clouds.

Quite recently d'Hendecourt and Muizon (1989) have claimed the discovery of interstellar carbon dioxide (CO_2) towards three infrared stars and suggested again the usage of $HOCO^+$ as a tracer of CO_2. Our results for $HOCO^+$ in the Galactic center and other molecular clouds could give some constraints on the grain surface chemistry for the formation of CO_2.

9.2 Implications for Interstellar Chemistry

The role of grains in interstellar chemistry has been often de-emphasized, except as a catalyst for the formation of H_2 molecules, largely because of the reasonable agreement between observational abundances and gas-phase calculations, at least for simple molecules (Irvine *et al.* 1985; Irvine and Knacke 1989). Although grain chemistry is highly uncertain compared with gas phase chemistry, and the grains constitute only about 1 % by mass of molecular clouds, the elements heavier than helium may exist in grains with comparable to or even greater abundances than the amounts in the gas phase, at least for certain elements (Irvine and Knacke 1989). Moreover, several molecules have been identified in grain mantles directly by infrared spectroscopy towards protostars embedded in molecular clouds (e.g. Hagen, Allamandola, and Greenberg

1980; Wilner 1984; Lacy *et al.* 1984). H_2O and CO, for example, have been identified in both the interstellar gas and solid phases.

Infrared spectroscopy of interstellar grains, however, has some limitations, because solid state spectra are not yet available except for a few simple molecules studied in the laboratory, because the interpretation of the broad spectral features attributed to interstellar grains is controversal, and above all, because observable sources are limited to a few protostars deeply embedded in molecular clouds. While radio observations of interstellar molecules identified clearly through their rotational spectra have many advantages compared to infrared spectroscopy, they are limited to gas phase species and there are few such molecules which trace purely grain processes. Consequently, there have been very few radio observations which clearly support grain processes. Our radio observations of interstellar molecules mentioned in previous chapters may be useful in this connection.

Our results for H_2S suggest that we may include H_2S as a candidate for production by grain surface processes. Although desorption should have to occur even in cold dark clouds to preserve the gas phase component, there has been little prior evidence for this phenomenon. However, the abundance of H_2S in quiescent clouds could be explained easily by grain surface formation followed by the desorption of the species, and the very high abundances in the Orion hot core and plateau strongly suggest evaporation of grain mantles. Our results for the H_2CS ortho/para ratios also suggest an efficient

exchange of material between grain surfaces and the gas phase in cold dark clouds. On the other hand, the upper limits for the ethyl cyanide abundance may indicate a lower desorption probability in cold dark clouds, at least for heavy molecules like CH_3CH_2CN and CH_2CHCN. Finally, we expect our $HOCO^+$ observations may give indirect evidence for energetic grain surface processes as well as some constraints on the gas phase chemistry.

We conclude that radio observations may be very useful for the study not only of gas phase processes but also of grain-related processes. They may at least give some constraints on highly uncertain grain processes, including accretion and desorption, surface reactions, evaporation of grain mantles, UV processing of grain mantles, and grain disruption by shocks. The understanding of interstellar grains would be increased most rapidly by carrying out studies of infrared spectroscopy, laboratory experiments, and radio observations simultaneously.

9.3 Future Observations

We plan to study H_2S further with higher angular resolution and sensitivity towards various types of sources, especially towards a region like Orion(KL) where the H_2S source sizes are estimated to be ~ 3" and ~ 7" for the hot core and the plateau, respectively. A map of the H_2S emission in Sgr B2 would reveal whether there exist actually two different velocity components as was suggested by H_2S

and $H_2{}^{34}S$ lines. This study could be interesting if H_2S traces active regions inside a dense molecular cloud.

The distributions of H_2S and H_2CS in cold dark clouds could be useful for studing abundance gradients within such clouds. Moreover, the H_2CS lines in the 3 mm region appear to be optically thin in most cases, and ortho-to-para ratios could be measured in a larger source sample as well as in several positions in a cloud. This ratio could also be measured using other molecules such as H_2S and H_2CCO.

Better upper limits for the abundances of HDS in Orion(KL), of H_2S in IC443B, and of $HOCO^+$ in molecular clouds outside the Galactic center would sharpen the arguments for their chemistry. Especially since interstellar CO_2 has been tentatively identified towards a few protostars (d'Hendecourt and Muizon 1989), $HOCO^+$ observations towards these sources would be useful for studying its chemistry.

APPENDIX A

Statistical Equilibrium and LVG Models

A.1 Cloud Model

The cloud model includes two coupled equations, the equations of statistical equilibrium and the equation of radiative transfer. The population of the energy levels of a molecule is determined by the statistical equilibrium equations, while the radiative transfer equation determines the radiation field inside the cloud, which is necessary to determine the radiative rates in the statistical equilibrium equations, and the emergent intensity from the cloud.

In statistical equilibrium, the rate of transitions that populate an energy level i is exactly balanced by the rate of transitions that depopulate the i^{th} level. For a k-level molecule there are k equations of the form,

$$n_i \sum_j R_{ij} = \sum_j n_j R_{ji},$$

where n_i and n_j are the populations of the i^{th} (E_i) and j^{th} (E_j) levels, respectively. R_{ij} is the rate of any transition that changes the molecule's excitation from the i^{th} level to the j^{th} level. With $E_i > E_j$ the transition rates are given by

$$R_{ij} = A_{ij} + B_{ij} J + C_{ij} n$$

$$R_{ji} = B_{ji} J + C_{ji} n .$$

The A_{ij}, B_{ij}, B_{ji} are the Einstein radiative rate coefficients, J is the intensity of the radiation field, C_{ij} the collision rate coefficients, and n the space density of collision partners. If the transitions are optically thin and the only continuum background is the cosmic black-body radiation, the radiation intensity J can be approximated by a black-body at $T_{bg} \sim 2.7$ K. However, if the transitions are optically thick, we have to solve the equation of radiative transfer to determine the radiation intensity at each point.

The radiative transfer equation is more difficult to solve, but it is simplfied considerably in the presence of systematic motion (Sobolev 1960; Castor 1970; Goldreich and Kwan 1974; Scoville and Solomon 1974; deJong, Chu, and Dalgarno 1975). If the velocity gradient is sufficiently large, an emitted photon travels a short distance compared with the cloud size before it is a Doppler width away from the velocity of the local material. The LVG approximation is valid for a cloud of radius R characterized by a local random motion ΔV_r of thermal or nonthermal origin if the velocity gradient dV/dr satisfies,

$$\Delta V_r \; / \; dV/dr \ll R .$$

A velocity gradient of ~ 1 km s^{-1} pc^{-1} easily satisfies this relation for dark clouds (Snell 1981). In the LVG approximation, the mean intensity of the radiation field at any point is determined by the local conditions at that point, which fix the local source function and the escape probability of a photon from the cloud. We consider here a spherically symmetric cloud with a velocity field of $v = \alpha \cdot r$. The input parameters necessary for the models to be considered here are the H_2 density, the kinetic temperature, and the molecular abundance of interest relative to H_2. The model solutions then give the line intensity, the optical depth, and the excitation temperature for the transitions included in the models. The input parameter values used for the models of H_2CS and $HOCO^+$ are given in the following section.

A.2 Results for H_2CS

We used the H_2CO collisional de-excitation rates (Green *et al.* 1978) for the corresponding H_2CS levels since those for H_2CS are not available, and collisional excitation rates have been calculated by assuming detailed balance. LVG models have been calculated for kinetic temperatures of 10 K (TMC-1), 20 K (Orion 3N1E), and 100 K (Orion KL). The input value ranges for the H_2 density and the H_2CS fractional abundance relative to H_2 are $n(H_2) = 10^{2.5}$ - 10^6 cm^3 and $f(H_2CS) = 10^{-5.5}$ - 10^{-13}, respectively. The calculations for T_{kin} ~ 10 K and 20 K include 16 levels for ortho-H_2CS and 15 levels for

para-H_2CS up to energy levels 70 K above the ground state, while for T_{kin} ~ 100 K, we have extrapolated the H_2CO collisional de-excitation rates up to energy levels of 300 K (the collisional de-excitation rates are not sensitive to kinetic temperatures or ΔJ values) and included 60 levels of ortho-H_2CS and 49 levels of para-H_2CS. We have carried out calculations using a velocity gradient dV/dr = 1 km s^{-1} pc^{-1} but since the quantity of significance in the calculations is the total column density divided by the line width, $N(H_2CS)/\Delta V$ (= $n(H_2CS)/dV/dr$), we have shown the calculation results as a function of $n(H_2CS)/dV/dr$. The results are shown in Figures A.1 to A.3.

A.3 Results for $HOCO^+$

We used the HNCO collisional de-excitation rates (S. Green, private communication) for the corresponding $HOCO^+$ levels since those for $HOCO^+$ are not available and both $HOCO^+$and HNCO have similar molecular constants and structures. The collisional excitation rates have been calculated by assuming detailed balance. We include a total of 72 levels up to energies of 200 K above the ground state in the K_a = 0, 1, and 2 ladders, and calculate for five different kintic temperatures (10 - 50 K) and for five different apparent background radiation temperatures (2.7 - 40 K). The apparent background radiation temperature is the temperature inferred from the background radiation intensity observed at the

point concerned in the LVG models. LVG models have been calculated for each kinetic temperature and background radiation temperature, and the input values of the H_2 density, $n(H_2) = 10^{3.5}$ - 10^7 cm^3, and the $HOCO^+$ fractional abundance relative to H_2, $f(HOCO^+) = 10^{-7.5}$ - 10^{-15}. We have carried out calculations using a velocity gradient dV/dr = 1 km s^{-1} pc^{-1}. For the same reason we mentioned above for H_2CS, we have shown the calculation results as a function of $n(HOCO^+)/dV/dr$ (= $N(HOCO^+)/\Delta V$), and some of them are illustrated in Figures A.4 to A.6.

Figure A.1a - c Excitation temperature (T_{ex}) versus $\log(n(H_2CS)/dV/dr)$ for $n(H_2) = 1 \times 10^5$ cm^{-3}. Transitions are indicated in the figures. (a) for T_{kin} = 10 K. (b) for T_{kin} = 20 K. (c) for T_{kin} = 100 K.

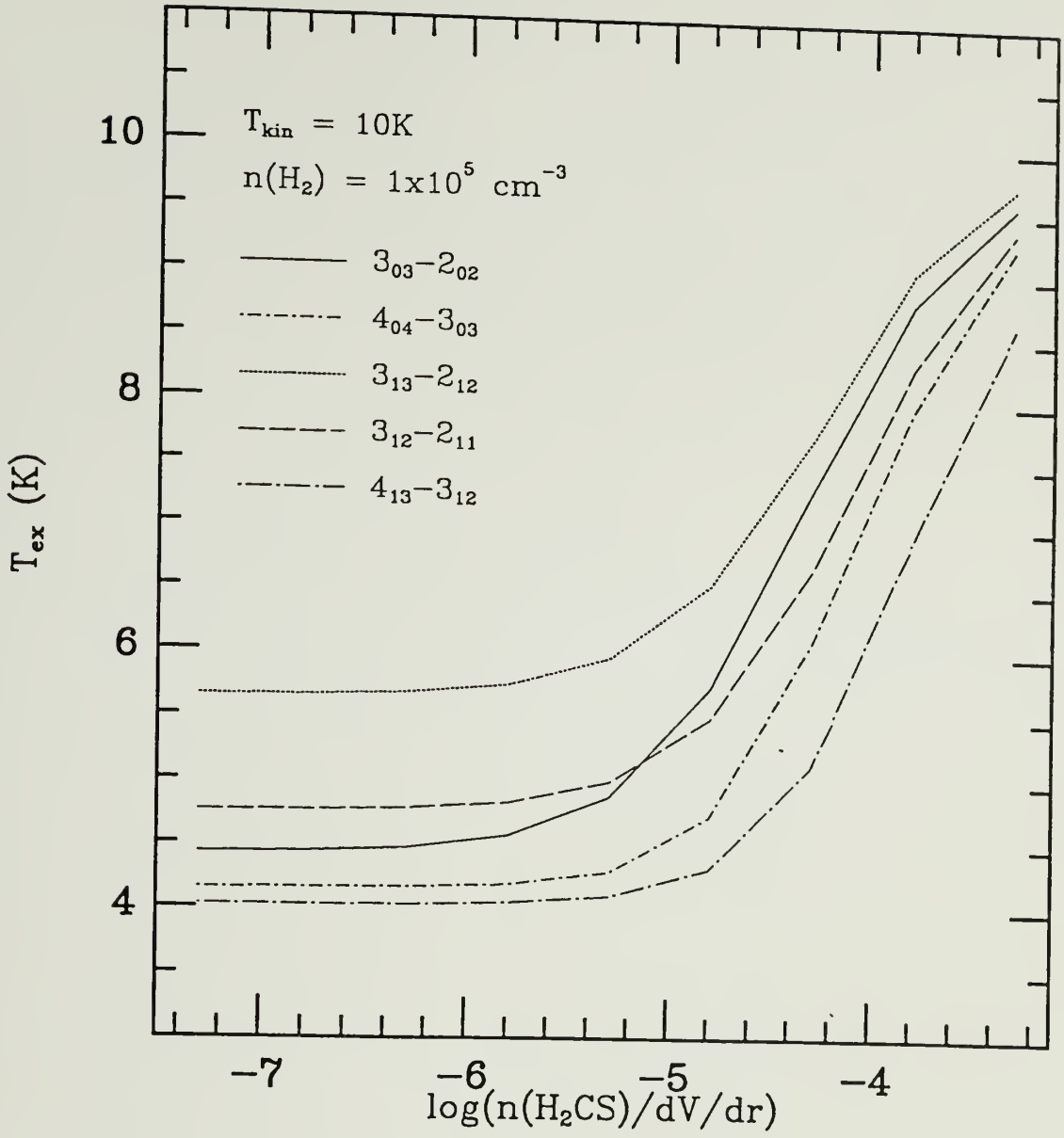
T_{kin} = 10K
$n(H_2)$ = 1x10^5 cm^{-3}
$3_{03}-2_{02}$
$4_{04}-3_{03}$
$3_{13}-2_{12}$
$3_{12}-2_{11}$
$4_{13}-3_{12}$
T_{ex} (K)
10
8
6
4
−7
−6
−5
−4
log(n(H$_2$CS)/dV/dr)

(a)

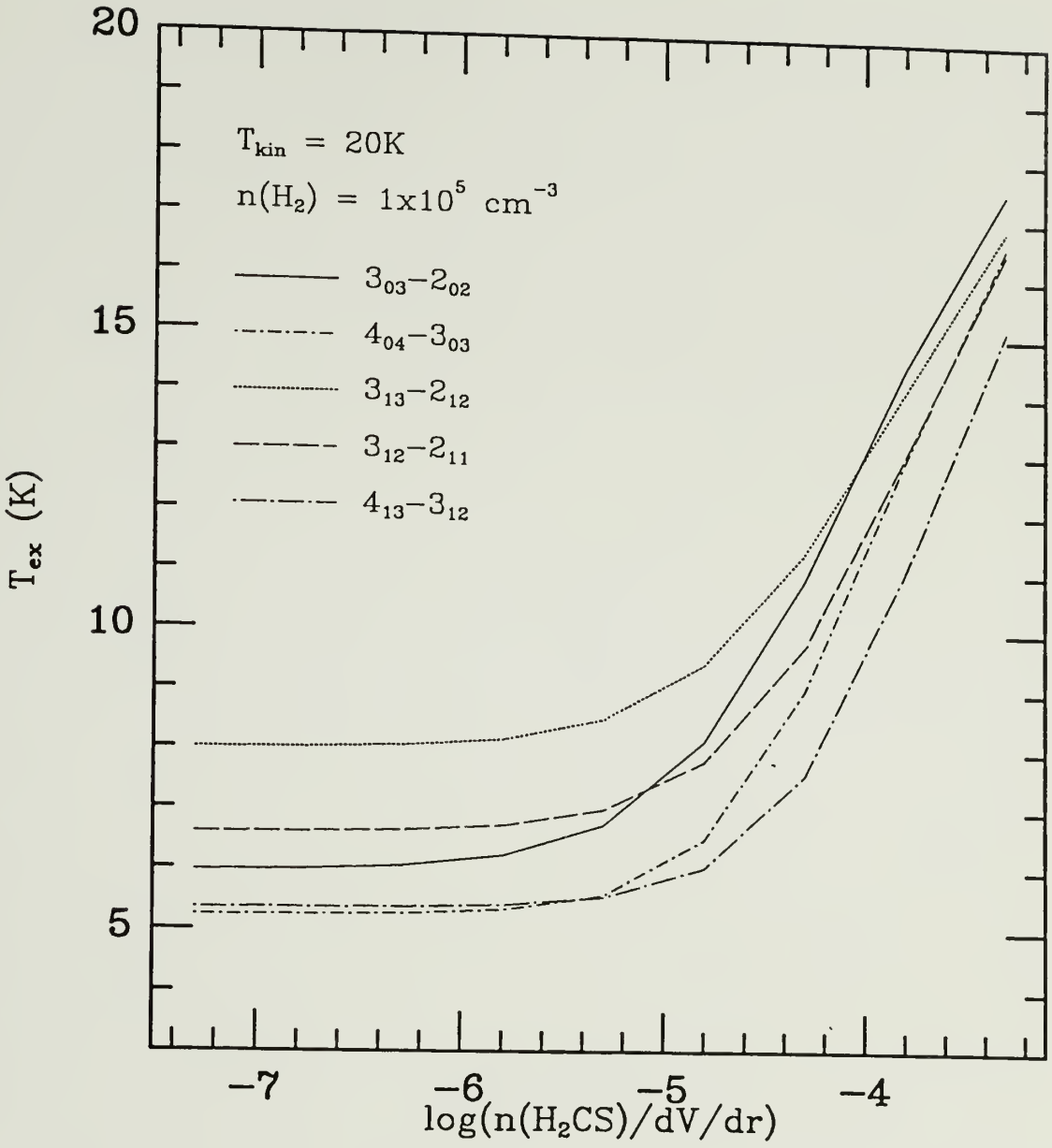
20
15
10
5
T_{kin} = 20K
$n(H_2)$ = 1x10^5 cm^{-3}
$3_{03}-2_{02}$
$4_{04}-3_{03}$
$3_{13}-2_{12}$
$3_{12}-2_{11}$
$4_{13}-3_{12}$
T_{ex} (K)
−7
−6
−5
−4
log(n(H_2CS)/dV/dr)

(b)

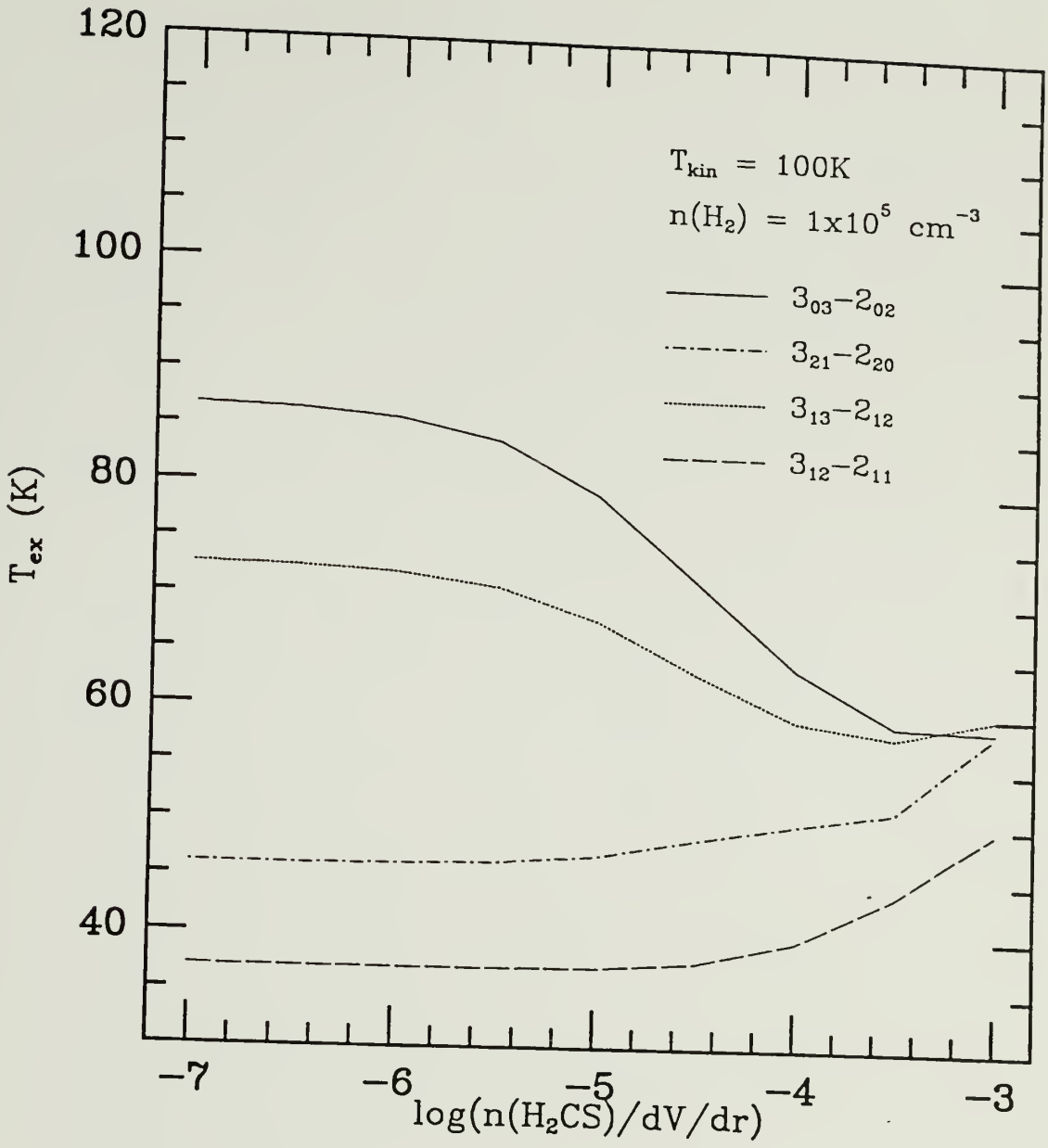
120
100
80
60
40
T_{ex} (K)
T_{kin} = 100K
$n(H_2)$ = 1x10^5 cm^{-3}
$3_{03}-2_{02}$
$3_{21}-2_{20}$
$3_{13}-2_{12}$
$3_{12}-2_{11}$
−7
−6
−5
−4
−3
log(n(H_2CS)/dV/dr)

(c)

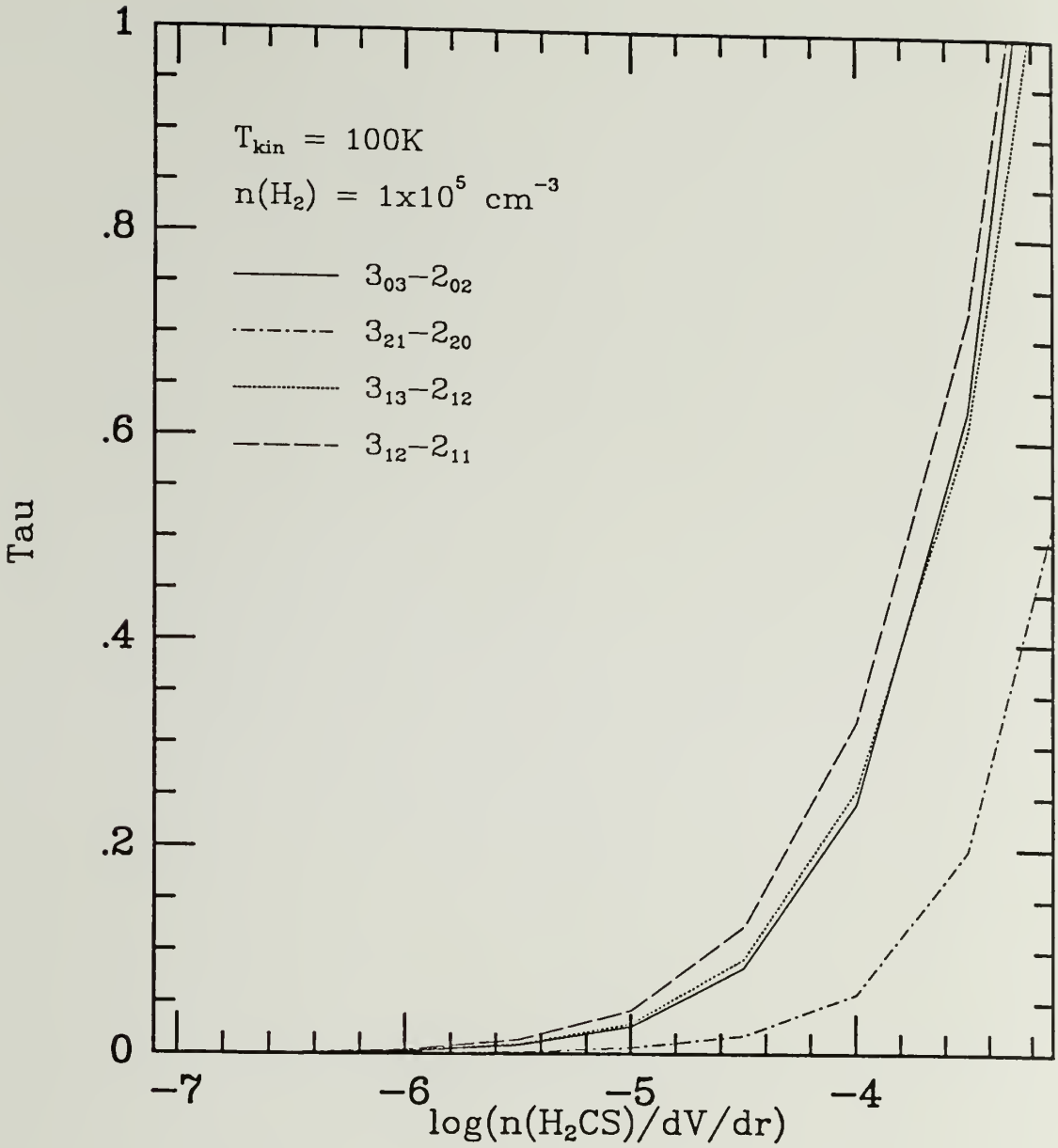
1
.8
.6
.4
.2
0
Tau
T_{kin} = 100K
$n(H_2)$ = 1x10^5 cm^{-3}
$3_{03}-2_{02}$
$3_{21}-2_{20}$
$3_{13}-2_{12}$
$3_{12}-2_{11}$
−7
−6
−5
−4
log(n(H_2CS)/dV/dr)

(c)

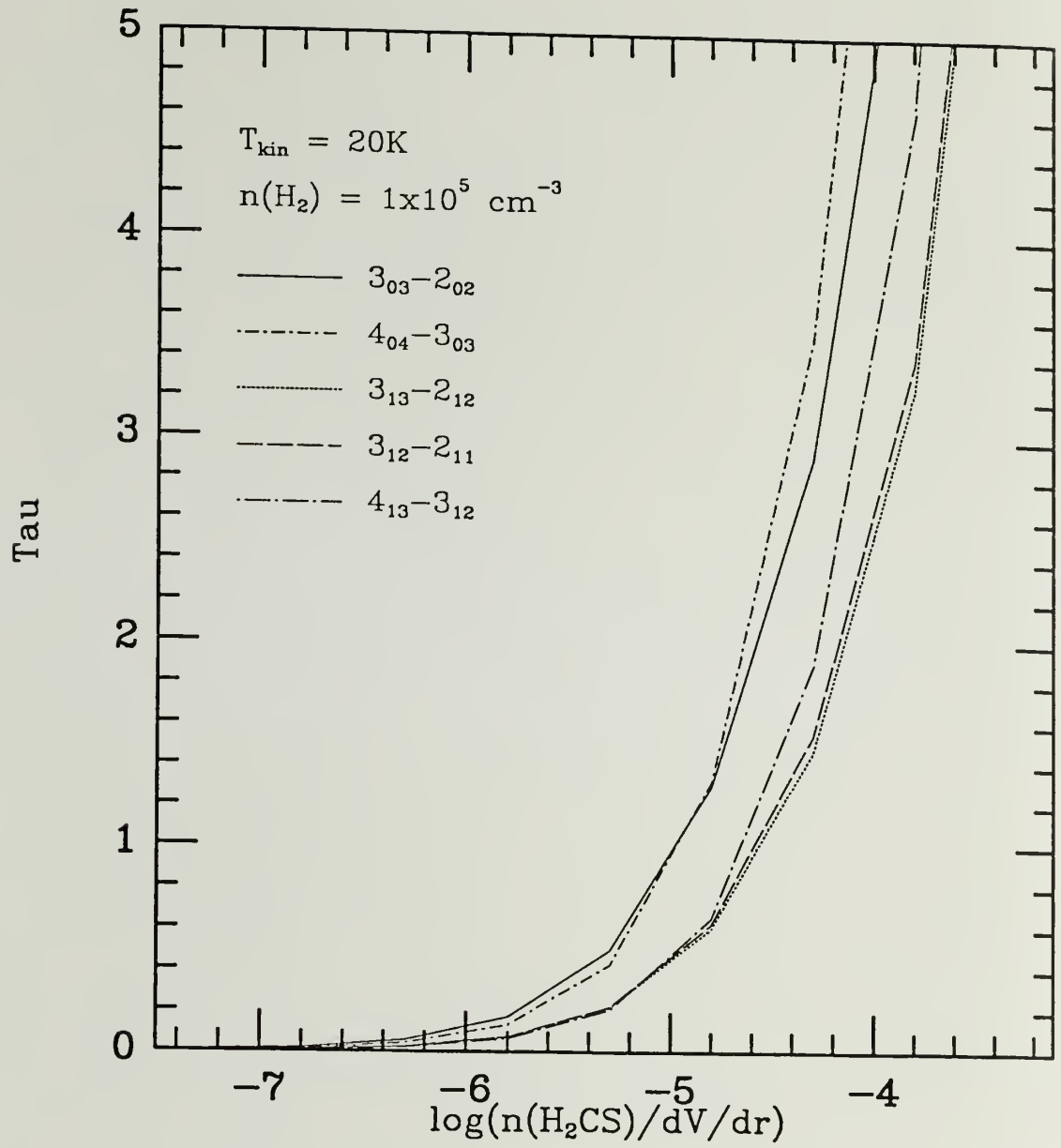
5
4
3
2
1
0
Tau
T_{kin} = 20K
$n(H_2)$ = 1x10^5 cm^{-3}
3_{03}–2_{02}
4_{04}–3_{03}
3_{13}–2_{12}
3_{12}–2_{11}
4_{13}–3_{12}
−7
−6
−5
−4
log(n(H_2CS)/dV/dr)

(b)

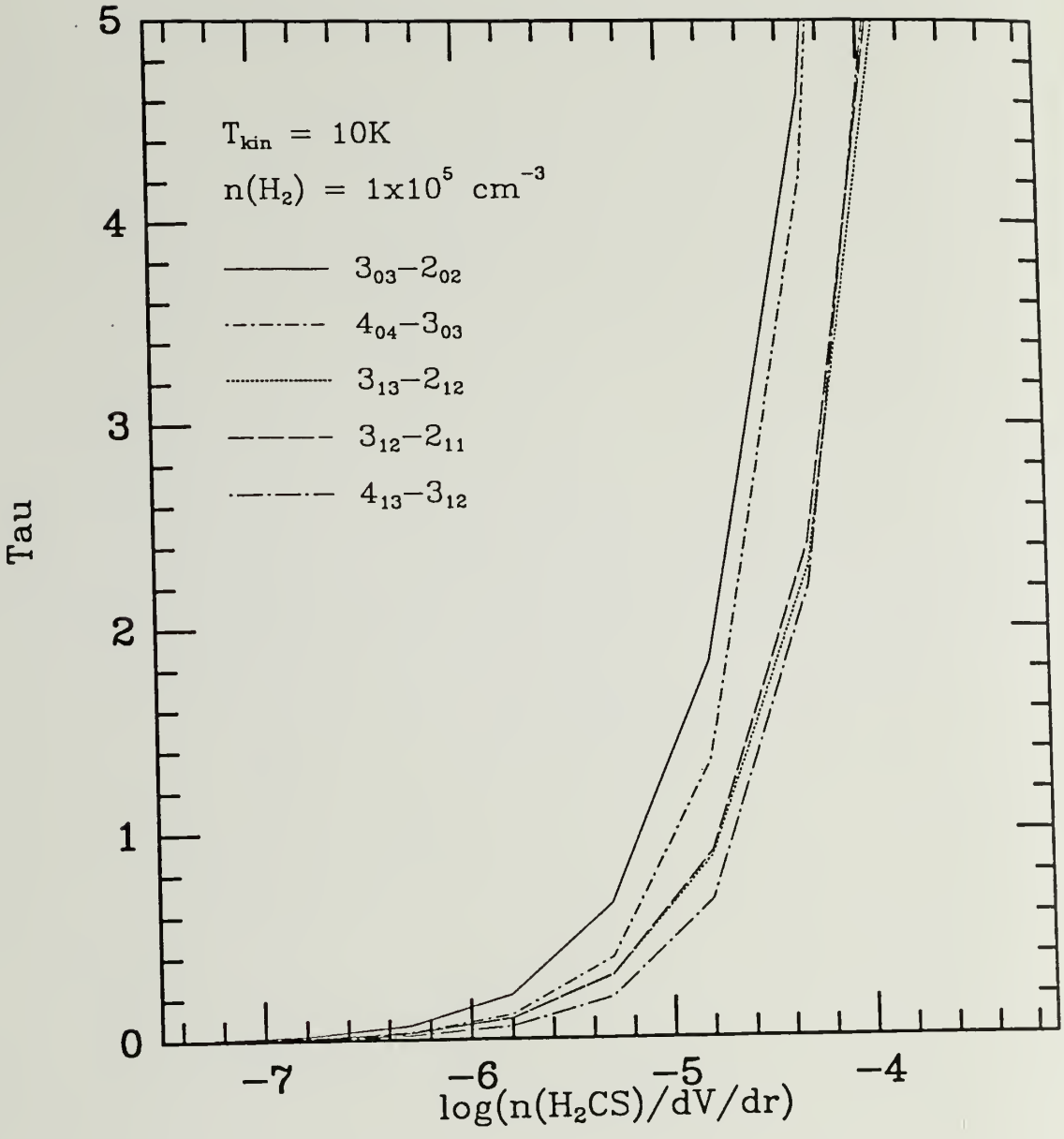
Tau
5
4
3
2
1
0
T_{kin} = 10K
$n(H_2)$ = 1x10^5 cm^{-3}
3_{03}–2_{02}
4_{04}–3_{03}
3_{13}–2_{12}
3_{12}–2_{11}
4_{13}–3_{12}
−7
−6
−5
−4
log(n(H_2CS)/dV/dr)

(a)

Figure A.2a - c Optical depth (Tau) versus $\log(n(H_2CS)/dV/dr)$ for $n(H_2) = 1 \times 10^5$ cm^{-3}. Transitions are indicated in the figures. (a) for $T_{kin} = 10$ K. (b) for $T_{kin} = 20$ K. (c) for $T_{kin} = 100$ K.

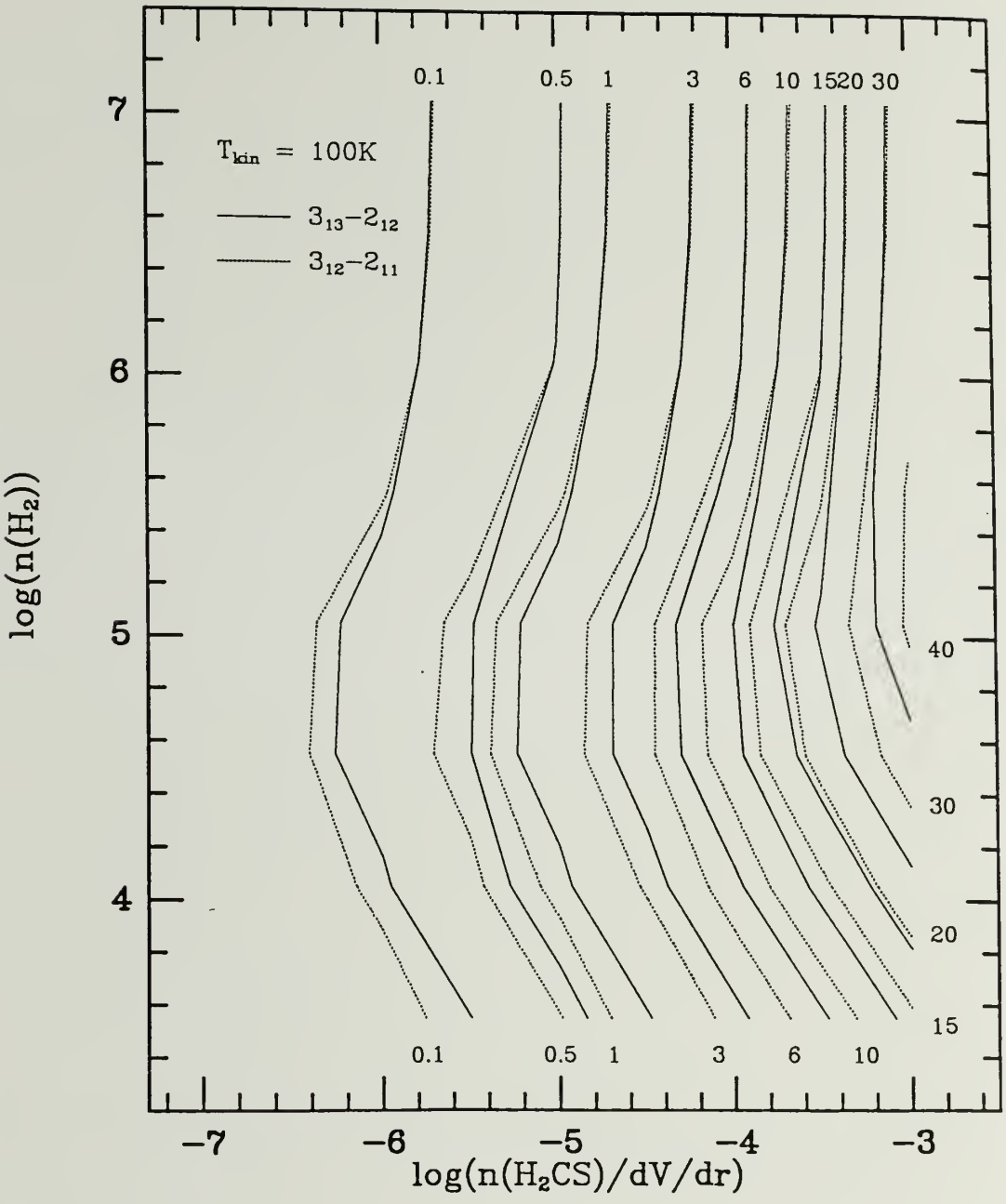
T_{kin} = 100K
$3_{13}-2_{12}$
$3_{12}-2_{11}$
0.1
0.5
1
3
6
10
15
20
30
40
log(n(H₂))
log(n(H₂CS)/dV/dr)
7
6
5
4
−7
−6
−5
−4
−3

(f)

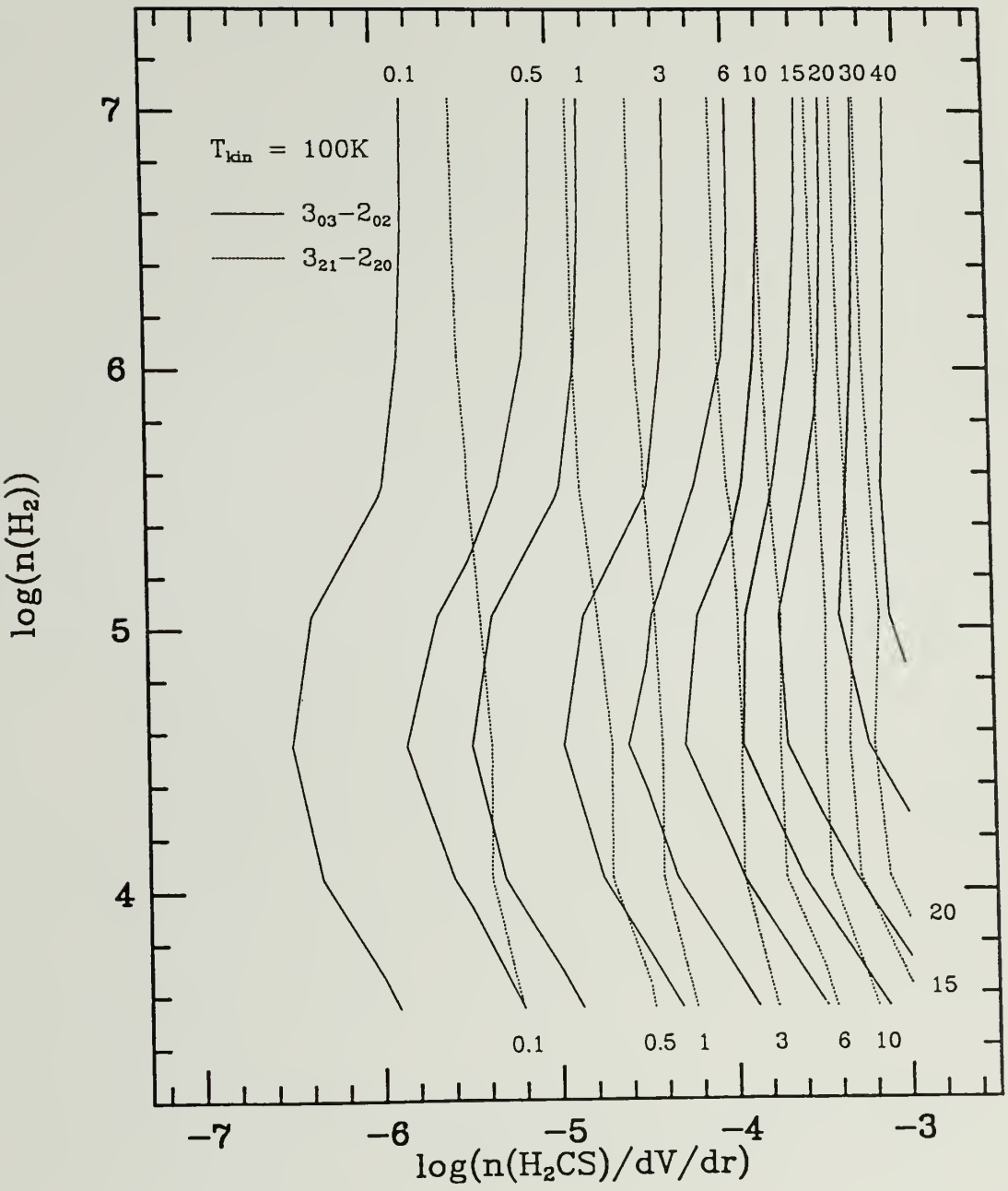
0.1
0.5
1
3
6
10
15
20
30
40
T_{kin} = 100K
$3_{03}-2_{02}$
$3_{21}-2_{20}$
7
6
5
4
log(n(H₂))
20
15
0.1
0.5
1
3
6
10
−7
−6
−5
−4
−3
log(n(H₂CS)/dV/dr)

(e)

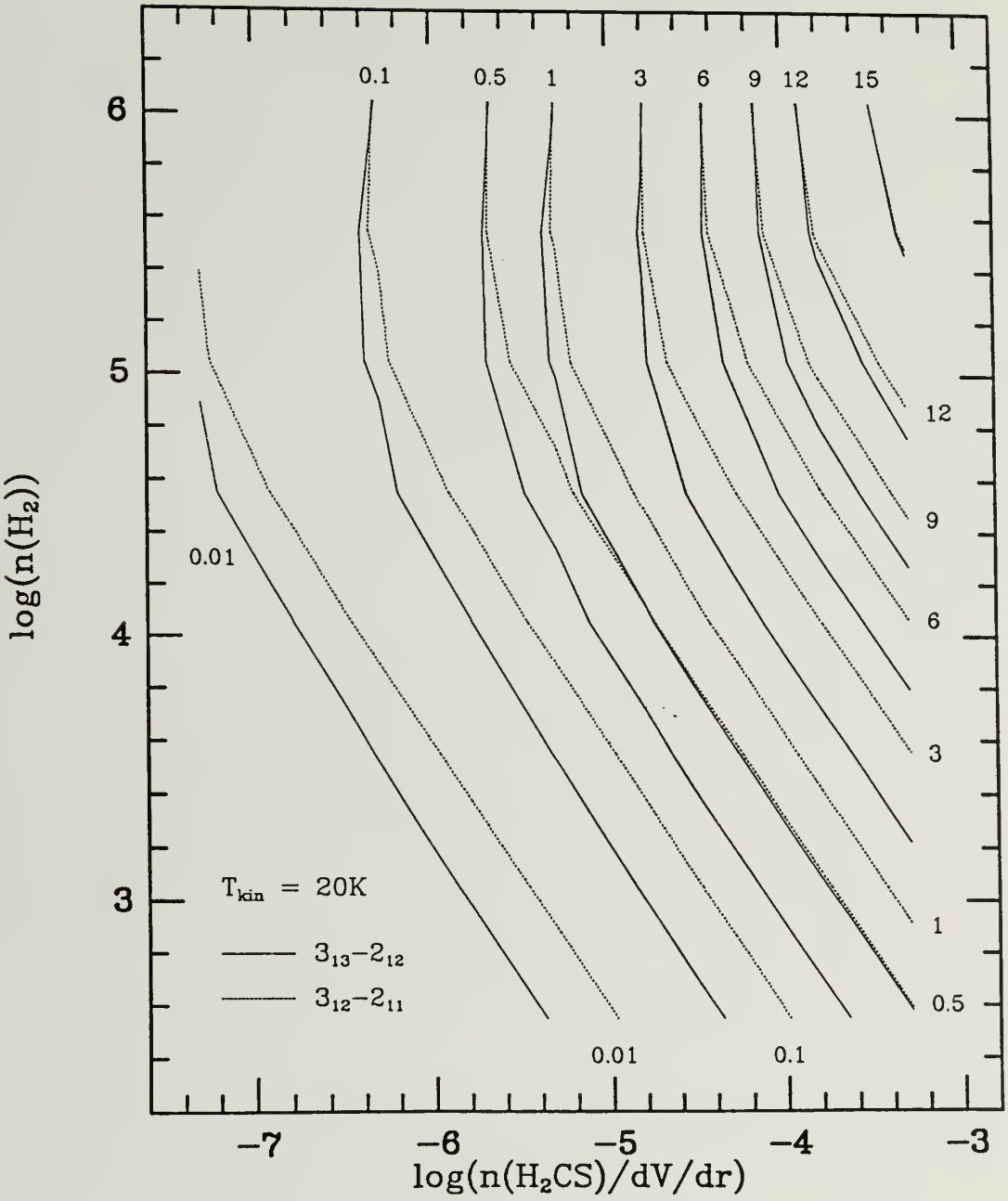
0.1
0.5
1
3
6
9
12
15
12
9
6
3
1
0.5
0.01
0.01
0.1
T_{kin} = 20K
$3_{13}-2_{12}$
$3_{12}-2_{11}$
log(n(H2))
log(n(H2CS)/dV/dr)
6
5
4
3
−7
−6
−5
−4
−3

(d)

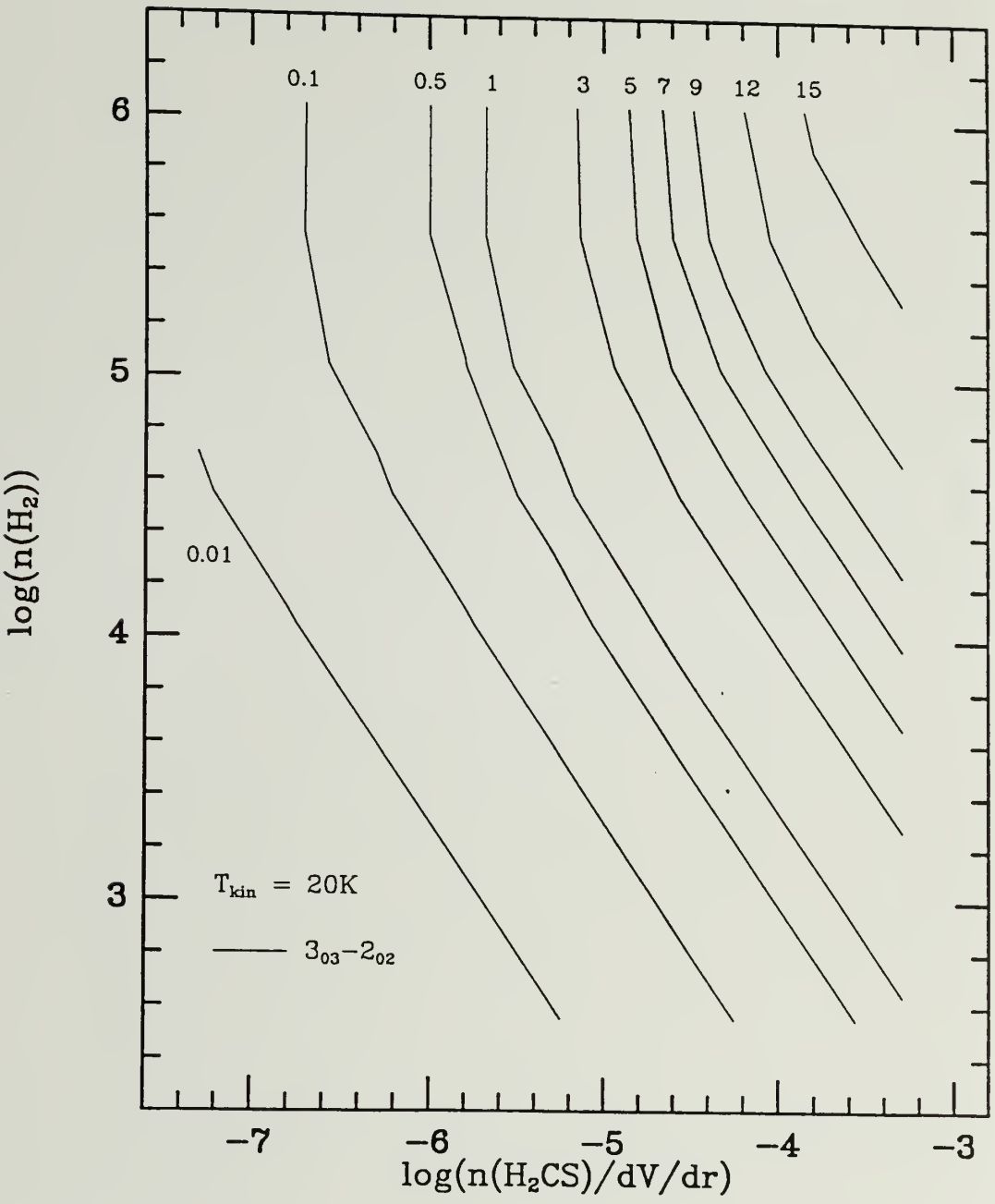
0.1
0.5
1
3
5
7
9
12
15
0.01
6
5
4
3
log(n(H2))
T_kin = 20K
3_03–2_02
−7
−6
−5
−4
−3
log(n(H2CS)/dV/dr)

(c)

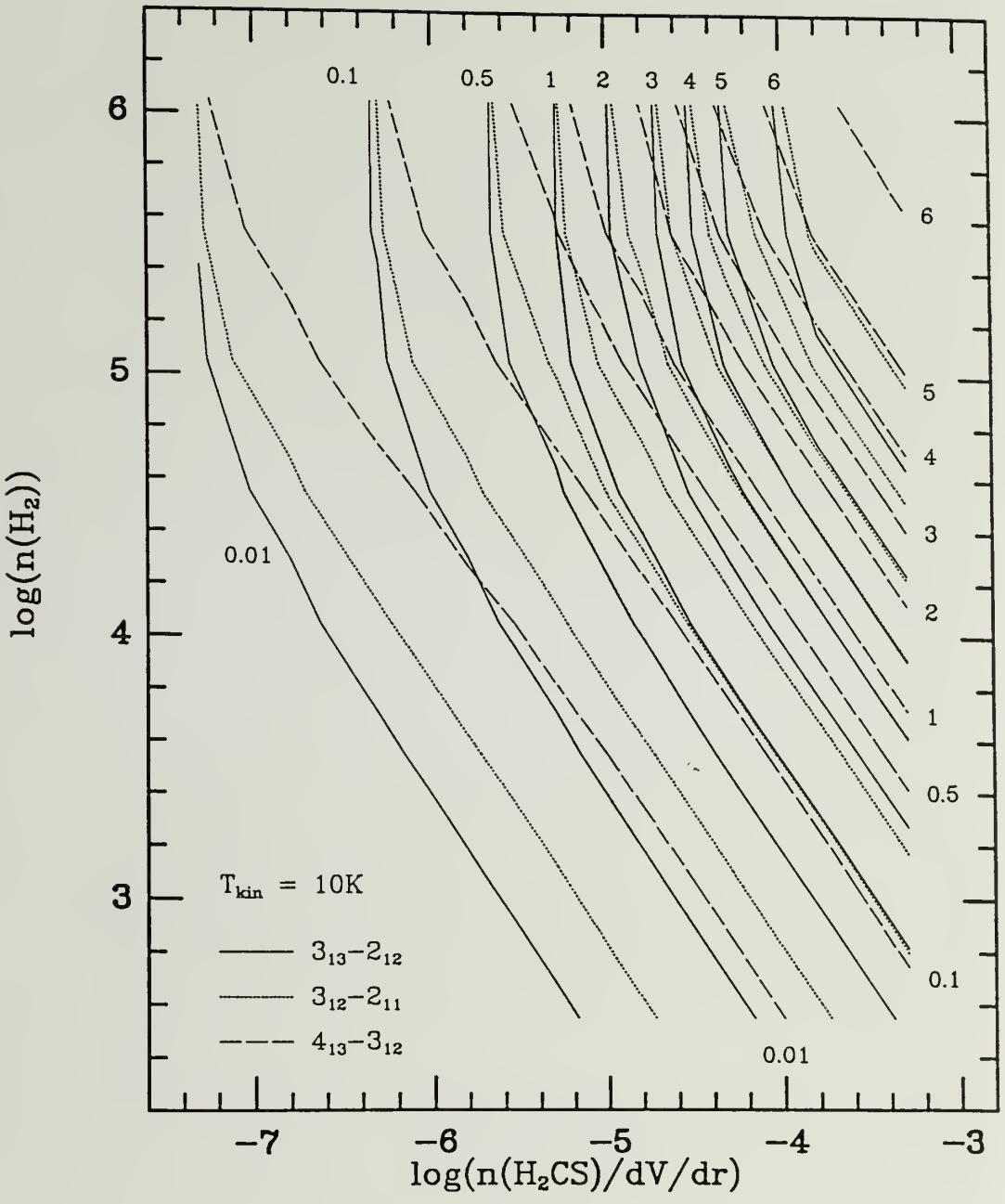
0.1
0.5
1
2
3
4
5
6
6
5
4
3
2
1
0.5
0.1
0.01
0.01
T_{kin} = 10K
$3_{13}-2_{12}$
$3_{12}-2_{11}$
$4_{13}-3_{12}$
log(n(H₂))
log(n(H₂CS)/dV/dr)
6
5
4
3
−7
−6
−5
−4
−3

(b)

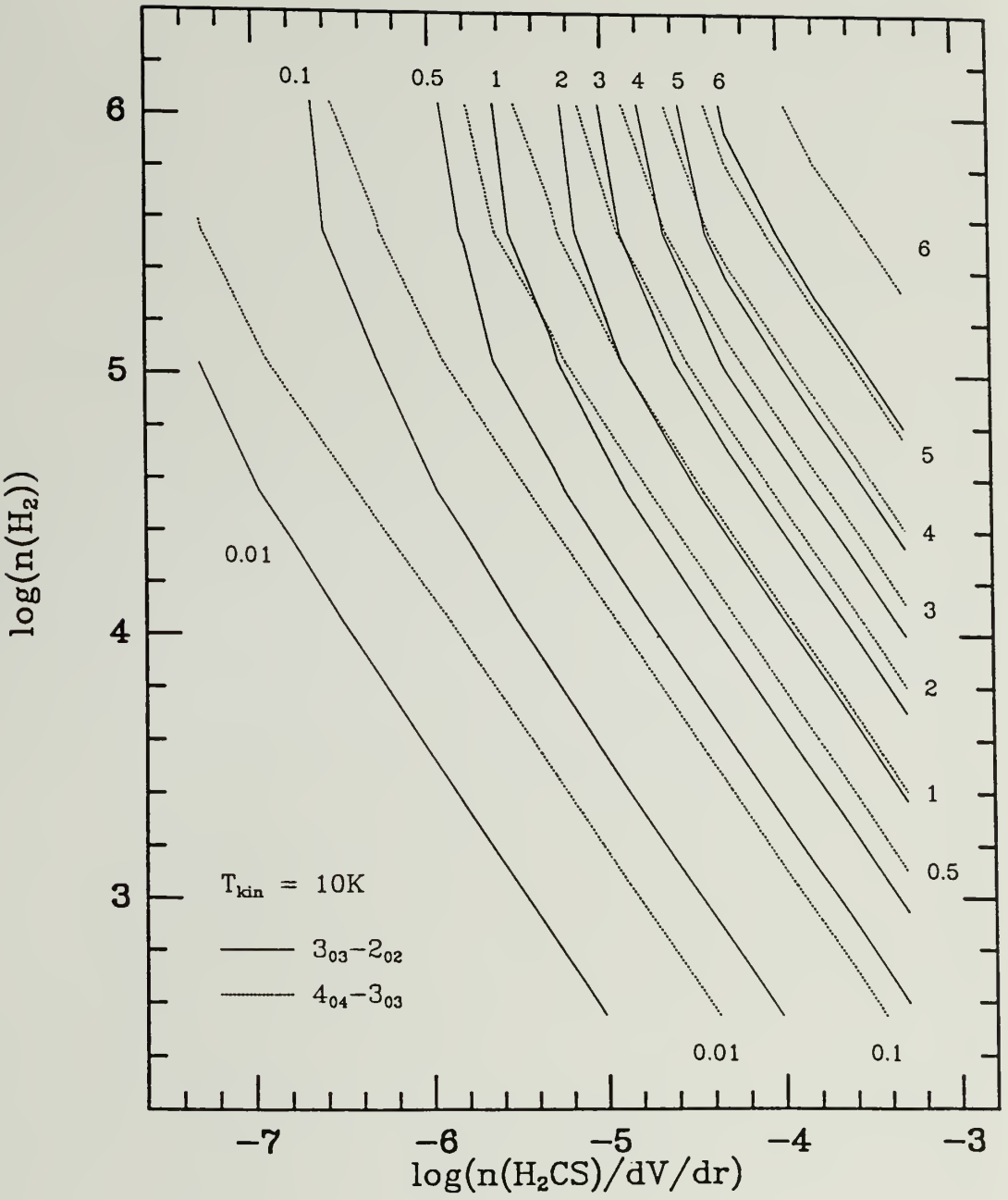
0.1
0.5
1
2
3
4
5
6
6
5
4
3
2
1
0.5
0.01
T_{kin} = 10K
$3_{03}-2_{02}$
$4_{04}-3_{03}$
0.01
0.1
log(n(H₂))
log(n(H₂CS)/dV/dr)
6
5
4
3
−7
−6
−5
−4
−3

(a)

Figure A.3a - f Constant antenna temperature curves. Contour levels are indicated in the figures. (a), (c), and (e) for para transitions for T_{kin} = 10, 20, and 100 K, respectively. (b), (d), and (f) for ortho transitions for T_{kin} = 10, 20, and 100 K, respectively.

Figure A.5a - b Optical depth (Tau) versus log($n(HOCO^+)/dV/dr$) for $n(H_2) = 3.2 \times 10^4$ cm^{-3}. (a) for T_{kin} = 10 K and T_{bg} = 2.7 K. (b) for T_{kin} = 50 K and T_{bg} = 10 K.

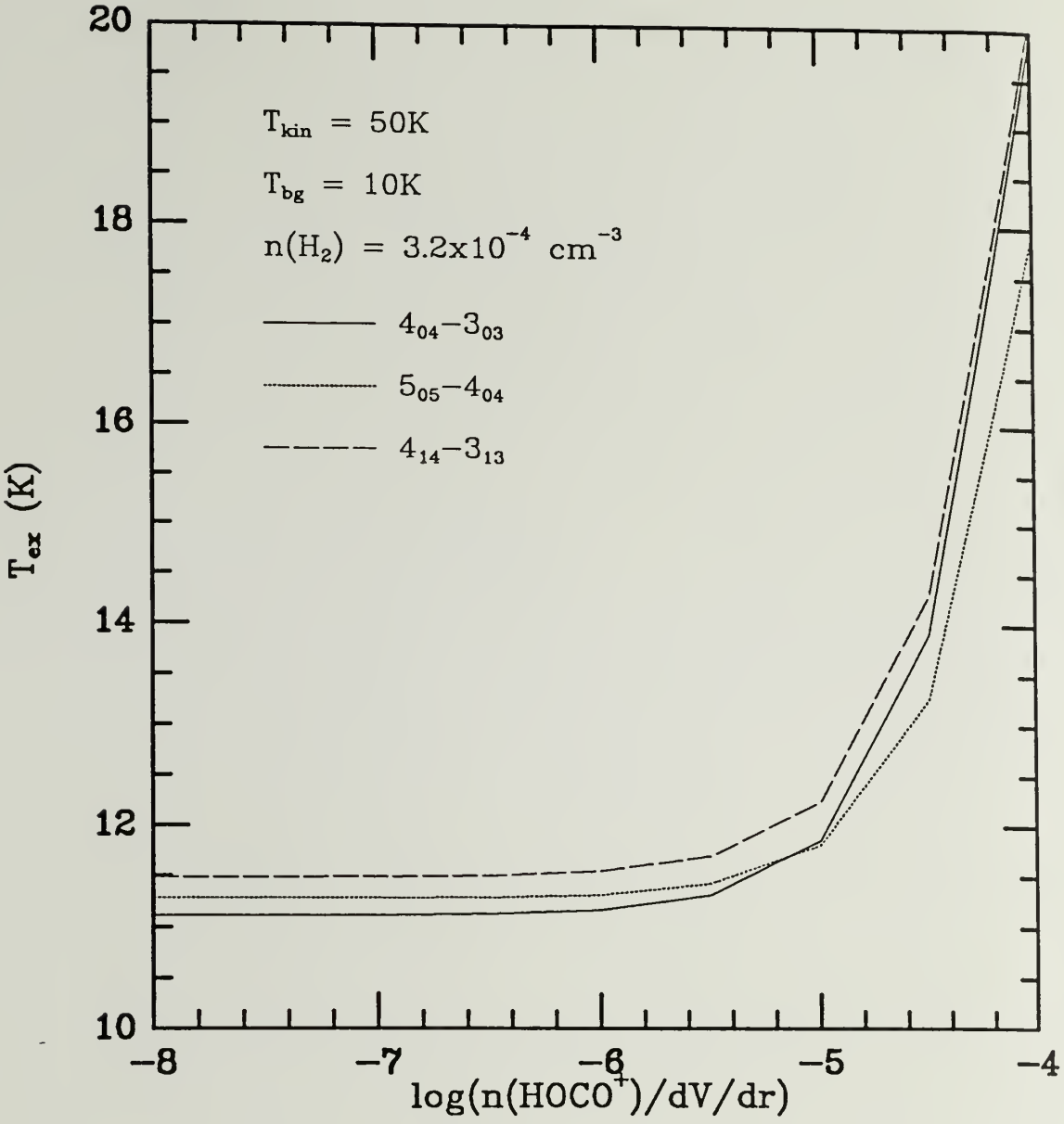
20
18
16
14
12
10
T_{ex} (K)
T_{kin} = 50K
T_{bg} = 10K
$n(H_2) = 3.2x10^{-4}$ cm^{-3}
$4_{04}-3_{03}$
$5_{05}-4_{04}$
$4_{14}-3_{13}$
−8
−7
−6
−5
−4
log(n(HOCO$^+$)/dV/dr)

(b)

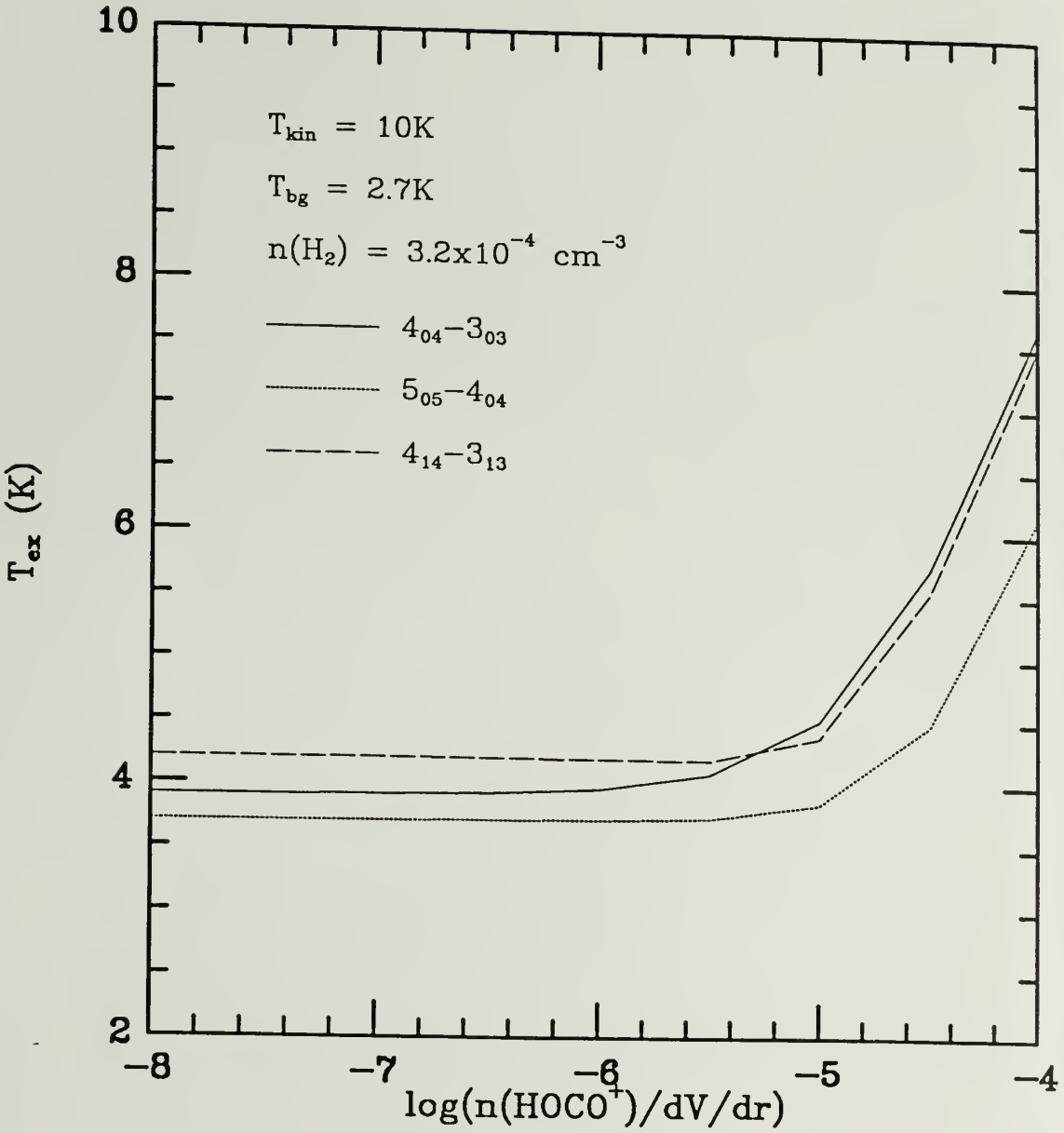
10
8
6
4
2
T_{ex} (K)
T_{kin} = 10K
T_{bg} = 2.7K
$n(H_2) = 3.2x10^{-4}$ cm^{-3}
$4_{04}-3_{03}$
$5_{05}-4_{04}$
$4_{14}-3_{13}$
−8
−7
−6
−5
−4
log(n(HOCO$^+$)/dV/dr)

(a)

Figure A.4a - b Excitation temperature (T_{ex}) versus $\log(n(HOCO^+)/dV/dr)$ for the volumn density $n(H_2) = 3.2 \times 10^4$ cm^{-3}. (a) for the kinetic temperature $T_{kin} = 10$ K and the background temperature $T_{bg} = 2.7$ K. (b) for $T_{kin} = 50$ K and $T_{bg} = 10$ K.

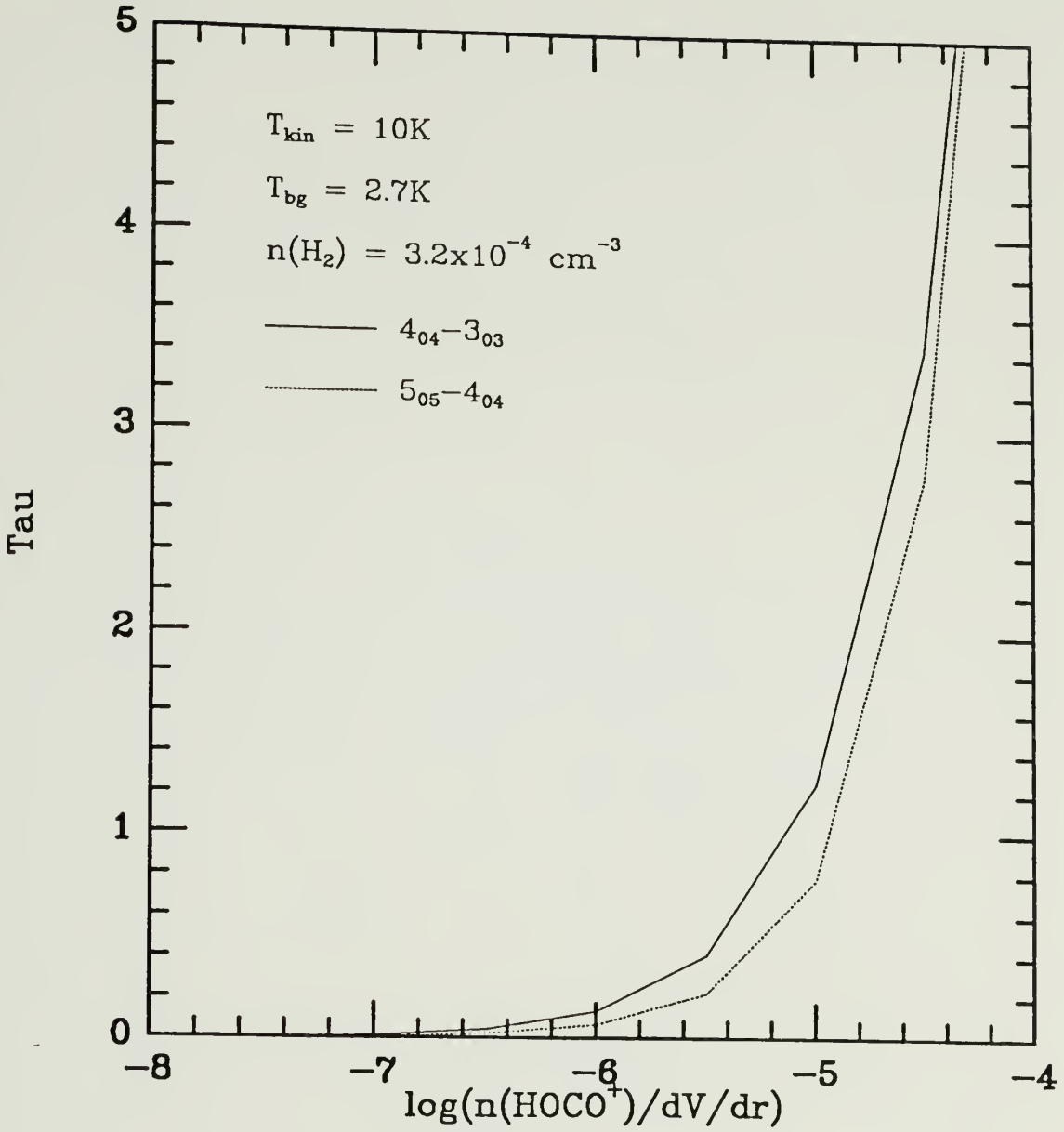
5
4
3
2
1
0
Tau
T_{kin} = 10K
T_{bg} = 2.7K
$n(H_2)$ = $3.2x10^{-4}$ cm^{-3}
$4_{04}-3_{03}$
$5_{05}-4_{04}$
−8
−7
−6
−5
−4
log(n(HOCO$^+$)/dV/dr)

(a)

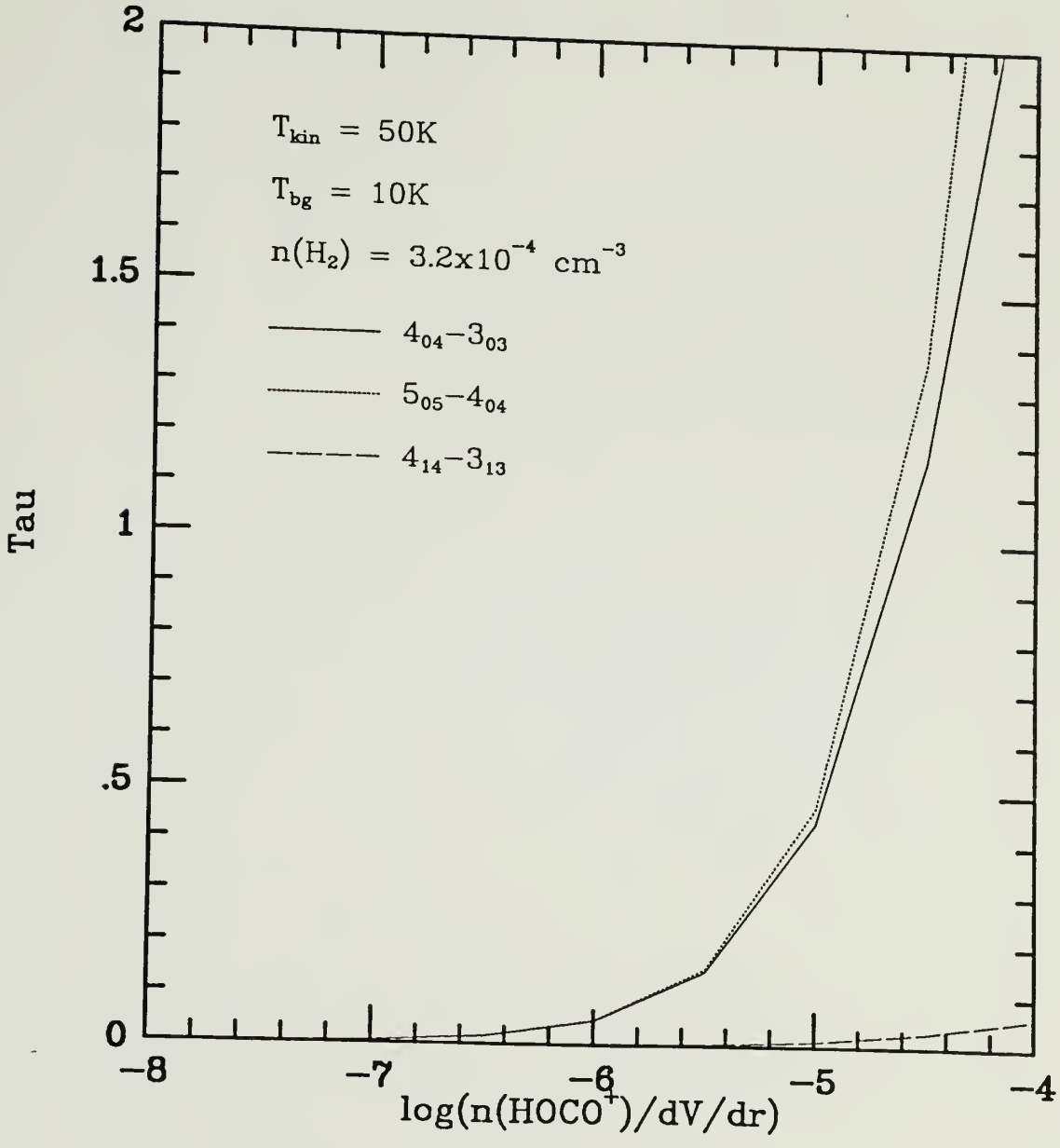
2
1.5
1
.5
0
Tau
T_{kin} = 50K
T_{bg} = 10K
$n(H_2)$ = 3.2x10^{-4} cm^{-3}
$4_{04}-3_{03}$
$5_{05}-4_{04}$
$4_{14}-3_{13}$
−8
−7
−6
−5
−4
log(n(HOCO$^+$)/dV/dr)

(b)

Figure A.6a - d Constant antenna temperature curves. Contour levels (K) are indicated in the figures. (a) for the 1_{01} - 0_{00} transition for T_{kin} = 10 K and T_{bg} = 2.7 K. (b) for the 4_{04} - 3_{03}, 5_{05} - 4_{04}, and 4_{14} - 3_{13} transitions for T_{kin} = 10 K and T_{bg} = 2.7 K. (c) for same transitions as in (b) for T_{kin} = 50 K and T_{bg} = 10 K. (d) for same transitions as in (b) for T_{kin} = 50 K and T_{bg} = 20 K.

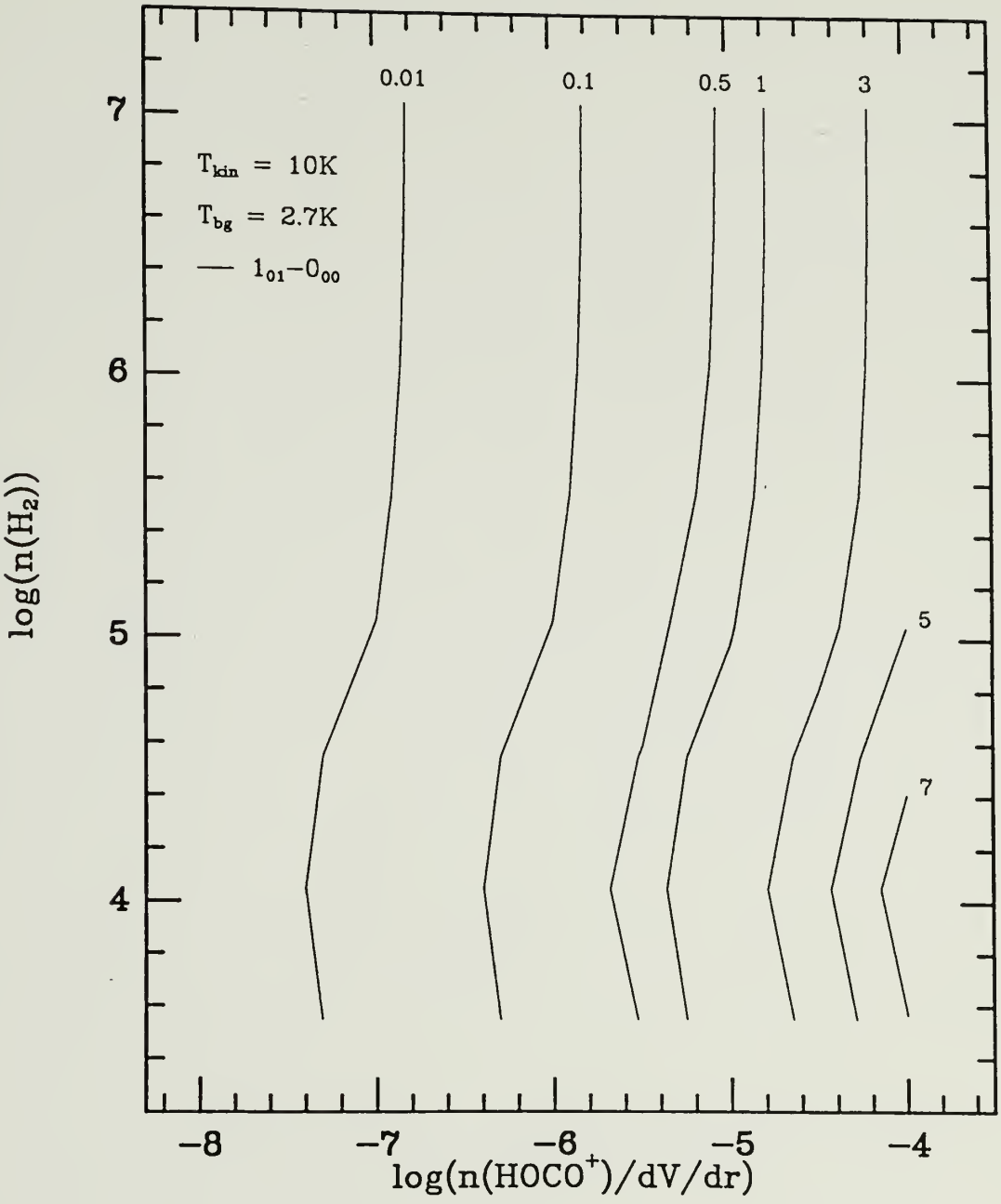
0.01
0.1
0.5
1
3
5
7
T_{kin} = 10K
T_{bg} = 2.7K
$1_{01}-0_{00}$
log(n(H₂))
7
6
5
4
−8
−7
−6
−5
−4
log(n(HOCO⁺)/dV/dr)

(a)

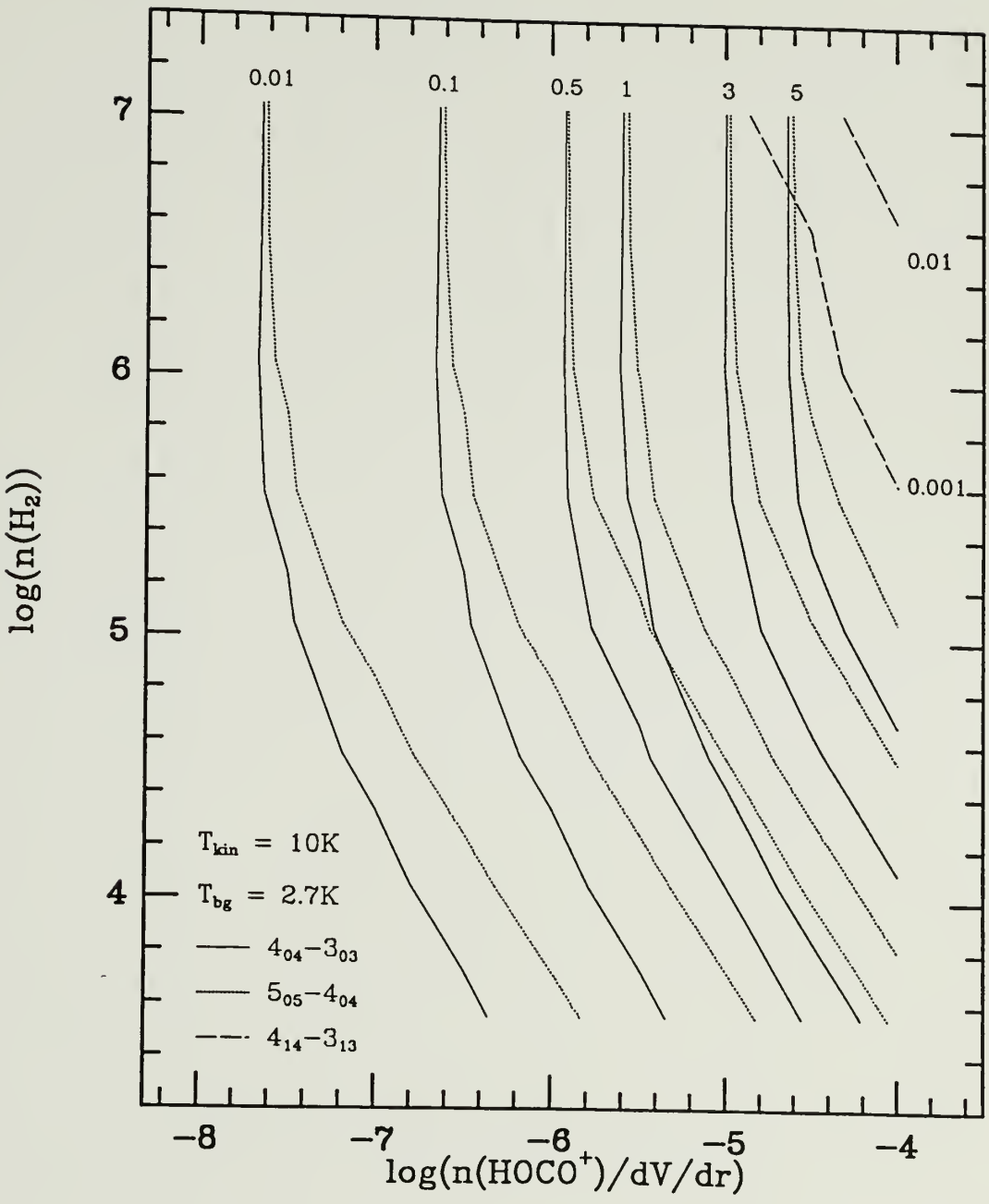
0.01
0.1
0.5
1
3
5
0.01
0.001
7
6
5
4
log(n(H2))
T_kin = 10K
T_bg = 2.7K
4_04–3_03
5_05–4_04
4_14–3_13
−8
−7
−6
−5
−4
log(n(HOCO+)/dV/dr)

(b)

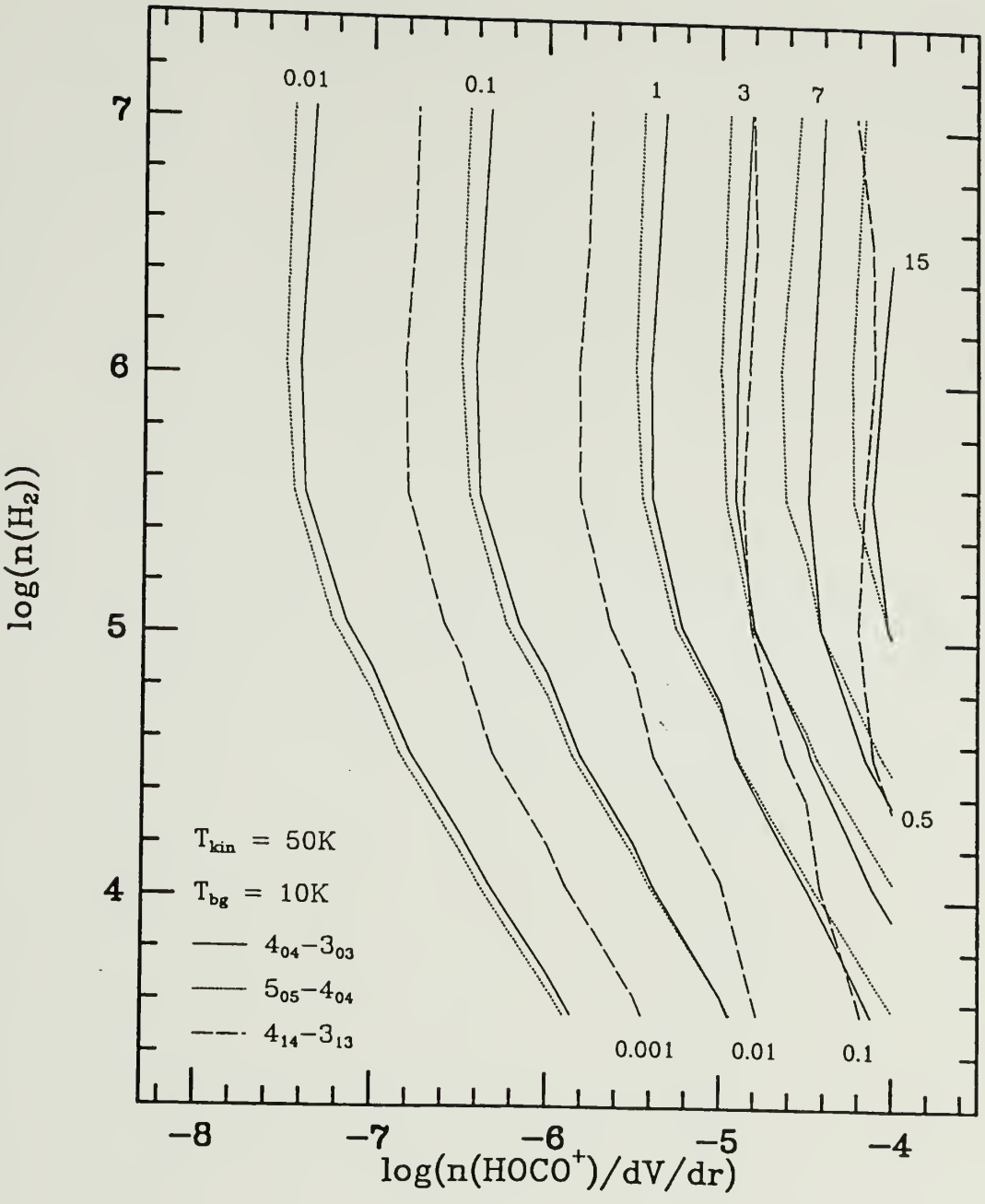
0.01
0.1
1
3
7
15
0.5
0.001
0.01
0.1
T_{kin} = 50K
T_{bg} = 10K
$4_{04}-3_{03}$
$5_{05}-4_{04}$
$4_{14}-3_{13}$
log(n(H₂))
log(n(HOCO⁺)/dV/dr)
7
6
5
4
−8
−7
−6
−5
−4

(c)

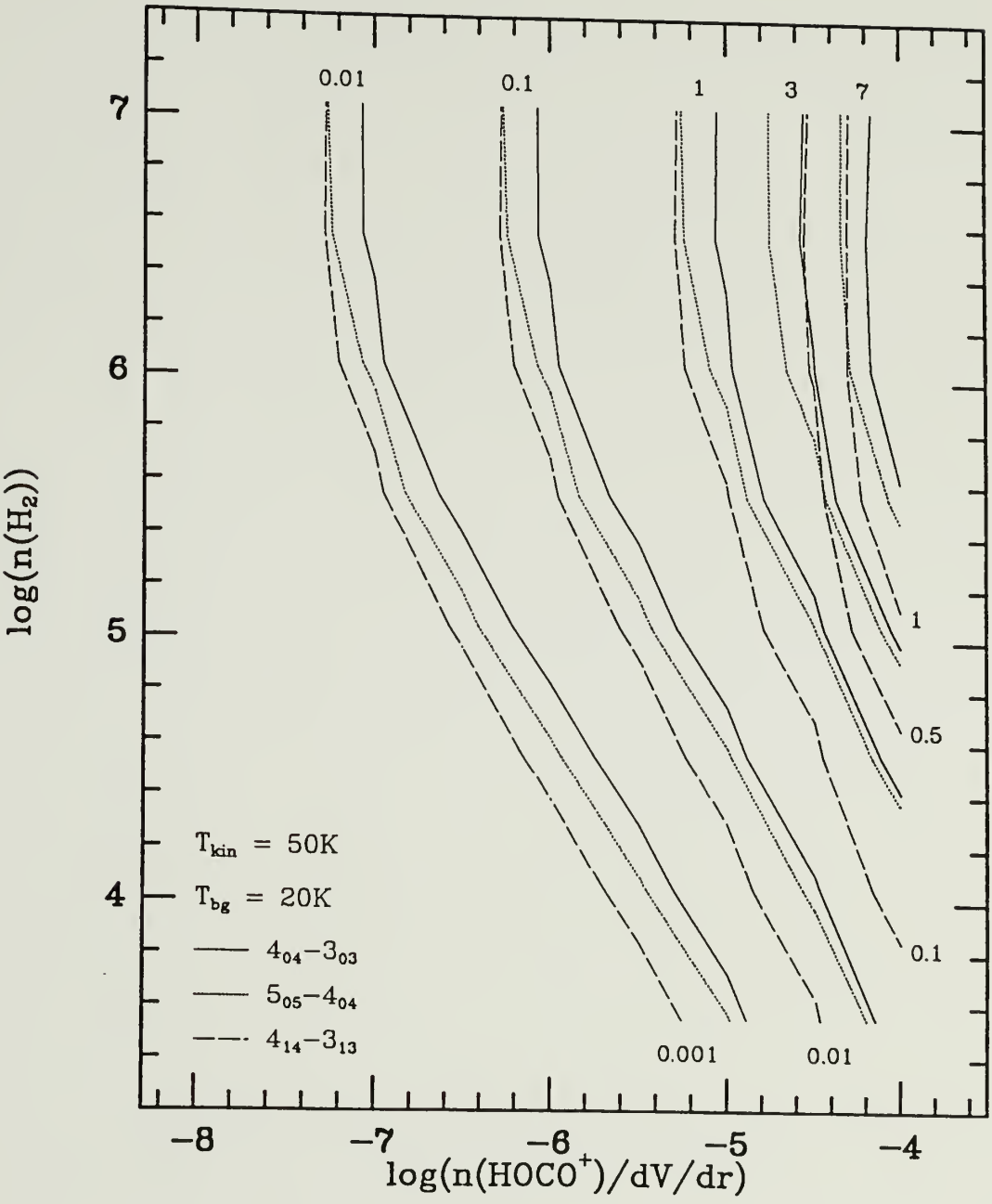
0.01
0.1
1
3
7
1
0.5
0.1
0.001
0.01
T_{kin} = 50K
T_{bg} = 20K
$4_{04}-3_{03}$
$5_{05}-4_{04}$
$4_{14}-3_{13}$
7
6
5
4
−8
−7
−6
−5
−4
log(n(H₂))
log(n(HOCO⁺)/dV/dr)

(d)

APPENDIX B

Abundances of Molecules in the Sgr A Cloud Complex

Data were obtained in 1988 June with the Swedish-ESO 15 m telescope in Chile, together with the observations of the $HOCO^+$ 4_{04} - 3_{03} and 5_{05} - 4_{04} transitions described in Chapter 8. Telescope parameters are given in Table 8.1 and observing methods in § 8.3. Observed molecules, transitions, and rest frequencies are included in Table B.1, and observed line parameters toward the cores of condensations in Sgr A (see Figure 8.1) are included in Table B.2. Each condensation is labeled A - G for convenience, as indicated in Table B.2. The Cloud A/S position is offset (Δl, Δb) = (1.4′, 0.4′) from the nominal position implied by M-0.13-0.08 (Cloud A). Sample spectra are shown in Figure B.1, including the $HOCO^+$ lines.

The column densities were determined from the following equation, assuming optically thin emission and neglecting any background radiation :

$$N_{molecule}(cm^{-2}) = 2\ \pi\ \nu^2\ k\ \Delta V\ T_R\ /\ h\ c^3 f\ A$$

where ν is the line frequency, ΔV the FWHP line width, T_R the brightness temperature assuming the source fills the main beam, f the fractional population in the upper level of the transition, and A the Einstein spontaneous emission coefficient.

To derive the total column density of HCO, we used the normalized theoretical relative intensities of 42 : 25 : 25 : 8 for (J=3/2-1/2 F=2-1) :(J=3/2-1/2 F=1-0) : (J=1/2-1/2 F=1-1) : (J=1/2-1/2 F=1-0) (Schenewerk, Snyder, and Hjalmarson 1986).

Methyl acetylene (CH_3CCH) has been observed via its J=5-4 and 6-5 transitions. However, since the K = 0, 1, and 2 components overlap with each other, we fit to gaussians by assuming the same V_{LSR} for each component. The gaussian fit results are given in Table B.3. Rotation temperatures of CH_3CCH have been derived from the rotation diagrams in Figure B.2. Askne *et al.* (1984) have suggested that methyl acetylene is an excellent kinetic temperature probe and a simple rotation diagram can be used to determine the kinetic temperature.

The molecular abundances have been calculated by assuming T_{ROT} and an LTE population distribution. We have used the rotation diagrams for CH_3CCH to derive its column densities and assumed T_{ROT} = 50 K for OCS since both species have similar electric dipole moments of less than 1 Debye (see Table B.1). We used T_{ROT} = 20 K for other molecules in Table B.1, whose electric dipole moments are greater than 1 Debye. We did not derive the column density for methanol because of its probable non-Boltzmann excitation. The calculated abundances for molecules are given in Table B.4 toward each core. In Table B.5 we list the fractional abundances relative to H_2 for the molecules observed in Sgr A, with those for TMC-1 and Sgr B2 from the tabulation of Irvine, Goldsmith, and Hjalmarson

(1987) for comparison. The molecular hydrogen column densities were derived from $N(^{13}CO)$ for each position from the map of Armstrong and Barrett (1984) assuming $[CO]/[^{13}CO] = 23$ and $[CO]/[H_2] = 10^{-4}$ (Penzias 1980).

TABLE B.1

Observed Molecules in Sgr A

Molecule	Transition	Rest Frequency[a] (GHz)	Dipole Moment[b] (Debye)
$H^{13}CO^+$	1 - 0	86.75429	4.48
$HC^{18}O^+$	1 - 0	85.16226	4.48
HCO	1_{01} - 0_{00} [c]	86.67082	1.36
HCS^+	2 - 1	85.34790	1.86
OCS	7 - 6	85.13911	0.72
C_3H_2	2_{12} - 1_{01}	85.33889	3.30
SiO	2 - 1	86.84700	3.10
^{29}SiO	2 - 1	85.75913	3.10
HC_5N	32 - 31	85.20135	4.33
CH_3OH	3_1 - 4_0 A^+	107.01385	0.89
HCOOH	4_{14} - 3_{13}	86.54613	1.40
CH_3CH_2OH	6_{06} - 5_{15}	85.26547	1.44
CH_3CCH	5 - 4 K=0	85.45730	0.75
	K=1	85.45567	
	K=2	85.45077	
	K=3	85.44260	
	K=4	85.43117	
	6 - 5 K=0	102.54798	
	K=1	102.54602	
	K=2	102.54014	
	K=3	102.53035	
	K=4	102.49902	

[a] From the tabulation of Lovas (1986).

[b] From the table of Blake *et al.* (1987).

[c] For the J = 3/2 - 1/2, F = 2 - 1 transition.

Figure B.1 Sample spectra obtained toward the core of M-0.13-0.08. I-bars indicate the observed antenna temperature scale of each spectrum. The spectrum of CH_3OH is reversed in this figure for ease of presentation (the line is actually in absorption). The spectra have a resolution of 0.69 MHz.

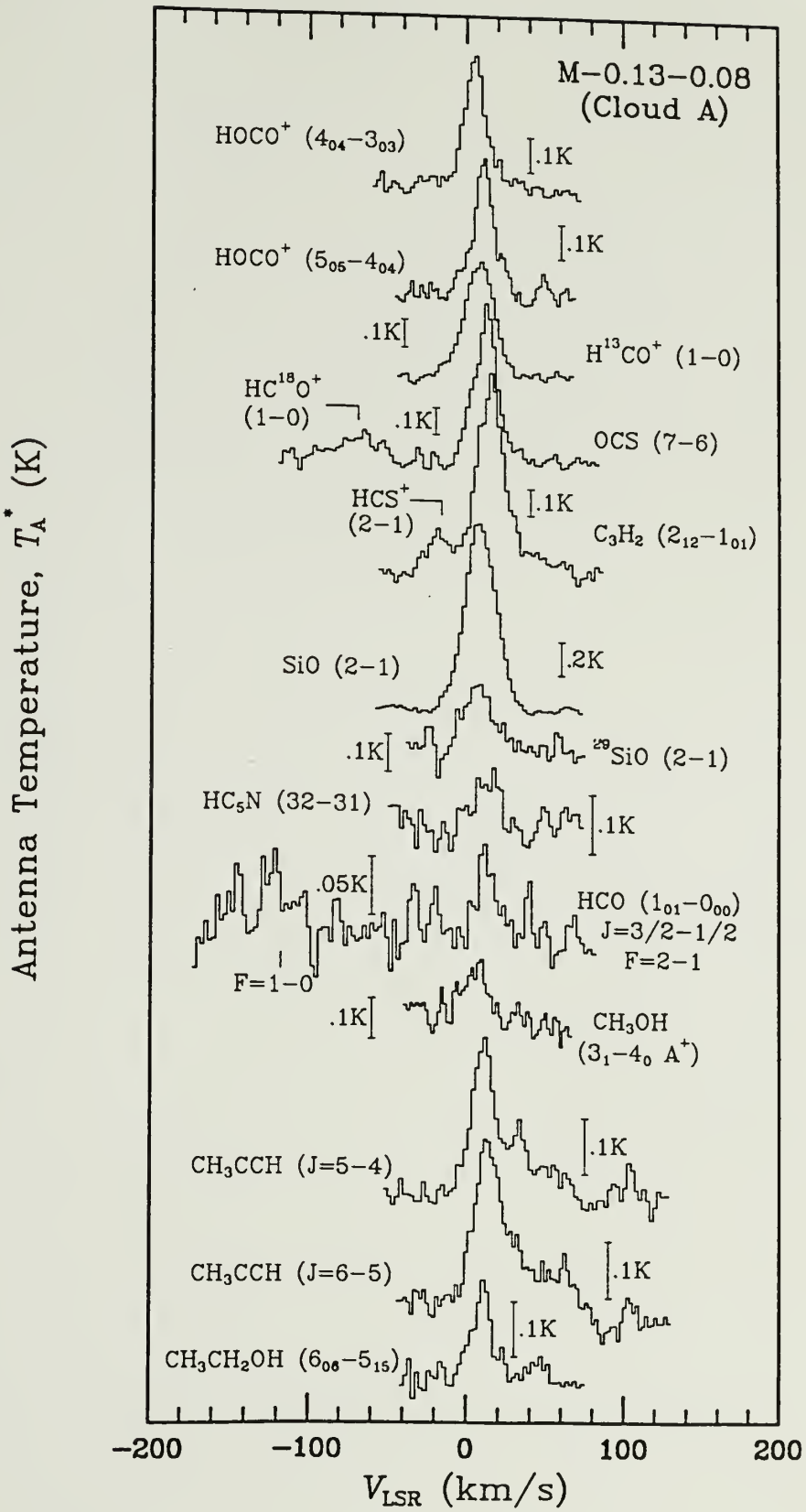
M−0.13−0.08
(Cloud A)
HOCO+ (4₀₄−3₀₃)
.1K
HOCO+ (5₀₅−4₀₄)
.1K
.1K
H13CO+ (1−0)
HC18O+
(1−0)
.1K
OCS (7−6)
HCS+
(2−1)
.1K
C3H2 (2₁₂−1₀₁)
SiO (2−1)
.2K
.1K
29SiO (2−1)
HC5N (32−31)
.1K
.05K
HCO (1₀₁−0₀₀)
J=3/2−1/2
F=2−1
F=1−0
.1K
CH3OH
(3₁−4₀ A+)
CH3CCH (J=5−4)
.1K
CH3CCH (J=6−5)
.1K
.1K
CH3CH2OH (6₀₆−5₁₅)
−200
−100
0
100
200
VLSR (km/s)
Antenna Temperature, T*A (K)

TABLE B.2

Line Parameters for the Observed Transitions

Molecule	(Transition)	T_A^* (K)	$\int T_A^* dV$ (K km s^{-1})	V_{LSR} (km s^{-1})
		M-0.13-0.08 (Cloud A)		
$H^{13}CO^+$	(1 - 0)	0.41	10.4	9.1
$HC^{18}O^+$	(1 - 0)	0.11	2.3	10.9
HCO	$(1_{01} - 0_{00})$[a]	0.09	1.0	11.7
HCS^+	(2 - 1)	0.16	1.7	13.2
OCS	(7 - 6)	0.60	10.4	12.1
C_3H_2	$(2_{12} - 1_{01})$	0.74	15.9	15.2
SiO	(2 - 1)	1.10	30.5	7.8
^{29}SiO	(2 - 1)	0.19	4.3	8.7
HC_5N	(32 - 31)	0.11	1.8	12.2
CH_3OH	$(3_1 - 4_0\ A^+)$	-0.15	-2.5	9.6
HCOOH	$(4_{14} - 3_{13})$	$\leq$ 0.06	—	—
CH_3CH_2OH	$(6_{06} - 5_{15})$	0.20	3.2	10.7
		M-0.13-0.08 (Cloud A/S)		
$H^{13}CO^+$	(1 - 0)	0.56	12.4	18.6
$HC^{18}O^+$	(1 - 0)	0.10	1.7	20.6
HCO	$(1_{01} - 0_{00})$[a]	0.05	1.0	19.0
HCS^+	(2 - 1)	0.15	1.7	27.4
OCS	(7 - 6)	0.64	13.4	19.4
C_3H_2	$(2_{12} - 1_{01})$	0.68	13.4	19.4
SiO	(2 - 1)	1.71	40.2	15.0
^{29}SiO	(2 - 1)	0.21	3.5	20.8
HC_5N	(32 - 31)	0.10	2.0	15.0
CH_3OH	$(3_1 - 4_0\ A^+)$	-0.14	-2.2	23.1
HCOOH	$(4_{14} - 3_{13})$	0.11	2.2	23.3
CH_3CH_2OH	$(6_{06} - 5_{15})$	0.22	3.3	18.0

(Continued on next page)

TABLE B.2

(Continued)

Molecule	(Transition)	T_A^* (K)	$\int T_A^* dV$ (K km s^{-1})	V_{LSR} (km s^{-1})
		M-0.02-0.07 (Cloud B)		
$H^{13}CO^+$	(1 - 0)	0.38	11.2	47.1
$HC^{18}O^+$	(1 - 0)	0.10	1.8	54.5
HCO	$(1_{01} - 0_{00})$	0.04	0.7	49.5
HCS^+	(2 - 1)	0.32	4.3	51.5
OCS	(7 - 6)	0.50	12.3	46.1
C_3H_2	$(2_{12} - 1_{01})$	0.45	13.1	51.4
SiO	(2 - 1)	1.44	46.4	41.2
^{29}SiO	(2 - 1)	0.20	5.6	47.3
HC_5N	(32 - 31)	0.08	1.4	46.7
CH_3OH	$(3_1 - 4_0\ A^+)$	-0.12	-2.3	44.2
HCOOH	$(4_{14} - 3_{13})$	0.05	1.0	47.4
CH_3CH_2OH	$(6_{06} - 5_{15})$	0.16	3.9	47.1
		M 0.06-0.04 (Cloud C)		
$H^{13}CO^+$	(1 - 0)	0.17	4.2	44.8
$HC^{18}O^+$	(1 - 0)	$\leq$ 0.05	—	—
HCO	$(1_{01} - 0_{00})$	$\leq$ 0.04	—	—
HCS^+	(2 - 1)	0.09	0.8	46.6
OCS	(7 - 6)	0.18	3.4	46.1
C_3H_2	$(2_{12} - 1_{01})$	0.20	4.0	49.0
SiO	(2 - 1)	0.58	11.4	41.2
^{29}SiO	(2 - 1)	$\leq$ 0.05	—	—
HC_5N	(32 - 31)	0.06	0.8	50.5
CH_3OH	$(3_1 - 4_0\ A^+)$	-0.09	-1.6	42.3
HCOOH	$(4_{14} - 3_{13})$	$\leq$ 0.05	—	—
CH_3CH_2OH	$(6_{06} - 5_{15})$	0.08	1.8	47.1

(Continued on next page)

TABLE B.2

(Continued)

Molecule	(Transition)	T_A^* (K)	$\int T_A^* dV$ (K km s^{-1})	V_{LSR} (km s^{-1})
		M 0.07-0.08 (Cloud D)		
$H^{13}CO^+$	(1 - 0)	0.42	11.2	47.0
$HC^{18}O^+$	(1 - 0)	0.07	1.0	53.5
HCO	$(1_{01} - 0_{00})$	$\leq$ 0.06	—	—
HCS^+	(2 - 1)	0.11	1.6	56.7
OCS	(7 - 6)	0.29	5.1	50.9
C_3H_2	$(2_{12} - 1_{01})$	0.38	8.8	56.3
SiO	(2 - 1)	1.00	28.1	48.3
^{29}SiO	(2 - 1)	0.18	2.4	44.9
HC_5N	(32 - 31)	0.05	0.7	46.0
CH_3OH	$(3_1 - 4_0\ A^+)$	-0.18	-2.5	46.2
HCOOH	$(4_{14} - 3_{13})$	$\leq$ 0.05	—	—
CH_3CH_2OH	$(6_{06} - 5_{15})$	0.10	1.8	54.3
		M 0.10-0.01 (Cloud E)		
$H^{13}CO^+$	(1 - 0)	0.26	4.7	44.8
$HC^{18}O^+$	(1 - 0)	0.06	1.1	41.4
HCO	$(1_{01} - 0_{00})$	$\leq$ 0.04	—	—
HCS^+	(2 - 1)	0.17	1.8	48.0
OCS	(7 - 6)	0.23	4.8	48.5
C_3H_2	$(2_{12} - 1_{01})$	0.23	6.3	53.9
SiO	(2 - 1)	0.70	12.9	48.3
^{29}SiO	(2 - 1)	0.10	1.5	41.6
HC_5N	(32 - 31)	0.06	0.8	43.6
CH_3OH	$(3_1 - 4_0\ A^+)$	-0.18	-2.5	46.2
HCOOH	$(4_{14} - 3_{13})$	$\leq$ 0.06	—	—
CH_3CH_2OH	$(6_{06} - 5_{15})$	0.14	1.9	44.6

(Continued on next page)

TABLE B.2

(Continued)

Molecule	(Transition)	T_A^* (K)	$\int T_A^* dV$ (K km s^{-1})	V_{LSR} (km s^{-1})
		M 0.11-0.08 (Cloud F)		
$H^{13}CO^+$	(1 - 0)	0.49	11.5	51.9
$HC^{18}O^+$	(1 - 0)	0.12	1.5	46.6
HCO	(1_{01} - 0_{00})	0.07	0.7	55.1
HCS^+	(2 - 1)	0.16	1.5	58.4
OCS	(7 - 6)	0.50	11.9	50.9
C_3H_2	(2_{12} - 1_{01})	0.36	7.2	58.7
SiO	(2 - 1)	1.47	44.8	53.1
^{29}SiO	(2 - 1)	0.24	5.6	49.7
HC_5N	(32 - 31)	0.10	1.6	48.5
CH_3OH	(3_1 - 4_0 A^+)	-0.13	-3.1	42.3
HCOOH	(4_{14} - 3_{13})	0.08	1.0	54.6
CH_3CH_2OH	(6_{06} - 5_{15})	0.15	3.2	49.5
		M 0.25+0.01 (Cloud G)		
$H^{13}CO^+$	(1 - 0)	0.22	5.6	35.2
$HC^{18}O^+$	(1 - 0)	0.06	0.8	37.1
HCO	(1_{01} - 0_{00})	$\leq$ 0.05	—	—
HCS^+	(2 - 1)	0.08	1.5	36.0
OCS	(7 - 6)	0.15	5.9	36.7
C_3H_2	(2_{12} - 1_{01})	0.19	7.5	39.4
SiO	(2 - 1)	0.52	19.0	31.6
^{29}SiO	(2 - 1)	0.12	1.6	31.7
HC_5N	(32 - 31)	0.09	0.6	19.7
CH_3OH	(3_1 - 4_0 A^+)	-0.17	-3.4	25.0
HCOOH	(4_{14} - 3_{13})	0.09	1.1	39.0
CH_3CH_2OH	(6_{06} - 5_{15})	0.10	2.0	42.5

[a] For J = 3/2 - 1/2, F = 2 - 1. NOTE.- Upper limits are 3 σ. Spectral resolution is 0.69 MHz and the typical rms value is ~20 mK.

TABLE B.3

Gaussian Fit Parameters for CH_3CCH

Transition		Cloud A		Cloud A/S		Cloud B	
		T_A^* (K)	ΔV (km s^{-1})	T_A^* (K)	ΔV (km s^{-1})	T_A^* (K)	ΔV (km s^{-1})
J=5-4	K=0	0.16	18.8	0.11	20.6	0.14	19.7
	K=1	0.15	11.5	0.10	17.0	0.15	24.9
	K=2	0.12	16.0	0.07	15.4	0.09	16.9
	K=3	0.06	21.8	0.08	17.0	0.08	20.4
	K=4	0.04	19.2	0.04	17.0	0.04	14.6
J=6-5	K=0	0.19	17.2	0.16	23.7	0.18	20.9
	K=1	0.13	19.0	0.18	14.7	0.16	21.1
	K=2	0.09	16.6	0.09	14.6	0.13	17.7
	K=3	0.09	15.0	0.10	15.8	0.11	18.0
	K=4	≤0.02	—	0.03	9.0	0.05	16.9

Transition		Cloud C		Cloud D		Cloud E	
		T_A^* (K)	ΔV (km s^{-1})	T_A^* (K)	ΔV (km s^{-1})	T_A^* (K)	ΔV (km s^{-1})
J=5-4	K=0	0.05	16.3	0.07	23.7	0.07	17.9
	K=1	0.07	10.7	0.10	15.6	0.06	25.1
	K=2	0.02	14.8	0.05	14.7	0.09	14.5
	K=3	0.04	19.5	0.05	18.5	0.07	18.8
	K=4	0.02	10.2	≤0.02	—	0.05	16.0
J=6-5	K=0	0.06	17.2	0.11	15.7	0.08	20.5
	K=1	0.07	15.0	0.12	13.9	0.10	17.0
	K=2	0.04	10.3	0.08	13.1	0.07	19.7
	K=3	0.05	13.0	0.10	10.6	0.05	21.5
	K=4	0.02	10.0	0.03	14.3	≤0.02	—

(Continued on next page)

TABLE B.3

(Continued)

Transition		Cloud F		Cloud G	
		T_A^* (K)	ΔV (km s^{-1})	T_A^* (K)	ΔV (km s^{-1})
J=5-4	K=0	0.10	25.2	0.14	21.4
	K=1	0.08	19.4	0.14	16.1
	K=2	0.08	14.6	0.08	18.8
	K=3	0.07	17.9	0.11	15.9
	K=4	0.03	13.1	≤0.02	—
J=6-5	K=0	0.11	18.6	0.15	21.7
	K=1	0.10	14.5	0.16	21.4
	K=2	0.06	15.8	0.12	12.2
	K=3	0.10	19.3	0.10	15.0
	K=4	0.03	14.2	0.03	14.2

Figure B.2 Rotation diagrams for CH_3CCH J = 5 - 4 and 6 - 5 transitions obtained at the center of each Cloud. Data are listed in Table B.3 and error bars indicate 3 σ values. I in the ordinate is $I =$

$$[3k\ (J+1)\ S(I,0)\ /\ 8\pi^3\ \nu\ \mu^2\ \{(J+1)^2 - K^2\}\ S(I,K)]\ \int T_A^* dV\ /\ \eta_B,$$

and see the notation in Hollis *et al.* (1981).

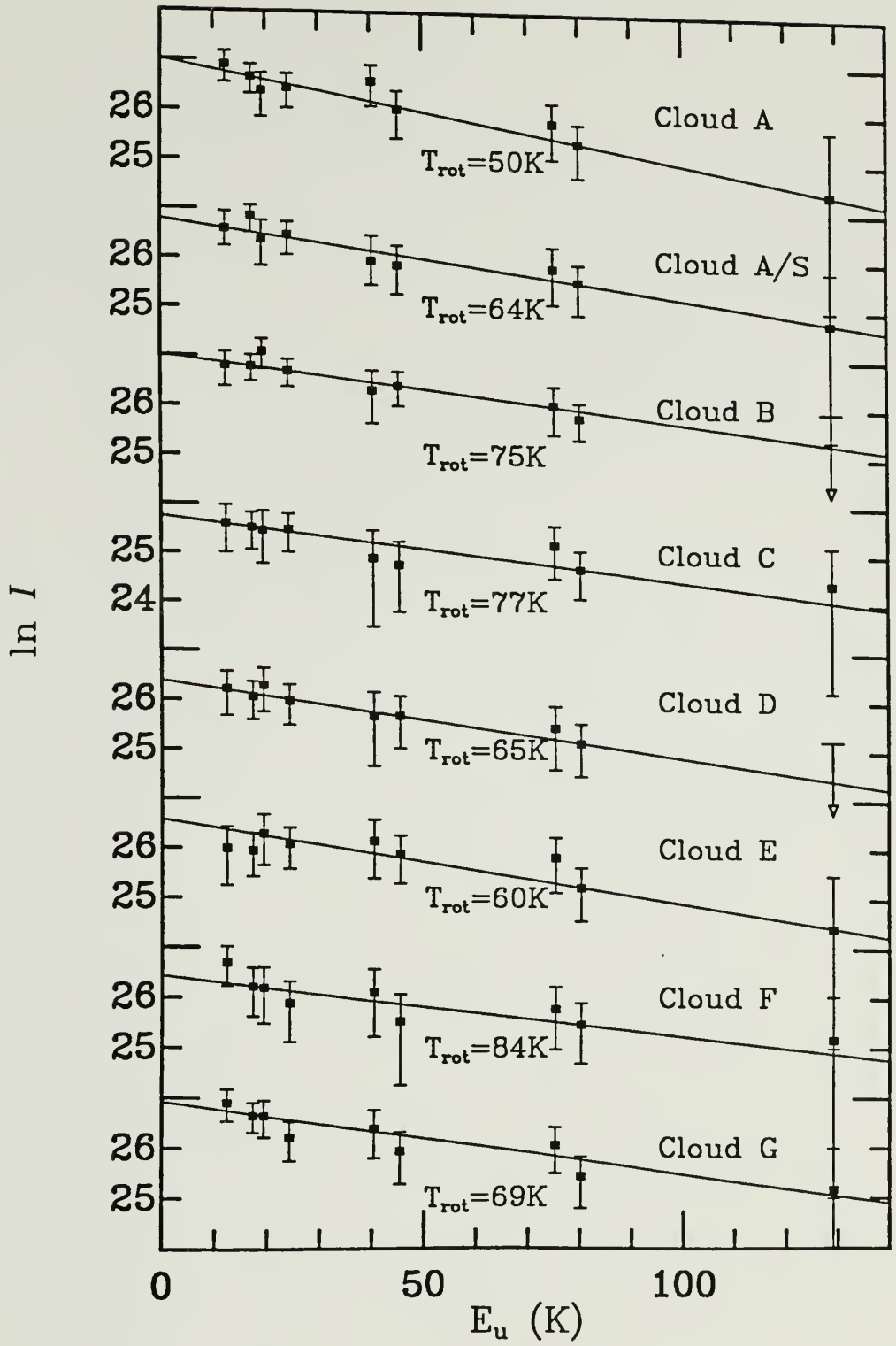
ln I
26
25
Cloud A
T_{rot}=50K
Cloud A/S
T_{rot}=64K
Cloud B
T_{rot}=75K
24
Cloud C
T_{rot}=77K
Cloud D
T_{rot}=65K
Cloud E
T_{rot}=60K
Cloud F
T_{rot}=84K
Cloud G
T_{rot}=69K
0
50
100
E_u (K)

TABLE B.4

Column Densities of Observed Molecules (cm^{-2})

Molecule \ Cloud	A/S	B	C	D	E	F	G
$H^{13}CO^+$	2(13)	2(13)	7(12)	2(13)	7(12)	2(13)	9(12)
$HC^{18}O^+$	3(12)	3(12)	≤2(12)	2(12)	2(12)	2(12)	1(12)
HCO	9(13)	6(13)	≤8(13)	≤1(14)	≤7(13)	6(13)	≤9(13)
HCS^+	2(13)	4(13)	8(12)	2(13)	2(13)	2(13)	2(13)
OCS	2(15)	2(15)	6(14)	9(14)	9(14)	2(15)	1(15)
C_3H_2	2(14)	2(14)	6(13)	1(14)	9(13)	1(14)	1(14)
SiO	1(14)	2(14)	4(13)	1(14)	5(13)	2(14)	7(13)
^{29}SiO	2(13)	3(13)	≤5(12)	1(13)	7(12)	3(13)	7(12)
HC_5N	8(13)	6(13)	3(13)	3(13)	3(13)	7(13)	3(13)
CH_3CCH	1(15)	2(15)	6(14)	1(15)	1(15)	2(15)	2(15)
HCOOH	2(14)	1(14)	≤1(14)	≤1(14)	≤1(14)	1(14)	1(14)
CH_3CH_2OH	9(14)	1(15)	5(14)	5(14)	5(14)	9(14)	5(14)

NOTE. - Numbers in parentheses are powers of 10. Positions given in Table B.2. Assumes optically thin emission and Boltzmann population distributions.

TABLE B.5

Comparison of Fractional Abundances relative to Molecular Hydrogen

Molecule	Sgr A	Sgr B2	TMC-1
HCO^+	—	8 (-9)	1 (-8)
$H^{13}CO^+$	3 (-10)	—	—
$HC^{18}O^+$	3 (-11)	—	—
HCO	1 (-9)	—	—
HCS^+	2 (-10)	2 (-10)	6 (-10)
OCS	2 (-8)	1 (-8)	2 (-9)
C_3H_2	2 (-9)	1 (-9)	2 (-8)
SiO	2 (-9)	4 (-10)	≤ 5 (-12)
^{29}SiO	3 (-10)	—	—
HC_5N	5 (-10)	4 (-10)	3 (-9)
CH_3CCH	2 (-8)	4 (-9)	6 (-9)
HCOOH	1 (-9)	2 (-9)	—
CH_3CH_2OH	1 (-8)	3 (-9)	—

NOTE.- Numbers in parentheses are powers of 10. Data for Sgr B2 and TMC-1 were adopted from the table of Irvine, Goldsmith, and Hjalmarson (1987).

BIBLIOGRAPHY

Allen, M. and Robinson, G. W. 1975, *Ap. J.*, **195**, 81.

Allen, M. and Robinson, G. W. 1977, *Ap. J.*, **212**, 396.

Andersson, M. 1985, in *(Sub)Millimeter Astronomy*, eds. P. A. Shaver and K. Kjar, ESO Conf. Workshop Proc. No.22, p. 353.

Armstrong, J. T., and Barrett, A. H. 1984, *Ap. J. Suppl.*, **57**, 535.

Askne, J., Hoglund, B., Hjalmarson, A., and Irvine, W. M. 1984, *Astr. Ap.*, **130**, 311.

Batrla, W., Wilson, T. L., Bastien, P., and Ruf, K. 1983, *Astr. Ap.*, **128**, 279.

Becklin, E. E., Gatley, I., and Werner, M. W. 1982, *Ap. J.*, **258**, 134.

Bogey, M., Demuynck, C., Destombes, J. L. 1984, *Astr. Ap.*, **138**, L11.

Booth, R. S. *et al.* 1989, *Astr. Ap.*, **216**, 315.

Brown, R. L. and Liszt, H. S. 1984, *Ann. Rev. Astr. Ap.*, **22**, 223.

Brown, P. D. and Millar, T. J. 1989, *M. N. R. A. S.*, **237**, 661.

Blake, G. A., Sutton, E. C., Masson, C. R., and Phillips, T. G. 1987, *Ap. J.*, **315**, 621.

Campell, B. and Thompson, R. I. 1984, *Ap. J.*, **279**, 650.

Castor, J. I. 1970, *M. N. R. A. S.*, **149**, 111.

Charnley, S. B., Dyson, J. E., Hartquist, T. W., and Williams, D. A. 1988, *M. N. R. A. S.*, **231**, 269.

Churchwell, E., and Hollis, J. M. 1983, *Ap. J.*, **272**, 591.

Churchwell, E., Wood, D., Myers, P. C., and Myers, R. V. 1986, *Ap. J.*, **305**, 405.

Cummins, S. E., Linke, R. A., and Thaddeus, P. 1986, *Ap. J. Suppl.*, **60**, 819.

Cupp, R. E., Kempf, R. A., and Gallagher, J. J. 1968, *Phys. Rev.*, **171**, 60.

Dalgarno, A., Black, J. H., and Weisheit, J. C. 1973, *Ap. Letters*, 14, 77.

Davis, D. S., Larson, H. P., and Smith, H. A. 1982, *Ap. J.*, 259, 166.

deJong, T., Chu, S. -L., and Dalgarno, A. 1975, *Ap. J.*, 199, 69.

DeNoyer, L. K. and Frerking, M. A. 1981, *Ap. J. (Letters)*, 246, L37.

Dent, W. A., Werner, M. W., Gately, I., Becklin, E. E., Hildebrand, R. H., Keene, J., and Whitcomb, S. E. 1982, in *The Galactic Center*, eds. G. R. Riegler and R. D. Blandford (New York: Am. Inst. Phys.), p. 33.

d'Hendecourt, L. B., Allamandola, L. J., and Greenberg, J. M. 1985, *Astr. Ap.*, 152, 130.

d'Hendecourt, L. B. and Muizon, Jourdain de, M. 1989, *Astr. Ap.*, in press.

Dopita, M. A. 1977, *Astr. Ap.*, 56, 303.

Drain, B. T. and Salpeter, E. E. 1979, *Ap. J.*, 231, 77.

Duley, W. W., Millar, T. J., and Williams, D. A. 1980, *M. N. R. A. S.*, 192, 945.

Evans, II, N. J. and Blair, G. N. 1981, *Ap. J.*, 246, 394.

Friberg, P. and Hjalmarson, A. 1989, in *Molecular Astrophysics*, ed. T. Hartquist (Cambridge: Cambridge University Press), in press.

Gardner, F. F., Höglund,B., Shukre, C., Stark, A. A., and Wilson, T. L. 1985, *Astr. Ap.*, 146, 303.

Gatley, I., Becklin, E. E., Werner, M. W., and Harper, D. A. 1978, *Ap. J.*, 220, 822.

Gately, I., Hasegawa, T., Suzuki, H., Garden, R., Brand, P., Lightfoot, J., Glencross, W., Okuda, H., and Nagata, T. 1987, *Ap. J. (Letters)*, 318, L73.

Geballe, T. R., Baas, F., Greenberg, J. M., and Schutte, W. 1985, *Astr. Ap.*, 146, L6.

Genzel, R. *et al.* 1978, *Astr. Ap.*, 66, 13.

Genzel, R. and Downes, D. 1977, *Astr. Ap.*, 61, 117.

Genzel, R. and Downes, D. 1982, in *Regions of Recent Star Formation*, eds. R. S. Roger and P. E. Dewdney (Dordrecht: Reidel), p. 251.

Genzel, R., Downes, D., Ho, P. T. P., and Bieging, J. H. 1982, *Ap. J. (Letters)*, **259**, L103.

Genzel, R., Watson, D. M., Townes, C. H., Dinerstein, H. L., Hollenbach, D., Lester, D. F., and Werner, M. 1984, *Ap. J.*, **276**, 551.

Gerry, M. C. L., Yamada, K., and Winnewisser, G. 1979, *J. Phys. Chem. Ref. Data*, **8**, 107.

Goldreich, P. and Kwan, J. 1974, *Ap. J.*, **189**, 441.

Goldsmith, P. F. and Mao, X.- J. 1983, *Ap. J.*, **265**, 791.

Goldsmith, P. F., Irvine, W. M., Hjalmarson, A., Elldér, J. 1986, *Ap. J.*, **310**, 383.

Goldsmith, P. F., Krotkov, R., Snell, R. L., Brown, R. D., and Godfrey, P. 1983, *Ap. J.*, **274**, 184.

Goldsmith, P. F., Snell, R. L., Hasegawa, T., and Ukita, N. 1987, *Ap. J.*, **314**, 525.

Graff, M. M., and Dalgarno, A. 1987, *Ap. J.*, **317**, 432.

Green, S., Garrison, B. J., Lester, Jr.,W. A., and Miller, W. H. 1978, *Ap. J. Suppl.*, **37**, 321.

Green, S., Schor, H., Siegbahn, P., and Thaddeus, P. 1976, *Chem. Phys.*, **17**, 479.

Greenberg, J. M. 1963, *Ann. Rev. Astr. Ap.*, **15**, 267.

Greenberg, J. M. 1989, in *Chemistry in Space*, eds. J. M. Greenberg and V. Pirronello (Dordrecht: Kluwer Academic Press), in press.

Greenberg, J. M., Allamandola, L. J., Hagen, W., van de Bult, C. E. P., and Baas, F. 1980, in *Interstellar Molecules*, ed. B. H. Andrew (Dordrecht: Reidel), p. 355.

Grim, R. J. A. and Greenberg, J. M. 1987, *Astr. Ap.*, **181**, 168.

Guélin, M., and Cernicharo, J. 1989, in *The Physics and Chemistry of Interstellar Molecular Clouds*, ed. G. Winnewisser (Berlin: Springer-Verlag), in press.

Güsten, R., and Henkel, C. 1983, *Astr. Ap.*, **126**, 136.

Güsten, R., Walmsley, C. M., and Pauls, T. 1981, *Astr. Ap.*, 103, 197.

Hagen, W., Allamandola, L. J., and Greenberg, J. M. 1980, *Astr. Ap.*, 86, L3.

Harris, A. Townes, C. H., Matsakis, D. N., and Palmer, P. 1983, *Ap. J. (Letters)*, 265, L63.

Hartquist, T. W., Oppenheimer, M., and Dalgarno, A. 1980, *Ap. J.*, 236, 182.

Hasegawa, T., Gately, I., Garden, R. P., Brand, P., Ohishi, M., Hayashi, M., and Kaifu, N. 1987, *Ap. J. (Letters)*, 318, L77.

Helminger, P., De Lucia, F. C., and Kirchhoff, W. H. 1973, *J. Phys. Chem. Ref. Data*, 2, 215.

Herbst, E., Adams, N. G., and Smith, D. 1983, *Ap. J.*, 269, 329.

Herbst, E., DeFrees, D. J., and Koch, W. 1989, *M. N. R. A. S.*, 237, 1057.

Herbst, E., Green, S., Thaddeus, P., and Klemperer, W. 1977, *Ap. J.* 215, 503.

Herbst, E. and Leung, C. M. 1986a, *M. N. R. A. S.*, 222, 689.

Herbst, E. and Leung, C. M. 1986b, *Ap. J.*, 310, 378.

Herd, C. R., Adams, N. G., and Smith, D. 1989, preprint.

Hildebrand, R. H., Whitcomb, S. E., Winston, R., Stiening, R. F., Harper, D. A., and Moseley, S. H. 1978, *Ap. J. (Letters)*, 219, L101.

Hollenbach, D. J. and Salpeter, E. E. 1971, *Ap. J.*, 163, 155.

Hollis, J. M., Snyder, L. E., Blake, D. H., Lovas, F. J., Suenram, R. D., and Ulich, B. L. 1981, *Ap. J.*, 251, 541.

Huang, Y.-L., Dickman, R. L., and Snell, R. L. 1986, *Ap. J. (Letters)*, 302, L63.

Irvine, W. M., Avery, L. W., Friberg, P., Matthews, H. E., and Ziurys, L. M. 1987, in *Interstellar Matter*, eds. J. M. Moran and P. T. P. Ho (New York: Gordon and Breach), p. 15.

Irvine, W. M., Friberg, P., Kaifu, N., Kawaguchi, K., Kitamura, Y., Matthews, H. E., Minh, Y. C., Saito, S., Ukita, N., and Yamamoto, S. 1989, *Ap. J.*, 342, 871.

Irvine, W. M., Goldsmith, P. F., and Hjalmarson, Á. 1987, in *Interstellar Processes*, eds. D. J. Hollenbach and H. A. Thronson, Jr. (Dordrecht: Reidel), p. 561.

Irvine, W. M., Good, J. C., and Schloerb, F. P. 1983, *Astr. Ap.*, 127, L10.

Irvine, W. M. and Hjalmarson, A. 1984, *Origins Life*, 14, 15.

Irvine, W. M., and Knacke, R. F. 1989, in *The Origin and Evolution of Planetary Atmospheres*, eds. S. K. Atreya, J. B. Pollack, and M. S. Matthews (Tucson: U.Arizona), p.3.

Irvine, W. M. and Schloerb, F. P. 1984, *Ap. J.*, 282, 516.

Irvine, W. M., Schloerb, F. P., Hjalmarson, Â., and Herbst E. 1985, in *Protostars and Planets II*, eds. D. C. Black and M. S. Matthews (Tucson: U. Arizona), p. 579.

Johansson, L. E. B., Andersson, C., Elldér, J., Friberg, P., Hjalmarson, A., Höglund, B., Irvine, W. M., Olofsson, H., and Rydbeck, G. 1984, *Astr. Ap.*, 130, 227.

Kahane, C., Frerking, M. A., Langer, W. D., Encrenaz, P., and Lucas, R. 1984, *Astr. Ap.*, 137, 211.

Kameya, O., Hasegawa, T. I., Hirano, N., Takakubo, K. 1989, *Ap. J.*, 339, 222.

Knacke, R. F., Geballe, T. R., Noll, K. S., and Tokunaga, A. T. 1985, *Ap. J. (Letters)*, 298, L67.

Knacke, R. F., McCorkle, S., Puetter, R. C., Erickson, E. F., and Kratschmer, W. 1982, *Ap. J.*, 260, 141.

Knowles, S. H., Johnston, K. J., Moran, J. M., Burke, B. F., Lo, K. Y., and Papadopoulos, G. D. 1974, *Ap. J.*, 79, 925.

Krugel, E., Stenholm, L. G., Steppe, H.,and Sherwood, W. A. 1983, *Astr. Ap.*, 127, 195.

Lacy, J. H., Baas, F., Allamandolar, L. J., Persson, S. E., McGregor, P. J., Lonsdale, C. J., Geballe, T. R., and van de Bult, C. E. P. 1984, *Ap. J.*, 276, 533.

Leger, A., Jura, M., and Omont, A. 1985, *Astr. Ap.*, 144, 147.

Lester, D. F., Werner, M. W., Storey, J. W. V., Watson, D. M., and Townes, C. H. 1981, *Ap. J. (Letters)*, 248, L109.

Leung, C. M., Herbst, E., and Huebner, W. F. 1984, *Ap. J. Suppl.*, 56, 231.

Linke, R. A., Guelin, M., and Langer, W. D. 1983, *Ap. J. (Letters)*, 271, L85.

Linke, R. A., Stark, A. A., Frerking, M. A. 1981, *Ap. J.*, 243, 147.

Lis, D. L. 1989, Ph. D. Thesis. University of Massachusetts.

Liszt, H. S. 1978, *Ap. J.*, 219, 454.

Liszt, H. S. and Vanden Bout, P. A. 1985, *Ap. J.*, 291, 178.

Loren, R. B. 1984, *MWO Spectral Line Detections from 128 to 357 GHz, 1979-1984*, Tech. Rept. AST 8116403-7.

Lovas, F. J. 1982, *J. Phys. Chem. Ref. Data*, 11, 251.

Lovas, F. J. 1986, *J. Phys. Chem. Ref. Data*, 15, 251.

Lovas, F. J. 1989, *Recommended Frequencies of the Interstellar Molecules*.

Matthews, H. E. and Sears, T. J. 1983a, *Ap. J. (Letters)*, 267, L53.

Matthews, H. E. and Sears, T. J. 1983b, *Ap. J.*, 272, 149.

Millar, T. J. 1982, *M. N. R. A. S.*, 199, 309.

Millar, T. J., Adams, N. G., Smith, D., Lindinger, W., and Villinger, H. 1986, *M. N. R. A. S.*, 221, 673.

Millar, T. J., Bennett, A., and Herbst, E. 1989, *Ap. J.*, 340, 906.

Millar, T. J. and Nejad, L. A. M. 1985, *M. N. R. A. S.*, 217, 507.

Mitchell, G. F. 1984, *Ap. J.*, 287, 665.

Minh, Y. C. and Irvine, W. M. 1989, in preparation.

Minh, Y. C., Irvine, W. M., and Ziurys, L. M. 1988, *Ap. J.*, 334, 175.

Minh, Y. C., Irvine, W. M., and Ziurys, L. M. 1989, *Ap. J. (Letters)*, 345, L63.

Minh, Y. C., Irvine, W. M., Ziurys, L. M., and McGonagle, D. 1989, in preparation.

Morris, M., Polish, N., Zuckerman, B., and Kaifu, N. 1983, *A. J.*, **88**, 1228.

Olano, C. A., Walmsley, C. M., and Wilson, T. L. 1988, *Astr. Ap.*, **196**, 194.

Oort, J. H. 1977, *Ann. Rev. Astr. Ap.*, **15**, 295.

Penzias, A. A. 1980, *Science*, **208**, 663.

Pineau des Forets, G., Roueff, E., and Flower, D. R. 1986, *M. N. R. A. S.*, **220**, 801.

Pineau des Forets, G., Roueff, E., and Flower, D. R. 1989, preprint.

Plambeck, R. L. and Wright, M. C. H. 1987, *Ap. J. (Letters)*, **330**, L61.

Plambeck, R. L., Wright, M. C. H., Welch, W. J., Bieging, J. H., Baud, B., Ho, P. T. P., and Vogel, S. N. 1982, *Ap. J.*, **259**, 617.

Poynter, R. L. and Pickett, H. M. 1984, *Submillimeter, Millimeter, and Microwave Spectral Line Catalogue* (JPL Pub. 80-23, Rev. 2).

Prasad, S. S. and Huntress, Jr., W. T. 1979, *Ap. J.*, **228**, 123.

Prasad, S. S. and Huntress, Jr., W. T. 1982, *Ap. J.*, **260**, 590.

Prasad, S. S., Tarafdar, S. P., Villere, K. R., and Huntress, Jr., W. T. 1987, in *Interstellar Processes*, eds. D. J. Hollenbach and H. A. Thronson, Jr. (Dordrecht: Reidel), p. 631.

Righini, G., Simon, M., and Joyce, R. R. 1976, *Ap. J.*, **207**, 119.

Saito, S., Kawaguchi, K., Yamamoto, S., Ohishi, M., Suzuki, H., and Kaifu, N. 1987, *Ap. J. (Letters)*, **317**, L115.

Schenewerk, M. S., Snyder, L. E., and Hjalmarson, A. 1986, *Ap. J. (Letters)*, **303**, L71.

Schloerb, F. P., Friberg, P., Hjalmarson, Á., Höglund, B., and Irvine, W. M. 1983, *Ap. J.*, **264**, 161.

Schloerb, F. P., Snell, R. L.,and Young, J. S. 1983, *Ap. J.*, **267**, 163.

Schmid-Burgk, J., Densing, R., Krugel, E., Nett, H., Roser, H. P., Schafer, F., Schwaab, G., van der Wal, P., and Wattenbach, R. 1989, *Astr. Ap.*, **215**, 150.

Scoville, N. Z., Sargent, A. I., Sanders, D. B., Claussen, M. J., Masson, C. R., Lo, K. Y., and Phillips, T. G. 1986, *Ap. J.*, **303**, 416.

Scoville, N. Z. and Solomon, P. M. 1973, *Ap. J.*, **180**, 31.

Scoville, N. Z. and Solomon, P. M. 1974, *Ap. J. (Letters)*, **187**, L67.

Scoville, N. Z., Solomon, P. M., and Penzias, A. A. 1975, *Ap. J.*, **201**, 352.

Sinclair, M. W., Fourikis, N., Ribes, J. C., Robinson, B. J., Brown, R. D., and Godfrey, P. D. 1973, *Australian J. Phys.*, **26**, 85.

Snell, R. L. and Wootten, A. 1979, *Ap. J.*, **228**, 748.

Smith, I. W. M. 1988, *M. N. R. A. S.*, **234**, 1059.

Smith, D., and Adams, N. G. 1985, in *Molecular Astrophsics*, eds. G. H. F. Diercksen *et al.* (Dordrecht: Reidel), p. 453.

Smith, J., Lynch, D. K., Cudaback, D., and Werner, M. 1979, *Ap. J.*, **234**, 902.

Snell, R. L. 1981, *Ap. J. Suppl.*, **45**, 121.

Sobolov, V. V. 1960, *Moving Envelopes of Stars* (Cambridge: Harvard University Press).

Spitzer, L., Drake, J. F., Jenkins, E. B., Morton, D. C., Rogerson, J. B., and York, D. G. 1973, *Ap. J. (Letters)*, **181**, L116.

Sutton, E. C., Blake, G. A., Masson, C. R., and Phillips, T. G. 1985, *Ap. J. Suppl.*, **58**, 341.

Swade, D. A. 1987, Ph. D. Thesis, University of Massachusetts.

Swade, D. A. 1989, *Ap. J. Suppl.*, **71**, 219.

Sweitzer, J. S. 1978, *Ap. J.*, **225**, 116.

Takayanagi, K., Sakimoto, K., and Onda, K. 1987, *Ap. J. (Letters)*, **318**, L81.

Thaddeus, P., Gûelin, M., and Linke, R. A. 1981, *Ap. J. (Letters)*, **246**, L41.

Thaddeus, P., Kutner, M. L., Penzias, A. A., Wilson, R. W., and Jefferts, K. B. 1972, *Ap. J. (Letters)*, 176, L73.

Tielens, A. G. G. M. and Allamandola, L. J. 1987, in *Interstellar Processes*, eds. D. Hollenbach and H. Thronson (Dordrecht: Reidel), p. 397.

Tielens, A. G. G. M. and Allamandola, L. J., Bregman, J., Goebel, J., d'Hendecourt, L. B., and Witteborn, F. C. 1984, *Ap. J.*, 287, 697.

Tielens, A. G. G. M. and Hagen, W. 1982, *Astr. Ap.*, 114, 245.

Turner, B. E.,and Thaddeus, P. 1977, *Ap. J.*, 211, 755.

Vanden Bout, P. A., Loren, R. B., Snell, R. L., and Wootten, A. 1983, *Ap. J.*, 271, 161.

Van Dishoeck, E. F., and Black, J. H. 1988, in *Physical Processes in Interstellar Clouds*, ed. M.Scholer (Dordrecht: Reidel),in press.

Vogel, S. N., Wright, M. C. H., Plambeck, R. L., and Welch, W. J. 1984, *Ap. J.*, 283, 655.

Walmsley, C. M., Hermsen, W., Henkel, C, Mauersberger, R., and Wilson, T. L. 1987, *Astr. Ap.*, 172, 311.

Watson, W. D. and Salpeter, E. E. 1972, *Ap. J.*, 174, 321.

Watson, W. D. and Walmsley, C. M. 1982, in *Regions of Recent Star Formation*, eds. R. S. Roger and P. E. Dewdney (Dordrecht: Reidel), p. 357.

Werner, M. W., Becklin, E. E., Gatley, I., Matthews, K., and Neugebaur, C. G. 1979. *M. N. R. A. S.*, 188, 463.

Wilner, S. P. 1984, in *Galactic and Extragalactic Infrared Spectroscopy*, eds. M. F. Kessler and J. P. Phillips (Dordrecht: Reidel), p. 37.

Wilson, T. L. and Walmsley, C. M. 1989, *Astr. Ap. Rev.*, 1, 141.

Winnewisser, G. and Herbst, E. 1987, *Topics in Current Chemistry*, 139, 119.

Wootten, A., Snell, R., and Evans II, N. J. 1980, *Ap. J.*, 240, 532.

Wynn-Williams, C. G., Becklin, E. E., and Neugebaur, G. 1974, *Ap. J.*, 187, 473.

Wynn-Williams, C. G., Werner, M. W., and Wilson, W. J. 1974, *Ap. J.*, **187**, 41.

Yamamoto, S., Saito, S., Kawaguchi, K., Kaifu, N., Suzuki, H., and Ohishi, M. 1987, *Ap. J. (Letters)*, **317**, L119.

Ziurys, L. M., Erickson, N. R., and Grosslein, R. M. 1988, in *Interstellar Matter*, eds. J. M. Moran and P. T. P. Ho (New York: Gordon and Breach), p. 255.

Ziurys, L. M. and Friberg, P. 1987, *Ap. J. (Letters)*, **314**, L49.

Ziurys, L. M., Snell, R. L., and Dickman, R. L. 1988, in *Molecular Clouds in the Milky Way and External Galaxies*, eds. R. L. Dickman, R. L. Snell, and J. S. Young (Berlin: Springer-Verlag), p. 184.

Ziurys, L. M., Wilson, T. L., and Mauersberger R. 1989, preprint.